



Depth profile of the fractal dimension associated to earthquakes distribution in the NW South America

Carlos A. Vargas¹ and Juan M. Salazar¹

(1) Universidad Nacional de Colombia, Bogota, Colombia
E-mail: cavargasj@unal.edu.co, jmsalazarr@unal.edu.co

Abstract: We have analyzed a seismological catalog of approximated 103.000 earthquakes with $0.1 \leq m_L \leq 6.8$ and depths ranging between 0 and 200 km. This catalog was estimated by the National Seismological Network of Colombia with 17 stations in the period 1993-2013. Data allowed calculate the spatial variations (dependence with depth) of the seismic regime (fractal dimension of the earthquakes distribution D) in a large portion of the Colombian territory. Variations of the fractal properties of seismicity were observed along depth, suggesting a stratified rheology and/or a differential behavior of the lithospheric system. Propagation wave results coming from other studies are agree with the estimations of this work.

Keywords: Fractal dimension, Earthquakes, Seismic regime, Colombia.

1. Introduction

The spatial and temporal distribution of earthquakes has been studied using different statistical techniques due to the complexity of these distributions [1-4]. Seismic activity is the result of the interaction between tectonic plates and of instabilities of the crust, mainly at the boundaries of these plates. The relative motion between them generates a stress concentration which generates a energy emission along fracture zones. The temporal distribution of this energy follows a power law and its spatial distribution is related to the occurrence of discrete events or earthquakes, which show a fractal structure [5-7].

The notion of fractal describes how certain structures have the property of self-similarity, characterized by fractal dimension.

Calculation of the fractal dimension of the spatial distribution of earthquakes is a statistical tool for the characterization of an earthquake zone [8].

In this paper we analyze some statistical properties of fractals and seismic activity throughout the territory of Colombia where few studies of this type have been conducted.

The goal of this paper is to study the fractal characteristics of the spatial distributions of earthquakes. First it shows the main characteristics of the data used in the analysis. Then shows how magnitudes of events follow the power law Gutenberg-Richter. Subsequently, we study the relationship between the spatial distribution of earthquakes with fractal dimensions both for epicenters and hypocenters. Finally presents an interpretation of the results.



2. Data

The data used in this study were provided by the National Seismological Network of Colombia. Were used over 100000 seismic events with magnitude greater than 3.2 between July 1, 1993 until January 15, 2013. The study area lies between longitudes 82°W and 65°W and between latitudes 4°S and 13°N. The study volume reaches depths of up to 200 km.

The catalog used incorporates the position of the seismic event, the event date and the Richter scale. Figure 1 shows the hypocentral location of the events used in this work, as well as the main fault systems generated by shallow seismicity in Colombia.

3. Gutenberg-Richter Law

The Gutenberg-Richter law relates the number of seismic events with the magnitude of the event, through the following equation [9-12].

$$\ln(N(M)) = a + bM,$$

Where M is the magnitude of the seismic event on the Richter scale, $N(M)$ is the number of seismic events with magnitude equal to or greater than M , b is the slope of the line formed by the value of $\ln(N(M))$ in function of M .

Figure 2 shows that the data follow the Gutenberg-Richter law and the slope obtained by linearizing the data is -0.873, this value is in a valid range of previous studies [13-16].

4. Fractal Distribution

A fractal is a distribution whose basic structure, fragmented or irregular, is repeated in different scales. A fractal dimension D is a ratio which provides a statistical value which compares as a pattern changes with the scale on which is measured [17].

$$D = -\frac{\ln(N)}{\ln(\varepsilon)},$$

N is the number of partitions of the same size and ε is the size of each partition. The box-counting method uses this relationship to determine the fractal dimension of the distribution. This method analyzes complex data patterns dividing usually box shaped in ever smaller parts. The essence of the process is to examine how observations change with the scale [18-20].

The first step in the study of the data was to find the fractal dimension D by the box-counting procedure of the epicenters in Figure 3 shows the results of the analysis.

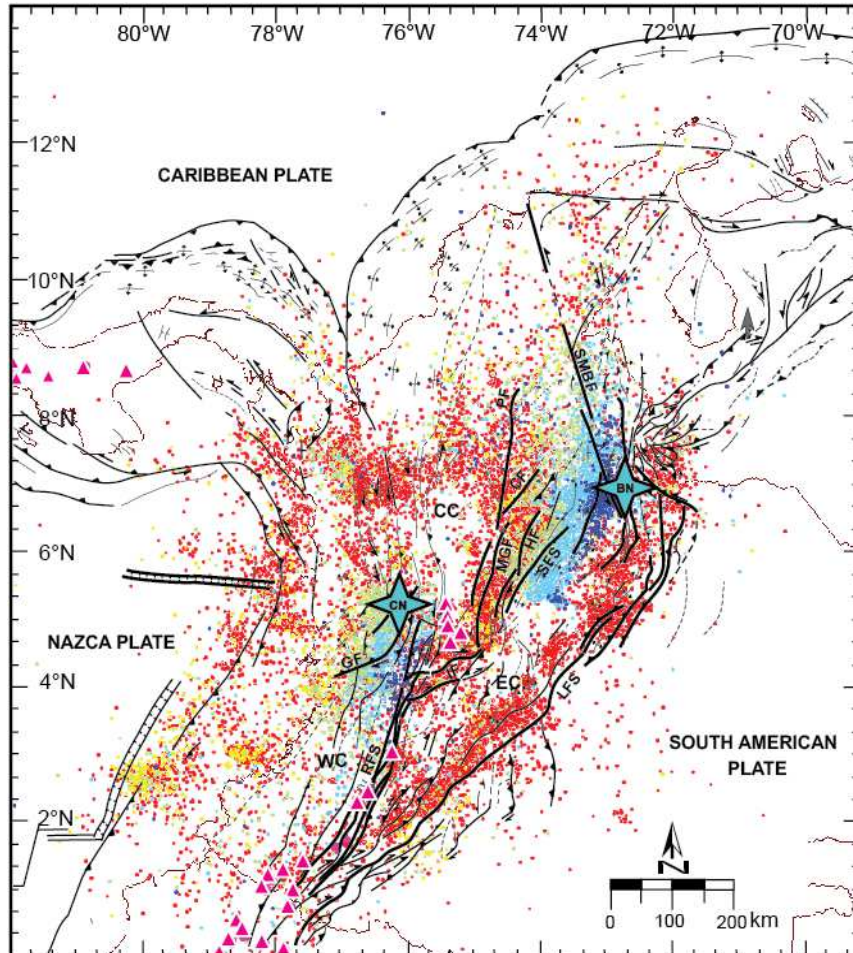


Figure 1. Tectonic setting of Colombia. Map is showing principal plate boundaries, fault systems and neotectonic faults, as well lineaments (dashed lines) and other minor tectonic features (thin lines). Dots represent hypocentral distribution of the approximately 100,000 earthquakes $6.7 \geq m_L > 1.0$ located by the CNSN between 1993 and 2013. Color scale, continuously varying, indicates the depth of events (red are surficial and dark blue are deeper events). Western Cordillera, WC; Central Cordillera, CC; Eastern Cordillera; Romeral fault system, RFS; Santa Marta-Bucaramanga fault, SMBF; Palestina fault, PF; Cimitarra fault, CF; Mulato-Getudo fault, MGF; Honda fault, HF; Salinas fault system, SFS; Garrapatas fault, GF; Llanos Fault System, LFS; Ibagué fault, IF; Bucaramanga nest, BN; Cauca nest, CN. Purple triangles correspond to active volcanos.

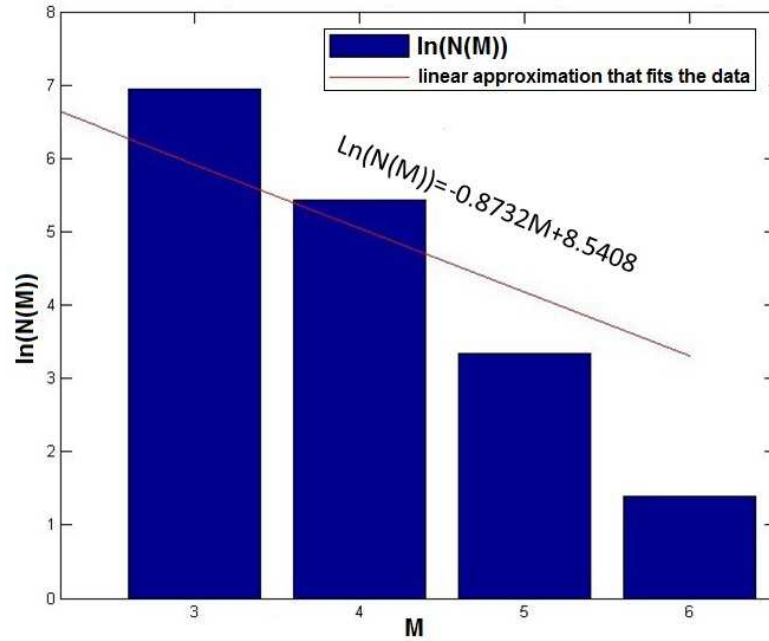


Figure 2. Distribution of the number of seismic events as a function of magnitude.

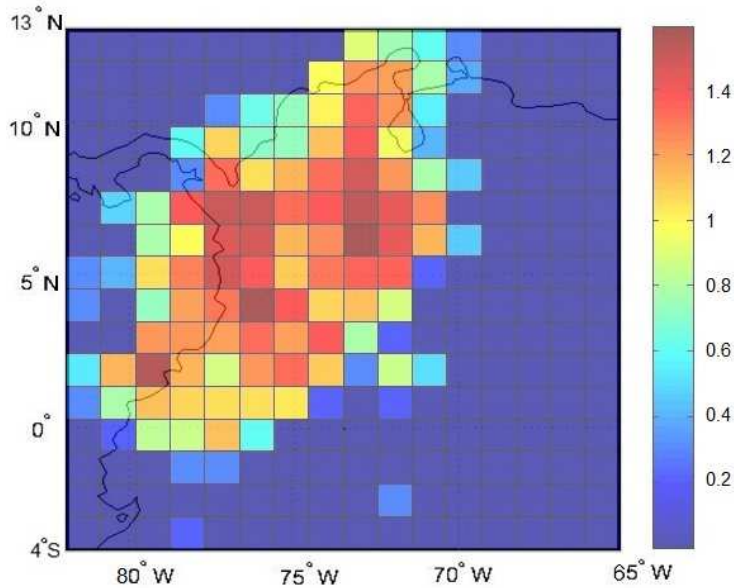
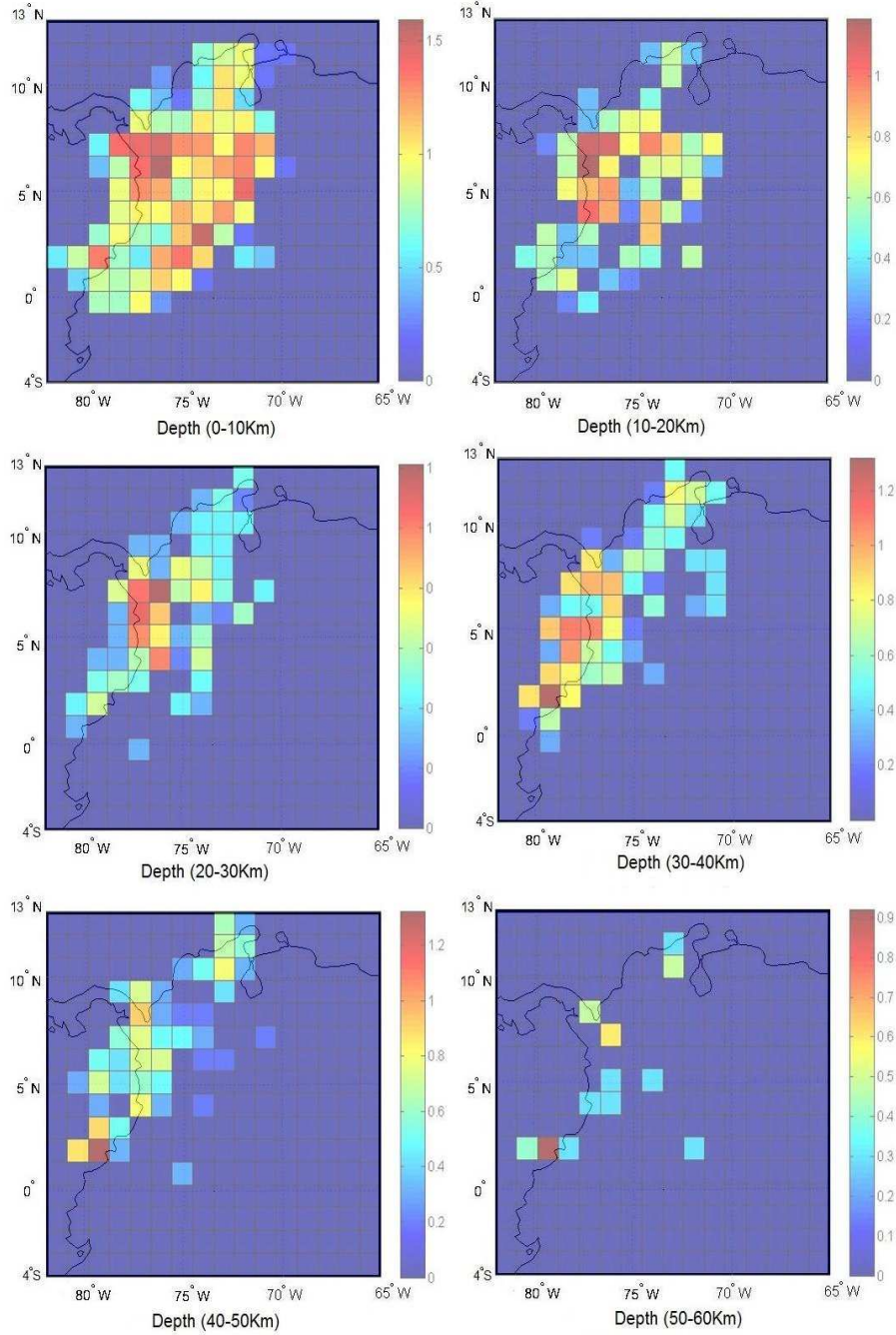
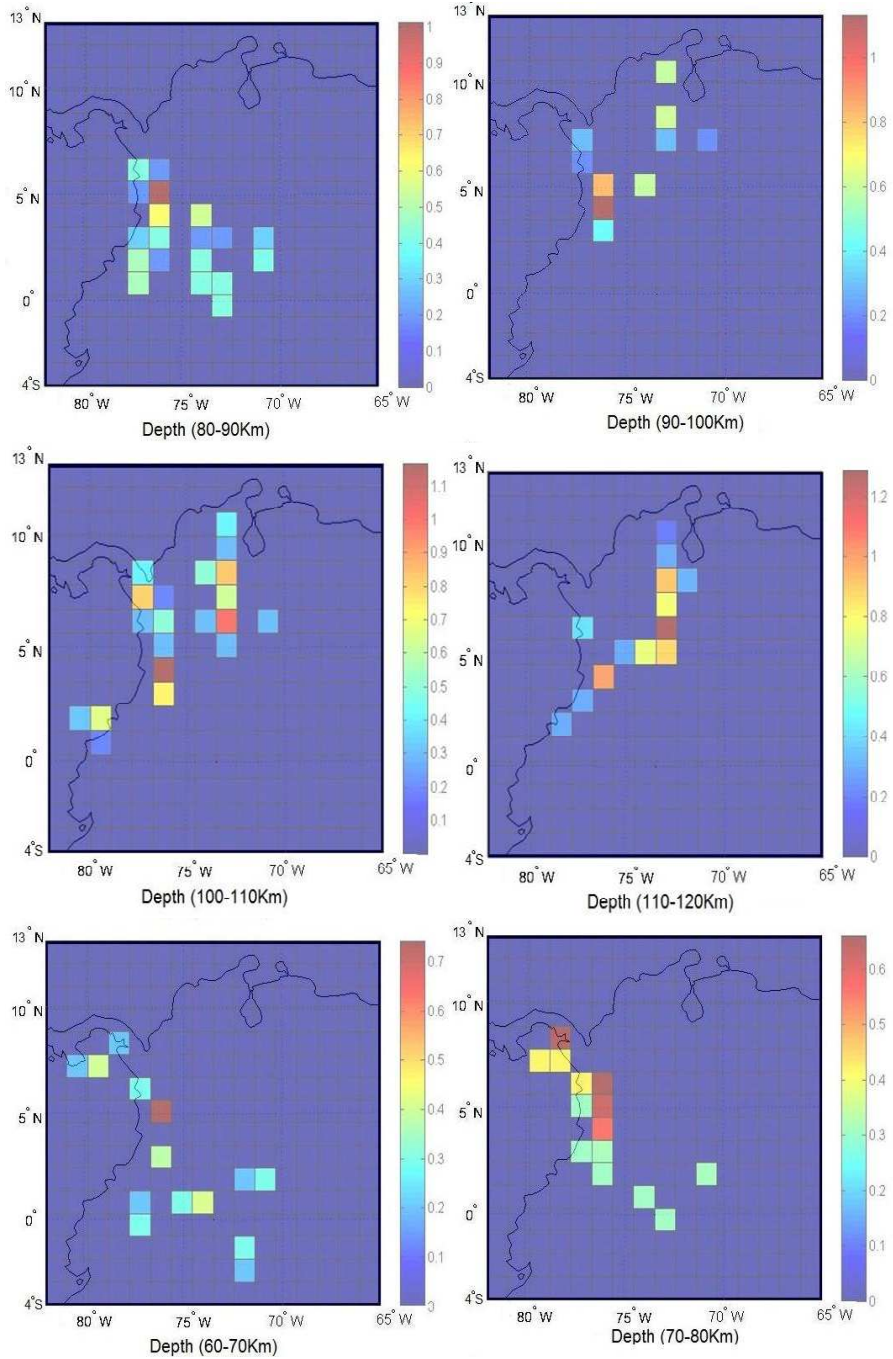
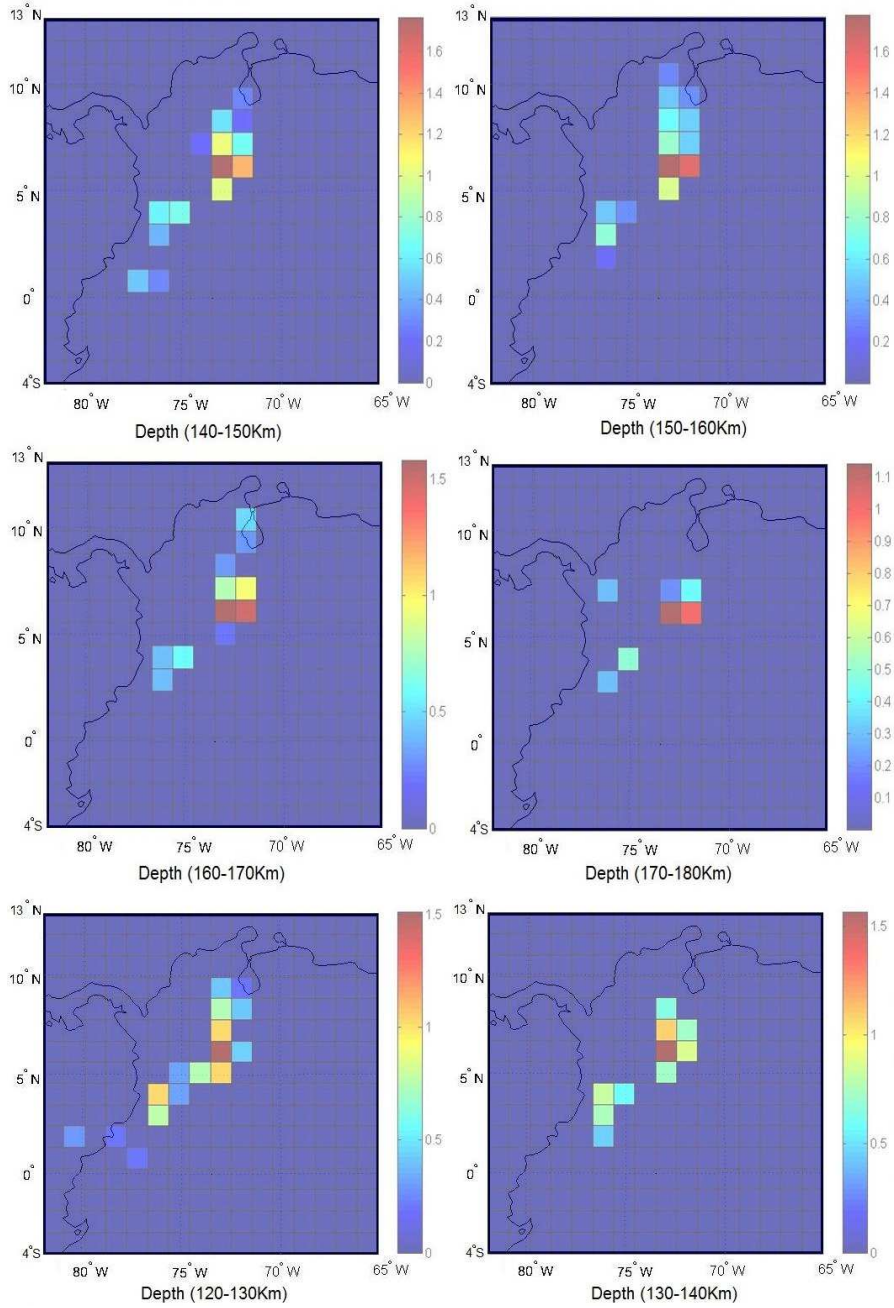


Figure 3. Fractal Dimension of the epicenters in the region of Colombia. In general are found higher values associated with areas where there is greater tectonic activity.







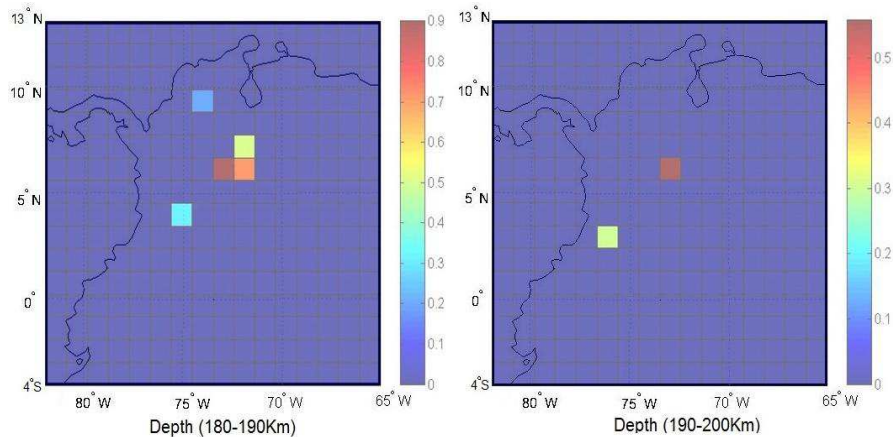


Figure 4. Fractal dimension for hypocenters in the region of Colombia in different depths.

For analysis of the epicenters were selected rectangular areas of dimension 1° in the NS direction and 1° in the WE direction. In each of the areas were taken magnitude values associated to the epicenters and determined its fractal dimension. In total were estimated 289 values of D , which are shown in Figure 3. Was subsequently determined the value of the fractal dimension for hypocenters through box-counting procedure. The results are shown in Figure 4. For this analysis were taken rectangular prisms whose base had dimensions of 1° in the NS direction and 1° in the WE direction and thickness of 10km. The prisms selected cover the territory of Colombia without overlap to a depth of 200km. In total were calculated 5780 values of fractal dimensions D with the hypocentral data. The results are shown in Figure 4 where the planes represent different depths.

5. Discussion and Conclusions

Figures 1 and 3 suggest that the maximum values of fractal dimension are found in the most seismically active areas. The activity is mainly located in the crust (Figure 4, sections up to 40 km in depth). From these depths are highlighted values in at least two seismic nests well identified (Figure 1): Bucaramanga (BN, 130-160km) and Cauca (CN, 70-120 km). In these zones, the possible instabilities tectonics in the range of depths identified suggest complex processes related to the convergence of the Nazca and Caribbean plates beneath the South American plate. High values in areas near the Isthmus of Panama and toward the Pacific coast, highlight a high complexity in the process of convergence between the three lithospheric plates that converge in this region of the planet.

The results obtained compared with other regions of the world that are among the tectonic plate boundaries show a relationship with the high values of b and



of fractal dimension. In Chile due to the convergence of the Nazca and Antarctic plates beneath the South American plate are found high values of b and of fractal dimension [8]. In Turkey due to the African Plate converges with the Eurasian Plate and the Anatolian Plate also are found high values of b and of fractal dimension [21].

References

1. H. Darooneha, C. Dadashinia, Analysis of the spatial and temporal distributions between successive earthquakes: Nonextensive statistical mechanics viewpoint. *Physica A*. vol. 387, 3647–3654, 2008.
2. V. German, Unified scaling theory for distributions of temporal and spatial characteristics in seismology. *Tectonophysics*, vol 424, 167–175, 2006.
3. C. Rajendran, K. Rajendran, The status of central seismic gap: a perspective based on the spatial and temporal aspects of the large Himalayan earthquakes. *Tectonophysics*, vol 395, 19– 39, 2005.
4. Y. Lu, S. Yang, L. Chen, J. Lei. Mechanism of the spatial distribution and migration of the strong earthquakes in China inferred from numerical simulation. *Journal of Asian Earth Sciences*, vol 40, 990–1001, 2011.
5. R. Zuo, P. Agterberg, Q. Cheng, L. Yao. Fractal characterization of the spatial distribution of geological point processes. *International Journal of Applied Earth Observation and Geoinformation*, vol 11, 394–402, 2009.
6. B. Enescu, K. Ito, Some premonitory phenomena of the 1995 Hyogo-Ken Nambu (Kobe) earthquake: seismicity, b -value and fractal dimension. *Tectonophysics*, vol 338, 297–314, 2001.
7. P. Mandal, M. Rodkin. Seismic imaging of the 2001 Bhuj Mw7.7 earthquake source zone: b -value, fractal dimension and seismic velocity tomography studies. *Tectonophysics*, vol 512, 1–11, 2011.
8. D. Pasten, V. Muñoz, A. Cisternas, J. Rogan, J. Valdivia. Monofractal and multifractal analysis of the spatial distribution of earthquakes in the central zone of Chile. *Physical Review E*, vol 84, 066123, 2011.
9. D. Rhoades. Estimation of the Gutenberg-Richter relation allowing for individual earthquake magnitude uncertainties. *Tectonophysics*, vol 258, 71-83, 1996.
10. T. Manzocchi, J. Walsh, A. Nicol. Displacement accumulation from earthquakes on isolated normal faults. *Journal of Structural Geology*, vol 28, 1685-1693, 2006.
11. Y. Kagan. Earthquake size distribution: Power-law with exponent $\beta \equiv 1/2$. *Tectonophysics*, vol 490, 103–114, 2010.
12. R. Hofmann. Individual faults can't produce a Gutenberg-Richter earthquake recurrence. *Engineering Geology*, vol 43, 5-9, 1996.
13. A. Caneva, V. Smirnov, Using the fractal dimension of earthquake distributions and the slope of the recurrence curve to forecast earthquakes in Colombia. *Earth Sciences Research Journal*. Res. J. 8, 3, 2004.
14. D. Cernadas, A. Osella, N. Sabbione. Self-similarity in the Seismicity of the South-American Subduction Zone. *Pure appl. geophys.* vol 152, 57–73, 1998.
15. P. Bhattacharya, R. Majumdar, J. Kayal. Fractal dimension and b -value mapping in northeast India. *Curr. Sci.* vol 82, 1486, 2002.



16. K. Nanjo, H. Nagahama, Observed correlations between aftershock spatial distribution and earthquake fault lengths. *Pure Appl. Geophys*, vol 157, 575, 2000.
17. R. Lopes, N. Betrouni, Fractal and multifractal analysis: A review. *Medical Image Analysis*, vol 13, 634–649, 2009.
18. K. Foroutan, P. Dutilleul, D. Smith. Advances in the implementation of the box-counting method of fractal dimension estimation. *Applied Mathematics and Computation*, vol 105, 195-210, 1999.
19. S. Buczkowski, P. Hildgen, L. Cartilier. Measurements of fractal dimension by box-counting: a critical analysis of data scatter. *Physica A*, vol 252, 23-34, 1998.
20. J. Jiménez, J. Ruiz de Miras. Fast box-counting algorithm on GPU. *Computer Methods and Programs in Biomedicine*. vol 108, 1229–12422, 2012.
21. O. Polat1, E. Gök, D. Yılmaz. Earthquake Hazard of the Aegean Extension Region (West Turkey). *Turkish Journal of Earth Sciences*, vol. 17, 593–614. 2008.



Semantic structuring of chaotic-standing sentences of natural language

Vavilenkova Nastya

National aviation university, Kiev, Ukraine

E-mail: a_vavilenkova@mail.ru

Abstract: The study represents the sentence as the basic unit of natural language content. Deep structures of any natural language sentences correspond to its semantic interpretation. The paper explores two ways of representing the semantic structure of sentences: finite state transition networks and logic-linguistic models. The examples demonstrate the advantages and disadvantages of both methods. An article proposes a new approach to the semantic structuring of chaotic-standing sentences by applying logic-linguistic models.

Keywords: Natural language, Logic-linguistic model, Transition network, Semantic modeling.

1. Introduction

The overall base of semantic analysis methods that can detect semantic relations between words is a thesaurus of language. At the mathematical level it is a directed graph, whose nodes are the words in their basic word forms and arcs define the relations between words and can also display a number of features. Thus thesaurus defines a set of binary relations on the set of words of natural language. Each sentence of natural language has structured minimum that can be represented as a logic-linguistic model of textual information. This model is based on predicate logic. Predicate is in the predicative relation to the subject, it is able to acquire different modal values. Predicate is a meaningful aspect because there are not only formal types of predicate sentences, but also semantic types of predicate. Deep structure of any natural language sentence corresponds to its semantic interpretation. That is, the semantic component should contain rules that transform the underlying structure of sentences generated by the syntactic component in their semantic representation [1]. When person speaks, he understands the contents of any sentences from any set of sentences, performing transaction association meaning of the words in the content of phrases and sentences. The rules of semantic components have to execute this unique procedure: to build the content of complex aggregate from the contents of its components.

Semantic analysis involves procedures aimed at automatic semantic processing of text and creation on its basis new linguistic objects. Semantic analysis is an algorithm that allows us to represent the semantic (content) structure of sentence and text as a strict formal system through analytical exploration of the relations between individual objects and events from the subject area. Semantic component is a set of concepts represented in words and phrases that are related to each other in content. These concepts form a semantic dictionary where

described units are grouped not formally (in alphabetical order), but according to the semantic sets (classes, groups, etc.). That dictionary is based on a hierarchical system of concepts representing its different semantic relations and it is necessary source of semantic information for applications of automatic text processing. The applying of such systems requires component that executes semantic analysis and work with the content of text. The purpose of semantic analysis is to determine the content characteristics for each word and phrase as a whole. Difficulties arise due to semantic ambiguity. Often, to remove this ambiguity, it is necessary to use “semantic articles” related to each other within the semantic network [2]. Analysis of the relations within the semantic network provides with an opportunity to get information that is obviously missed in phrase but without this information any adequate understanding of the phrase is impossible. Difficulties of such implementing are associated with a large amount of semantic networks and multiplicity of analysis. Representation of the sentence that obtained at the stage of semantic analysis is called semantic graph of sentence.

2. The method of augmented transition networks

A finite state transition network is represented by set of nodes and directed arcs connecting them. These nodes correspond to nonterminal symbols and arcs to terminal symbols. Sentence is a minimal and basic communication unit of the language. Sentences should be holistic and transmit information across the complexity of dependencies and relations [3]. Syntactic relations in sentences are called according to the function of dependent member of sentence: identification relations (between the subject and the attributive, complement, adverbial), adverbial relations (between predicate and adverbials), complement relations (between predicate and complement), predicate relations (between subject and predicate). Based on this classification and the assumption that each sentence in natural language has a certain structural minimum, it is possible to build a finite state transition network for any sentence (Fig. 1) [4].

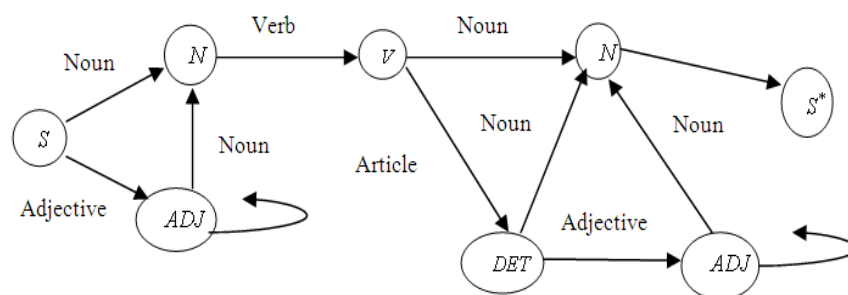


Fig.1. Finite state transition network

Where S is initial node, and S* is final node.
Terms of use of the finite state network:



1. We have to choose one of the directed arcs, which comes from this node and go through it.
2. When the arc is passed, we have to choose one of the terminal symbols subset corresponding to that arc.
3. Continue the process until a node S^* would be reached.

So, it is possible now to write an order of consideration of network nodes (Fig.1) for the sentence «Digital logic circuits require two levels of signal».

Procedure for consideration of nodes would be:

$$S \rightarrow ADJ \rightarrow ADJ \rightarrow N \rightarrow V \rightarrow ADJ \rightarrow N \rightarrow DET \rightarrow N \rightarrow S^*$$

Thus, using a specific network (Fig. 1), we are able to reach final state S^* , so the sentence «Digital logic circuits require two levels of signal» is perceived. However, the proposed finite state transition network (FTN) is not universal. If we change the word order within the natural language sentence or increase the number of a certain type members of sentences, the network will not be able to bring the user to the final state S^* . For sentence to be perceived, cycles should be input into the FTN for almost every of its terminal symbols. Thus the network will have an infinite number of states.

In addition, the proposed network is able to work with rules of recursive origination. Within these rules, a single left symbol reconstitutes right symbol, for example $Cq \rightarrow A_1 q A_2$. Since, there is no way to implement recursion as a part of FTN, a clause of natural language can be described by a single network.

That is, the recursion can be done by extending the model of finite network and enabling a FTN to call the second such network. This procedure should be able to run in any node. In this case, the grammar is represented by set of FTNs, each of which corresponds to a grammatical analysis of natural language sentences. Then the analysis of T chain is the following algorithm:

1. We start examination of terminal symbol S in the initial network.
2. We pass an arc and perceive terminal symbol at each step.
3. If necessary, some nodes, instead of passing the original arc should assigns control to another FTN, referring to the grammar.
4. A called network starts analysis with its own original symbol S' , using the next symbol of T chain as its first input symbol.
5. In turn, if necessary, called network can initiate related FTN, etc.
6. When reaching the final node S'^* , called network assigns control to the initial network, which has been analyzing a input chain T.
7. The process continues until you reach the final terminal symbol of original network S^* .

While studying of how the transition network analyzes the natural language sentences, it is necessary to distinguish between two components of the algorithm: the actual network and program management. Management program is responsible for memorizing word which is read from the input chain T and also for a sequence of calls and network's place active at the moment. In FTN without recursion, controlling program simply checks whether the read word is label for one of the arcs, which comes from the currently active node (terminal symbol).

Consider the example of a set of networks for FTN, which has the ability to call other networks like procedure. Let's analyze the sentence: «The microprocessor is an integrated circuit which has the properties of a complete central processing». For the analysis of a input sentence it is proposed to use a set of networks $M=\{(A),(B),(C),(D)\}$ (Fig.2).

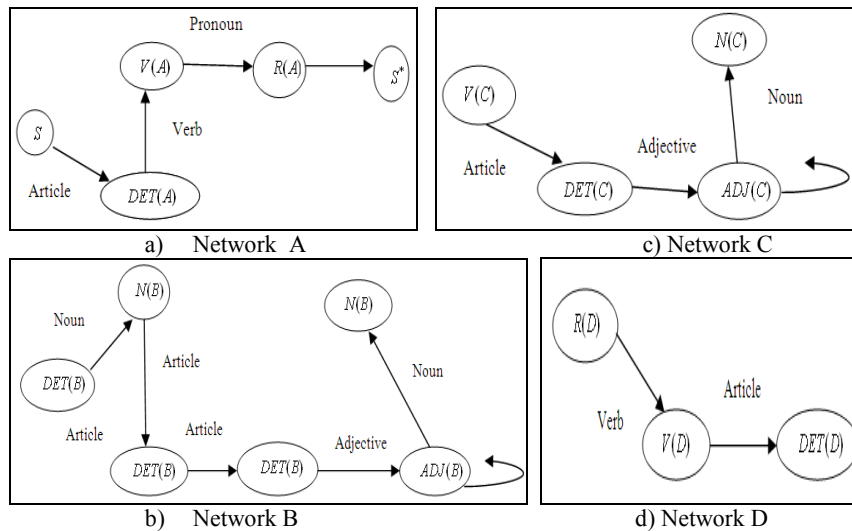


Fig.2. Set of FTNs

1. The analysis begins with the state S of the network (A).
2. The control is passed to $DET(A)$ and the input word will be «The».
3. The network (B) contains a set of possible states for describing the noun, which is the next word in the chain. However, called network (B) for word «microprocessor» has only one proper arc $DET(B) \rightarrow N(B)$, where $DET(B)$ – initial terminal symbol of network (B).
4. Procedure of consideration of the chain at the moment is $S \rightarrow DET(A) \rightarrow N(B)$, current word «is».
5. From the initial FTN's node $V(A)$ the network (C) is called whose initial node is $V(C)$.
6. The transition on network (C) occurs, and result will be as the following sequence of stages: $V(C) \rightarrow DET(C) \rightarrow ADJ(C) \rightarrow N(C)$.
7. After returning to the original network (A), the active node $R(A)$ will be the word «which», and the sequence of stages that led to this node:

$$S \rightarrow DET(A) \rightarrow N(B) \rightarrow V(C) \rightarrow DET(C) \rightarrow ADJ(C) \rightarrow N(C).$$
8. From node $R(A)$ the network (D) is called, and initial terminal symbol is $R(D)$.
9. Analysis of a set of states of network (D) makes possible to define the following sequence of stages: $R(D) \rightarrow V(D) \rightarrow DET(D)$ then comes another call of network where the initial state $DET(B)$, i.e., the word «the».



10. After analyzing the network (B) a sequence of stages is formed as follows:

$$DET(B) \rightarrow N(B) \rightarrow DET(B) \rightarrow DET(B) \rightarrow ADJ(B) \rightarrow ADJ(B) \rightarrow N(B).$$

11. From the network (B) it is returned first to the called network (D), and then to original network (A), which following state is finite S^* .

12. Thus, the call of FTN within input set led to the following sequence of stages:

$$S \rightarrow DET(A) \rightarrow N(B) \rightarrow V(C) \rightarrow DET(C) \rightarrow ADJ(C) \rightarrow N(C) \rightarrow R(D) \rightarrow V(D) \rightarrow \\ \rightarrow DET(B) \rightarrow N(B) \rightarrow DET(B) \rightarrow DET(B) \rightarrow ADJ(B) \rightarrow ADJ(B) \rightarrow N(B) \rightarrow S^*.$$

This approach is generally correct, but the implementation is very labor-intensive, requires large amount of actions and takes much time. The larger is the network, the harder is to use it. The implementation approach using FTN is possible, if the correct number of nodes in the network is provided. This option is available when working with a specific type of sentences. In his work on transformational grammar, Chomsky [5] notes that in formal linguistics we research the concept, i.e. order the structure of natural language sentence, rather than its execution. Thus, the practice of using the proposed approach shows the impossibility of using it for semantic structuring of sentences. And as the structure of natural language sentences is very diverse, the approach using FTN is not rational and universal.

3. Semantic structuring of chaotic-standing sentences of natural language

The considered method of augmented FTN gives a possibility to trace visually the syntactic and semantic relations in complex natural language sentences. By a similar principle we can identify the relation between sentences in any text. Nowadays, to research texts a content analysis is used. Its main purpose is to identify the content of text arrays to further meaningful interpretation of the discovered numerical patterns [6]. The basic idea of content analysis is to discover the procedures by which we can find corresponding indicators studied phenomena and characteristics in the text. Content analysis is used as the primary method aims to obtain the most important information about the subject area. This method, used in combination with others, as an auxiliary procedure for processing data obtained in other researches.

The object of content analysis is the content of various electronic documents interpreted through statistical calculation of meaningful units: concepts expressed in words and terms, themes, expressed in the form of paragraphs of texts and articles [7].

A disadvantage of content analysis is that the researcher should take into account not only mentions that may encounter in the text, but also elements of its contextual use. For this purpose a detailed system of rules for each case use should be developed. Also, the positive and negative ratings are assigned to key content units manually and not automatically; content units are also discovered not automatically but by experts. Searching of natural language sentences by building its logic-linguistic models allow us to analyze the content of sentences: by detecting similar elements and analyzing predicate variables of constructed



models. For example, we have a set of sentences: «Robots can also tell the difference between two temperatures. Ukraine is a sovereign state with its territory, high and local bodies of state power, government. He was one of the greatest scientists and thinkers in history. The simplest and earliest type of robot was a fixed sequence type. The development in robotics is towards adaptive robots having sensory abilities».

Let's form the logic-linguistic models for each of the sentences of preset text (formal representation and model with substitution specific words) [8].

$$P_1 \& P_2(x_1, c_1, x_2[x_3[x_4\{c_{41}\}]]), \quad (1)$$

where $P_1 \& P_2$ – predicate; x_1 – predicate variable subject; c_1 – predicate constant; x_2, x_3, x_4 – predicate variable arguments; c_{41} – predicate constant, that indicates the characteristic of argument x_4 .

$$\text{Can \& tell}(\text{robots, also, difference[between[temperatures \{two\}]]}), \quad (1')$$

$$P'_1 \& P'_2\{c'_{21}\}(x'_1, x'_2\{c'_{21}\}, x'_3\{c'_{31} \& c'_{32}\}[x'_4[x'_5]], x'_6), \quad (2)$$

$$\text{Is \& state}\{\text{sovereign}\} \left(\text{Ukraine, territory}\{its\}, \text{bodies}\{high \& local\} \right), \quad (2')$$

$$\left[\text{state}\{power\} \right], \text{government}$$

$$P''(x''_1, x''_2[x''_3\{c''_{31}\}[x''_4]] \& x''_2[x''_5\{c''_{51}\}[x''_4]]), \quad (3)$$

$$\text{Was} \left(\text{he, one}\{scientists\}\{greatest\}\{history\} \& \right), \quad (3')$$

$$\left(\text{one}\{thin ker s\}\{greatest\}\{history\} \right)$$

$$P'''(x'''_{11} \& x'''_{12}\{c'''_{11} \& c'''_{12}\}, x'''_2[x'''_3[x'''_4]]), \quad (4)$$

$$\text{Was}(\text{type \& robot}\{\text{simplest \& earliest}\}, \text{fixed}\{sequence\}\{type\}). \quad (4')$$

The obtained models allow you to compare predicates and subjects of sentences without searching keywords. For example, model (3) and (4) have the same predicate, but the subjects have completely different semantic value, and therefore can't be the same in content. The subject of model (2) is word «Ukraine», predicate variables (arguments) of this sentence do not overlap in meaning with the subjects and objects of logic-linguistic model (1), (3), (4). This can be checked by using electronic semantic dictionary. Comparison of the same subjects of model (1) and (4) reveals that the words «robot» and «robots» - are nouns used in the singular and plural respectively. Predicate constant «also» informs that in text should be mentioned about the subject of logic-linguistic model earlier in this text. Thus, a sentence that is described by logic-linguistic model (4) should precede sentence (1). The remaining sentences are unrelated by content. Such conclusions were made by comparison the main components of the elementary logic-linguistic models of textual information. If we complicate the comparison criteria and selection algorithm we can improve the comparative analysis of logic-linguistic patterns of natural language sentences.



Thus, we can make a permutation of sentences in preset text: «The simplest and earliest type of robot was a fixed sequence type. Robots can also tell the difference between two temperatures. Ukraine is a sovereign state with its territory, high and local bodies of state power, government. He was one of the greatest scientists and thinkers in history».

4. Conclusions

Semantic structuring of natural language sentences in text is not possible without the implementation of semantic analysis. The results of this analysis can be present as a semantic graph, FTN and in the form of logic-linguistic models. Researches demonstrate that the FTN can visualize relations between words in natural language sentences, but it is not easy in use. This is due to a variety of sentence structures and the number of used words. Speaking about relations between sentences in the text, the transition networks are not designed to handle large amounts of information.

The logic-linguistic models are able to display semantic-syntactic relations in natural language sentences. A detailed study of its components (predicates, subjects and objects), comparison and also application of synonymic dictionary allow to determinate common content components. Due to logic-linguistic models of textual information it is possible to trace semantic relations between sentences and structure them in a document.

References

1. V. Sh. Rubashkin. *Presentation and analysis of the meaning in intelligent information systems*, M., Science, 1989, 192 p.
2. V. A. Zvegintsev. New in foreign linguistics. *Linguistic semantics*: Vol. 10, M., Progress, 1981, 568 p.
3. M. A. Krongauz. *Semantic*, M., Publishing Center "Academy", 2005, 352 p.
4. E. B. Hunt. *Artificial Intelligence*, Academic Press, Inc., 1975, 560 p.
5. N. Chomsky. *Three models of language*. Cyber collection, Vol. 2, 1961, pp. 81-92.
6. R. G. Buharaev and D. S. Sulaymanov. *Semantic analysis in question-answer systems*. Kazan, Publishing of university of Kazan, 1990, 124 p.
7. <http://opros-center.info>. Factor. South-Russian Research Center, content analysis.
8. A. I. Vavilenkova. *Logic-linguistic model as a way to express the syntax of text information*. Mathematical machines and systems, Institute of Mathematical Machines and System Problems of the National Academy of Sciences of Ukraine, 2010, pp. 134-137.





Synergetic approach to unmanned air vehicle control with “attractor-repeller” strategy of nondeterministic obstacles avoidance*

Gennady E. Veselov (Prof.), Andrey A. Sclyarov

Southern Federal University,
Dept. of Synergetics and Control Processes
44, Nekrasovky str., Taganrog, 347928, Russia
E-mail: gev@sfedu.ru, s.andrey.88@mail.ru

Abstract: In the paper we show the new approach to four-motors unmanned air vehicle (UAV) control at the environment with rigid obstacles of various shapes. This approach is based on principles and methods of synergetic control theory. A modern UAVs operating under urban condition are subjected with strict requirement to maneuvering ability. So, among another types of UAVs we may mark a four-motors UAV or quadcopter as mostly maneuverable and suitable one for operating under restricted space conditions.

In the report we explore analysis of mathematical model of four-motors UAV accounting of external disturbance action and synthesis of nonlinear synergetic control law for this robot by using method of analytical design of aggregated regulators (ADAR). For mobile robot adaptation to external environment, we have developed attractor-repeller strategy of nondeterministic obstacles avoidance. The essence of this strategy is that desired ensemble of UAV end states presented as attracting manifolds, i.e. attractors, and obstacles at quadcopter pass presented as three-dimensional repeller (drive back) surface deforming the phase space of mobile robot therefore forming an avoidance trajectory. A bypass direction is formed according to condition of minimal motion resistance in the fully nondeterministic environment or according condition of shorter bypass way at obstacle known parameters. This approach is also could be applied to dynamically changeable obstacles but we might have information about obstacle speed in that case.

We should also note that due to application of integral adaptation method, the obtained synergetic law of spatial control is invariant to piecewise constant external disturbances raised at action of external forces to UAV

Keywords: quadrocopter, sinergetics, attractors, reppers, adaptation, the “attractor-repeller” bypassing strategy.

1. Introduction

Now the unmanned air vehicles (UAVs) are used in many fields of human activity, i.e. in geodesy for mapping of terrain elevation, at police departments for violation record and tracking criminals; in military for reconnaissance

* This research was partially supported by Russian Foundation for Basic Research grants #13-08-00794A and #13-08-01015A



missions. A modern UAVs operating under urban condition are subjected with strict requirement to maneuvering ability. So, among all existed types of UAVs we may mark a four-motors UAV or quadcopter as most maneuverable and suitable one for operating under restricted space conditions. Another advantage of this type of frame is specific simplicity of structure and fabrication low price. As well as quadcopters are designed to operate at restricted space, so the problem of creation the strategy of nondeterministic obstacles avoidance is very actual for this type of mobile robot. The main approaches used for mobile robots control under obstacle environment are: methods of fuzzy logics, methods of artificial neural network, methods of finite automaton, method of position-trajectory control, and synergetic control theory.

Methods of fuzzy logics used to solve difficultly formalize engineering problems, such as obstacles avoidance, basing on predefined expert data base. For implementation of obstacles avoidance with this method, we need to provide on fuzzy membership function input the current position of mobile robot and distance between obstacles and control object [1-4]. Then the fuzzy function will output the control laws as trust power of mobile robot servo drivers.

As well as fuzzy logics method, artificial neural network algorithms are used for obstacles avoidance. For mobile robot control is used artificial neural network learned on defined set of situations. This network define robot behavior according dynamically changed obstacles [5, 6]. This method was spreading due to opportunity to implement the coordinated control strategies of un-formalized control objects in the problems with a-priory known external environment.

Because of modern microcontrollers computing power capabilities grow, the new tends are to solve complex nonlinear problems with software-algorithms solutions, i.e. finite automaton in order to determine classes of situations. This situation also applies to the problem of obstacles avoidance: for some class of obstacles were developed a special algorithms (including ones based on finite automaton) to bypass stationary objects as well as traditional recognition algorithms for object prohibit movement of mobile robot [7-11].

The general lack of these approaches is necessity to have a-priory data about mobile robot operating environment. This fact, in turn, restricts application area of that system with some set of various situations. Moreover, these approached did not account the internal dynamics of control objects and servo drivers of mobile robots.

In order to overcome these lacks, we developed the analytical method of mobile object position-trajectory control at the a-priory unformalized environments [12]. In this approach we account the nonlinear links between segments of control object, and present the behavior of mobile robot as unsteady one at the obstacle proximity. These properties allows position-trajectory control method to be invariant to obstacle location. But the lacks of explored method are avoidance efficiency dependence on obstacle shape; i.e. for linear obstacles the method of position-trajectory control shows the worst result [12]. Besides these method does not account internal dynamics of servo drivers, this fact leads to unreasonable energy loss occurs at overcoming of internal contradictions



between algorithms of higher and lower levels of control system hierarchy structure.

Nowadays, in order to solve the multi-dimensional nonlinear problems, i.e. mobile robot control with taking into account the dynamics of its servo drives, the new integral study – synergetics, is formed. This study explore the processes of self-organization and embrace modern knowledge of nature, including engineering sciences. Based on new knowledge about the nature of processes in the complex nonlinear systems, there was formulated new applied synergetic control theory (SCT) [13], which used the principle of self-organization. As a part of this theory was developed the method of analytical design of aggregated regulators (ADAR) [13-15]. This method provides control law design without linearization or another simplifications. In this method the control targets act as invariant manifolds, and account of system nonlinear dynamics is provided by asymptotic transfer from one invariant manifold to another one with sequential reducing dimension of manifolds.

This control task approach does not need to strictly correspond of real object parameters to ones of controller model; we need only providing entry of closed-loop system into area of attraction of invariant manifolds; on these manifolds, in turn, the desired end state of control object is maintained.

If we explore the mobile robot control under environment with obstacles, the end targets (the defined point into phase space or some desired trajectory) could be presented as attracting manifolds or attractors, and obstacles could be presented as repelling manifolds or repellers.

The synergetic control theory methods we already applied to obstacles avoidance algorithms [16-18]. But the lacks of these works as well as method of position-trajectory control [12] are accounting obstacle size and its matching to defined shape, i.e. circle; this is difficult to accomplish in real conditions of mobile robots operation. This fact drives us to create new synergetic “attractor-repeller” strategy of nondeterministic obstacles avoidance, which is presented in this paper.

To provide spatial control of mobile robot (MR) with four-propeller vertical-attitude takeoff frame, in the paper we propose to use principles and methods of synergetic control theory (SCP) [19-21] in order to implement “attractor-repeller” strategy of nondeterministic obstacles avoidance.

2. Mathematical description and control problem statement

The quadcopter (Fig. 1) is a type of flight vehicle with vertical trust vector [22, 23] drove by four rotors with rotation speed $\Omega_1, \Omega_2, \Omega_3, \Omega_4$ and mounted at the robot center of masses M , on the two decussate metallic beams, rotating corner-wise in the opposite directions (Fig. 2).



Fig. 1. The quadcopter

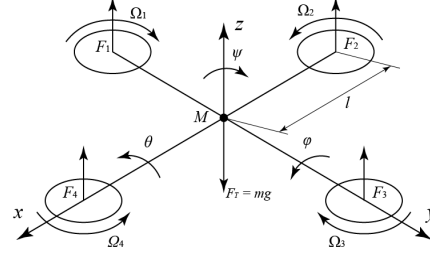


Fig. 2. The quadcopter motion scheme

To design of high level control strategies we need to build quadcopter math. model as a rigid body. UAV motion may be explored as a sum of linear motion of center of masses and spherical motion of body against center of masses [23]. Quadcopter center of masses is on crossing of beams on which the propellers are mounted. The motion mode of UAV is described by the following system of differential equation [23]:

$$\begin{aligned}
 \frac{dx}{dt} &= V_x; & \frac{dy}{dt} &= V_y; & \frac{dz}{dt} &= V_z; \\
 m \frac{dV_x}{dt} &= (\sin \psi \sin \varphi + \cos \psi \sin \theta \cos \varphi) U_1; \\
 m \frac{dV_y}{dt} &= (-\cos \psi \sin \varphi + \sin \psi \sin \theta \cos \varphi) U_1; \\
 m \frac{dV_z}{dt} &= U_1 \cos \theta \cos \varphi - mg; \\
 \frac{d\theta}{dt} &= \omega_\theta; & \frac{d\varphi}{dt} &= \omega_\varphi; & \frac{d\psi}{dt} &= \omega_\psi; \\
 I_{xx} \frac{d\omega_\varphi}{dt} &= (I_{yy} - I_{zz}) \omega_\theta \omega_\psi - J_{TP} \omega_\theta \Omega + U_2; \\
 I_{yy} \frac{d\omega_\theta}{dt} &= (I_{zz} - I_{xx}) \omega_\varphi \omega_\psi + J_{TP} \omega_\varphi \Omega + U_3; \\
 I_{zz} \frac{d\omega_\psi}{dt} &= (I_{xx} - I_{yy}) \omega_\varphi \omega_\theta + U_4,
 \end{aligned} \tag{1}$$

where x, y, z are coordinated of center of gravity of robot; V_x, V_y, V_z , are projections of vector of robot linear velocity; θ is pitch angle; φ is roll angle, ψ is yaw angle, ω_θ – angular velocity in pitch; ω_φ is roll angle angular velocity; ω_ψ is yaw angle angular velocity m is robot mass; I_{xx}, I_{yy}, I_{zz} are moments of inertia around axle x, y and z ; U_1, U_2, U_3, U_4 are UAV control channels; Ω is common velocity of four propellers; J_{TP} is common angular momentum of inertia around propeller axle as follows:

$$J_{TP} = J_P + \eta N^2 J_M \tag{2}$$



where J_p is motor moment of inertia, J_M is propeller moment of inertia, N is reducing gear ratio, η is reducing gear coefficient of performance. Equations of correlation of control channels U_1, U_2, U_3, U_4 with velocities of propeller rotations $\Omega_1, \Omega_2, \Omega_3, \Omega_4$ has the form:

$$\begin{aligned} U_1 &= b(\Omega_1^2 + \Omega_2^2 + \Omega_3^2 + \Omega_4^2) \\ U_2 &= lb(-\Omega_2^2 + \Omega_4^2) \\ U_3 &= lb(-\Omega_1^2 + \Omega_3^2) \\ U_4 &= d(-\Omega_1^2 + \Omega_2^2 - \Omega_3^2 + \Omega_4^2) \\ \Omega &= -\Omega_1 + \Omega_2 - \Omega_3 + \Omega_4 \end{aligned} \quad (3)$$

where l is the distance between center of quadcopter and center of propeller, b and d are aerodynamics components of trust and resistance coefficient. As a parameter of stabilization, the propellers rotation speed is passed into drive system. So we can extract the desired high level control channels from eq. system (3):

$$\begin{aligned} \Omega_1 &= \sqrt{\frac{1}{4b}U_1 - \frac{1}{2bl}U_3 - \frac{1}{4d}U_4}; \\ \Omega_2 &= \sqrt{\frac{1}{4b}U_1 - \frac{1}{2bl}U_2 + \frac{1}{4d}U_4}; \\ \Omega_3 &= \sqrt{\frac{1}{4b}U_1 + \frac{1}{2bl}U_3 - \frac{1}{4d}U_4}; \\ \Omega_4 &= \sqrt{\frac{1}{4b}U_1 + \frac{1}{2bl}U_2 + \frac{1}{4d}U_4}. \end{aligned} \quad (4)$$

In order to control quadcopter hierarchy at low level we need to formalize a dynamics of its drives rotation. Since 4-rotors UAVs have small dimensions, then synchronous micro-motors with permanent magnets (PSDM) are used as the drives for rotating the rotor. These engines have a small size, stable instantaneous angular speed, and high energy performance. PSDM dynamics is described by the following differential equations [19-21]:

$$\begin{aligned} \frac{d\omega}{dt} &= \frac{p}{J} \left(\frac{mp}{2} (\Phi_0 i_{sq} + (L_{sd} - L_{sq}) i_{sd} i_{sq}) - M_c \right); \\ \frac{di_{sq}}{dt} &= \frac{1}{L_{sq}} (-r_s i_{sq} - L_{sd} \omega i_{sd} - \Phi_0 \omega + u_{sq}), \\ \frac{di_{sd}}{dt} &= \frac{1}{L_{sd}} (-r_s i_{sd} + L_{sq} \omega i_{sq} + u_{sd}), \end{aligned} \quad (5)$$

where Φ_0 is magnets magnetomotive force (MMF); ω is micro-motor rotor rotation electric frequency coincides with the rotational speed of the i -th propeller of quadcopter Ω_i ; i_{sd}, u_{sd} is the projection of the current and voltage of the stator winding on d -axis of rotating coordinate system; i_{sq}, u_{sq} is the



projection of the current and voltage of the stator winding on axle q ; r_s is the resistance of the stator winding; L_{sd}, L_{sq} are inductances of the stator winding; p is number of pole pairs; m is the number of phases of the stator winding, M_c is the moment of rotor rotation resistance. Let us take into consideration the fact that PSDM mathematical model (5) is written without accounting eddy currents, hysteresis, saturation and iron loss. It is also necessary to consider the fact that each winding magnetic field distribution along the circumference of the stator and the rotor are take as sinusoidal, stator windings are symmetrical, and the magnets permeability is constant. Also, the magnetic state of the magnets in any mode at any time is determined by the points of one return line and no field of the stator currents are induced in the magnet body [19].

Thus, an objective of synthesizing a design strategy for coordinating control is the rotation speed of four engines $\Omega_1, \Omega_2, \Omega_3, \Omega_4$, which provides asymptotically stable movement of the UAV to a given position x_0, y_0, z_0 in order to keep a given yaw angle ψ_0 . The synthesized control strategies are control inputs for quadcopter micromotor control subsystems [19-21]. It should be noted that the construction of control laws for model (1)-(4) with taking into account the dynamics of drive subsystems (5) by the classical methods of control theory is not a trivial task [14], so we propose to use the principles and methods of the synergetic control theory (SCT) [13-15] in order to design UAV control laws.

3. Design procedure

In the SCT, the set of criteria for system control is usually expressed in the form of an appropriate system of invariants. Invariants act as control objectives, they deliver intended technological problem, but a synergetic design procedure is reduced to finding control laws under which these invariants are satisfied. As invariants for a mobile robot let us choose moving of its center of gravity into coordinates x_0, y_0, z_0 , as well as keeping the quadcopter UAV orientation angle ψ in a given direction ψ_0 . Thus, a subset of the objectives for the drive subsystem has the form

$$\Sigma_1 = \{x = x_0, y = y_0, z = z_0, \psi = \psi_0\}. \quad (6)$$

For the implementation of the synergetic control method according to the procedure of ADAR method[13 - 15, 19 - 21], decompose the original system (1) with the subset of targets (6), for this we introduce the first set of macro variables:

$$\begin{aligned} \Psi_1 &= \omega_\theta - \gamma_1; \\ \Psi_2 &= \omega_\varphi - \gamma_2; \\ \Psi_3 &= \omega_\psi - n_1(\psi_0 - \psi); \\ \Psi_4 &= V_z - n_2(z_0 - z); \end{aligned} \quad (7)$$

where γ_1 and γ_2 are internal control laws for system [13 - 15], n_1 and n_2 are positive constants. Introduced macrovariables Ψ_3 and Ψ_4 serve for keeping subset targets (6) for UAV angular orientation and height. The system of macro



variables (7), according to SCP, shall satisfy solution $\Psi_1 = 0$, $\Psi_2 = 0$, $\Psi_3 = 0$ and $\Psi_4 = 0$ of functional equations:

$$\begin{aligned}\Psi_1 + \lambda_1 \Psi_1 &= 0; \\ \Psi_2 + \lambda_2 \Psi_2 &= 0; \\ \Psi_3 + \lambda_3 \Psi_3 &= 0; \\ \Psi_4 + \lambda_4 \Psi_4 &= 0.\end{aligned}\quad (8)$$

Solution of functional equation system (8) are control laws U_1, U_2, U_3, U_4 , providing transfer of closed-loop system representative point (RP) into neighborhood of manifolds $\Psi_1 = 0$, $\Psi_2 = 0$, $\Psi_3 = 0$ and $\Psi_4 = 0$ intersection. The result is dynamic decomposition of initial system (1). As a result, the behavior of mobile robot at the intersection of manifolds will be described as

$$\begin{aligned}\frac{dx}{dt} &= V_x; \quad \frac{dy}{dt} = V_y; \quad \frac{dz}{dt} = n_2(z_0 - z); \\ m \frac{dV_x}{dt} &= (\sin \psi \sin \varphi + \cos \psi \sin \theta \cos \varphi) U_1; \\ m \frac{dV_y}{dt} &= (-\cos \psi \sin \varphi + \sin \psi \sin \theta \cos \varphi) U_1; \\ m \frac{dV_z}{dt} &= U_1 \cos \theta \cos \varphi - mg; \\ \frac{d\theta}{dt} &= \gamma_1; \quad \frac{d\varphi}{dt} = \gamma_2; \quad \frac{d\psi}{dt} = n_1(\psi_0 - \psi).\end{aligned}\quad (9)$$

In order to accomplish the purposes of the remaining subset conditions (6), namely $x = x_0$ and $y = y_0$, we shall introduce the collection of macro variables

$$\begin{aligned}\Psi_5 &= \beta_{11}(x_0 - x) + \beta_{12}(y_0 - y); \\ \Psi_6 &= \beta_{21}(x_0 - x) + \beta_{22}(y_0 - y);\end{aligned}\quad (10)$$

where β_{11} , β_{12} , β_{21} , and β_{22} are positive constants, besides $\beta_{11}\beta_{22} \neq \beta_{12}\beta_{21}$. Macrovariables system (10), according to SCP, must satisfy solution $\Psi_5 = 0$ and $\Psi_6 = 0$ of functional equations:

$$\begin{aligned}\Psi_5 + \lambda_5 \Psi_5 + \lambda_6 \Psi_5 + \lambda_7 \Psi_5 &= 0; \\ \Psi_6 + \lambda_8 \Psi_6 + \lambda_9 \Psi_6 + \lambda_{10} \Psi_6 &= 0.\end{aligned}\quad (11)$$

The joint solution of equations (10) and (11), with the decomposed mathematical model (9) results in "internal" control laws γ_1 and γ_2 . The resulting "internal" control laws need to substitute to "external" controls U_1, U_2, U_3, U_4 , which are solutions of the functional equation (8). As a result, taking into account the mathematical model of the mobile robot (1), the constraint equations (3) - (4) and "external" controls U_1, U_2, U_3, U_4 , we can get a coordinating strategy speed control for quadcopter four motors $\Omega_1, \Omega_2, \Omega_3, \Omega_4$.

When we determined the coordinating control strategies of the upper level of the hierarchy it is necessary to synthesize control laws of actuators [20], namely synchronous motors with permanent magnets. As the first invariant, according to the SCT, we choose the micro-motor frequency ω stabilization equal to ω_0 ,

which in turn will lead to the stabilization of rotational speed of a single i -th propeller Ω_i . As the second invariant we choose equality of the longitudinal component of the stator current to zero value, to provide maximum electrical torque [19]. Thus, a subset of goals for the PSDM will have the form

$$\Sigma_2 = \{\omega = \omega_0, i_{sd} = 0\}. \quad (12)$$

To suppress the external disturbances acting on the UAV drive at flight, it is necessary to apply, according to the SCT, integrated adaptation [13 - 15], namely to complete the PSDM mathematical model (5) with equations of data perturbation evaluations:

$$\begin{aligned} \frac{dz}{dt} &= \eta(\omega - \omega_0); \\ \frac{d\omega}{dt} &= \frac{p}{J} \left(\frac{mp}{2} (\Phi_0 i_{sq} + (L_{sd} - L_{sq}) i_{sd} i_{sq}) - z \right); \\ \frac{di_{sq}}{dt} &= \frac{1}{L_{sq}} (-r_s i_{sq} - L_{sd} \omega i_{sd} - \Phi_0 \omega + u_{sq}); \\ \frac{di_{sd}}{dt} &= \frac{1}{L_{sd}} (-r_s i_{sd} + L_{sq} \omega i_{sq} + u_{sd}), \end{aligned} \quad (13)$$

where z is evaluation of external disturbances affecting the rotor speed, η is the constant factor.

For the implementation of the synergetic control according to the procedure of ADAR method, decompose the original system (13) with the subset of targets (12), for this we introduce the first set of macro variables:

$$\begin{aligned} \Psi_7 &= \beta_{31} i_{sd} + \beta_{32} (i_{sq} - \gamma_3); \\ \Psi_8 &= \beta_{41} i_{sd} + \beta_{42} (i_{sq} - \gamma_3), \end{aligned} \quad (14)$$

where γ_3 is "internal" control law of PSDM system, β_{31} , β_{32} , β_{41} , and β_{42} are positive constants, besides $\beta_{31}\beta_{42} \neq \beta_{32}\beta_{41}$. The introduced manifolds Ψ_7 and Ψ_8 serve for stabilization projection of stator winding current to d axle, that was indicated in the subset of objectives (12). System (14) of macrovariables, according to SCT, shall satisfy solution $\Psi_7 = 0$ and $\Psi_8 = 0$ of functional equations:

$$\begin{aligned} \dot{\Psi}_7 + \lambda_{11} \Psi_7 &= 0; \\ \dot{\Psi}_8 + \lambda_{12} \Psi_8 &= 0. \end{aligned} \quad (15)$$

The solution of the system of functional equations (15) are the laws of PSDM "external" control u_{sq} and u_{sd} , providing closed-loop system RP transfer into intersection of manifolds $\Psi_7 = 0$ and $\Psi_8 = 0$, the result is the dynamic decomposition of system (13). As a result, the dynamics of PSDM at the intersection of manifolds will be described as

$$\begin{aligned} \frac{dz}{dt} &= \eta(\omega - \omega_0); \\ \frac{d\omega}{dt} &= \frac{mp^2}{2J} \Phi_0 \gamma_3 - z, \end{aligned} \quad (16)$$



To keep the shaft speed of the micromotor ω around ω_0 taking into account external disturbances, let us introduce the following macro variable:

$$\Psi_9 = \omega + \alpha z. \quad (17)$$

and corresponding main functional equation [1,2]:

$$\Psi_9 + \lambda_{13} \Psi_9 = 0. \quad (18)$$

The joint solution of equations (17) and (18), with the PSDM decomposed mathematical model (16) results in "internal" control law γ_3 . Then, to get PSDM "external" control laws u_{sq} and u_{sd} , let us substitute "internal" control γ_3 into system solution (15). As a result we get synthesized PSDM control law stabilizing the speed of the quadcopter four engines $\Omega_1, \Omega_2, \Omega_3, \Omega_4$ under piecewise constant external perturbations arising from the UAV flight. However, the synthesized control laws do not take into account the obstacles at the way of MR. In order quadcopter had the opportunity to perform technological objectives formulated by designers, it needs to supplement synthesized UAV coordinating control strategy with a new "attractor-repeller" non-deterministic strategy of obstacle bypass.

4. Organization of an "Attractor-repeller" non-deterministic strategy of obstacle bypass

In synergic control theory differs energy, technology and auxiliary invariants. With regard to UAV control, technology invariants are $\Psi_4 = 0, \Psi_5 = 0$ and $\Psi_6 = 0$, since they are implementing the ultimate technological challenge of the quadcopter center of gravity transfer into the given point of three-dimensional coordinate system. This three-dimensional point, in terms of the SCT, is an attractor, i.e. attracting manifold in the phase space of the control object. So, for the implementation of the sustainable movement to the attractor, in the control system of mobile robot we must submit every obstacle in the form of a repeller, i.e. surface whose points are repelling manifolds of the phase space of a mobile robot. This "Attractor-repeller" strategy of bypassing non-deterministic obstacles should be applied at the level of technological invariants by modifying the corresponding macro variables. The procedure can be modified as follows:

$$\Psi(x, y, z) = \Psi(\tilde{x}, \tilde{y}, \tilde{z}); \quad (19)$$

$$\begin{bmatrix} \tilde{x} \\ \tilde{y} \\ \tilde{z} \end{bmatrix} = M_x(\alpha) \cdot M_y(\beta) \cdot M_z(\gamma) \cdot \begin{bmatrix} x \\ y \\ z \end{bmatrix}, \quad (20)$$

where $\Psi(x, y, z)$ is macrovariable corresponded to technological invariant, responsible for transfer of RP to attractor; x, y, z are MR coordinates; $\tilde{x}, \tilde{y}, \tilde{z}$ are modified coordinates of MR, $M_x(\alpha), M_y(\beta), M_z(\gamma)$ are rotation matrixes around axles x, y, z at angles α, β , and γ . Expressions (19) and (20), in its essence, represent a process of distortion of the MR phase space in the vicinity of $\Psi(\tilde{x}, \tilde{y}, \tilde{z}) = 0$. Angles α, β , and γ responsible for shape of distortions and are expressed as:



$$\alpha = \rho_1 F_r; \quad \beta = \rho_2 F_r; \quad \gamma = \rho_3 F_r; \quad (21)$$

where ρ_1, ρ_2, ρ_3 are factors determining the behavior of non-deterministic strategy bypass obstacles; F_r is force which acts on the surface repeller to control. Since MR acts at indeterminate external environment, the force F_r should be invariant to the size and shape of the obstacle. This condition can be satisfied if the force F_r of equation (21) define as a function of empirical equation

$$F_r = G \frac{\pi}{2} e^{-\xi \left((x-x_r)^2 + (y-y_r)^2 + (z-z_r)^2 \right)}, \quad (22)$$

wherein x, y, z are MR current coordinates, x_r, y_r, z_r are coordinates of the point closest to the obstacle surface, G is gain of F_r , ξ -rate is ratio of the reaction function (22) when approaching a surface with obstacles. According to properties of empirical function (22), if the distance from the obstacle surface to MR is large, repeller force tends to zero ($F_r \rightarrow 0$) that corresponds to the normal movement of the UAV along a predetermined path. However, with the convergence of the obstacle, strength of the repeller increases and asymptotically tends to $\pi / 2$ ($F_r \rightarrow \pi / 2$ at $G = 1$), which corresponds to the distortion of the phase space of the robot and thus bypass obstacles. This "Attractor-repeller" strategy allows the mobile robot to perform obstacle avoidance, regardless of their size and shape.

The use of "Attractor-repeller" strategy of robot deflection from the obstacle is also suitable for bypass of moving objects. To do this, just modify the empirical function of repeller power with the velocity vector of the moving barrier:

$$F_r = \rho G \frac{\pi}{2} e^{-\xi \left((x-(x_r+V_x))^2 + (y-(y_r+V_y))^2 + (z-(z_r+V_z))^2 \right)}, \quad (23)$$

where V_x, V_y, V_z are projections of speed vector of moving obstacle at three-dimensional coordinate system.

5. Computer simulation

Let us perform a computer study of the synthesized closed-loop control system of 4-propeller UAVs in non-deterministic environment with obstacles. As the parameters of the UAV as a control object we take the following values:

$$m = 6 \text{ kg}; \quad l = 0.3 \text{ m}; \quad b = 121.5 \times 10^{-6}; \quad d = 2.7 \times 10^{-6};$$

$$I_{xx} = 0.6 \text{ kg} \times \text{m}^2; \quad I_{yy} = 0.6 \text{ kg} \times \text{m}^2; \quad I_{zz} = 0.6 \text{ kg} \times \text{m}^2.$$

Also as parameters actuators, namely PSDM, take the following values

$$L_{sd} = 0.0025 \text{ Gn}; \quad L_{sq} = 0.0064 \text{ Gn}; \quad p = 4;$$

$$\Phi_0 = 0.0581 \text{ Weber}; \quad J = 0.003 \text{ kg} \cdot \text{m}^2; \quad r_s = 0.175 \text{ Ohm};$$

Let us take as an internal controller parameter values

$$n_1 = n_2 = 0.2; \quad \lambda_1 = \lambda_2 = 0.5; \quad \lambda_3 = 1; \quad \lambda_4 = \lambda_5 = 0.5; \quad \lambda_6 = 0.2; \quad \lambda_7 = 0.05;$$

$$\lambda_8 = 0.5; \quad \lambda_9 = 0.2; \quad \lambda_{10} = 0.05; \quad \lambda_{11} = \lambda_{12} = r_s / L_{sq}; \quad \lambda_{13} = 1/J;$$

$$\alpha = 10; \quad \eta = 10; \quad \beta_{11} = \beta_{31} = 1; \quad \beta_{12} = \beta_{32} = 2; \quad \beta_{21} = \beta_{41} = 3; \quad \beta_{22} = \beta_{42} = 4.$$

Define the target coordinates $x_0 = 100 \text{ m}$, $y_0 = 260 \text{ m}$, $z_0 = 40 \text{ m}$ and angle $\psi_0 = 0$ rad. As a parameter of attractor-repeller strategy let us take $\rho_1 = \rho_3 = 0$ and $\rho_2 = 1$, that corresponds UAV bypass above the obstacle (fig. 3).

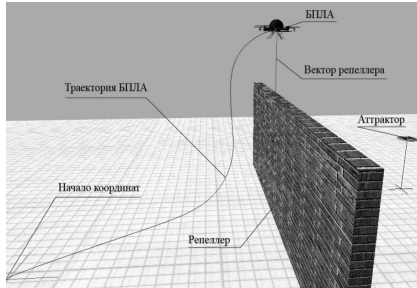


Fig. 3. UAV bypassing a-priori unknown obstacle

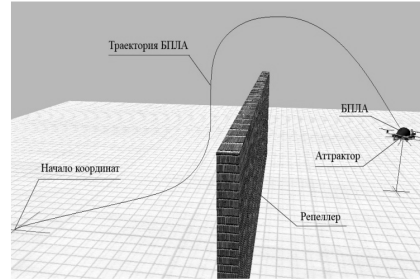


Fig. 4. Keeping UAV at attractor

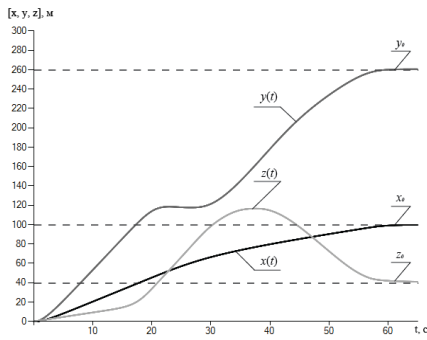


Fig. 5. Transients of UAV center of gravity linear motion

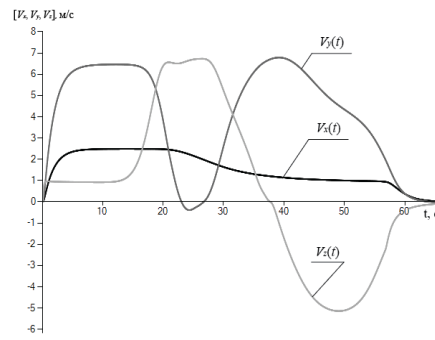


Fig. 6. Transients of linear speeds

The presented simulation results show that the synthesized closed-control system (1-5), taking into account (19)-(23), provide the system introduced invariants, movement to a given point in three-dimensional space, and the invariance to the size and shape of the obstacles at the way of UAV (Fig. 3 and Fig. 8).

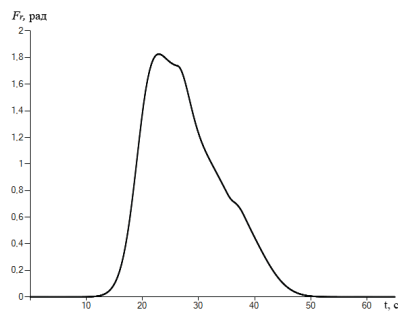


Fig. 7. Repeller force module

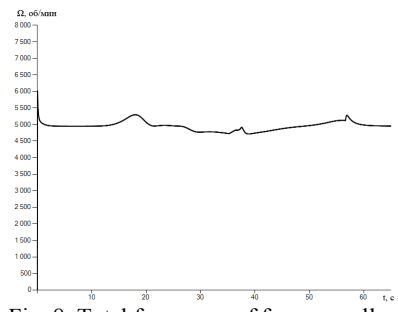


Fig. 8. Total frequency of four propellers rotation



Conclusion

Thus, the article presents an important scientific result: the procedure for analytical synthesis of the coordinating strategy of vector control for unmanned aerial vehicle using the full non-linear models of motion and taking into account the internal dynamics of the actuators. Also developed a "Attractor-repeller" procedure of bypass of non-deterministic non-stationary obstacles of various shapes. This control strategy provides asymptotical stability of closed-loop systems and precise implementation of defined invariants. Presented synergetic control law takes into account the piecewise constant random external disturbances by applying it to the integrated adaptation.

References

1. Dilip Kumar Pratihar, Kalyanmoy Deb, Amitabha Ghosh. A genetic-fuzzy approach for mobile robot navigation among moving obstacles. *International Journal of Approximate Reasoning* 20 – (1999) – 145–172.
2. R. Abiyev, D. Ibrahim, B. Erin. Navigation of mobile robots in the presence of obstacles. *Advances in Engineering Software* 41 - (2010) - 1179–1186.
3. Gyula Mester. Motion Control of Wheeled Mobile Robots. *SISY 2006 4th Serbian-Hungarian Joint Symposium on Intelligent Systems*. – (2006) – 119-130.
4. Khairulmizam Samsudin, Faisal Arif Ahmad, Syamsiah Mashohor. A highly interpretable fuzzy rule base using ordinal structure for obstacle avoidance of mobile robot. *Applied Soft Computing* 11 – (2011) – 1631–1637.
5. Jose M. Cuadra Troncoso, Jose R. Alvarez Sanchez, Felix de la Paz Lopez. Discretized ISO-learning neural network for obstacle avoidance in reactive robot controllers. *Neurocomputing* 72 - (2009) - 861–870.
6. Nirmal Baran Hui, Dilip Kumar Pratihar. A comparative study on some navigation schemes of areal robot tackling moving obstacles. *Robotics and Computer-Integrated Manufacturing* 25 - (2009) - 810–828.
7. Chaoxia Shi, Yanqing Wang, Jingyu Yang. A local obstacle avoidance method for mobile robots in partially known environment. *Robotics and Autonomous Systems* 58 - (2010) - 425 – 434.
8. E. Einhorn, Ch. Schröter, H.M. Gross. Attention-driven monocular scene reconstruction for obstacle detection, robot navigation and map building.
9. Alexey S. Matveeva, Chao Wang, Andrey V. Savkin. Real-time navigation of mobile robots in problems of border patrolling and avoiding collisions with moving and deforming obstacles.
10. Volkan Sezer, Metin Gokasan. A novel obstacle avoidance algorithm: “Follow the Gap Method”. *Robotics and Autonomous Systems* 60 - (2012) - 1123–1134.
11. Jeongdae Kim, Yongtae Do. Moving obstacle avoidance of a mobile robot using a single camera. *Procedia Engineering* 41 - (2012) - 911 – 916.
12. Pshihopof V.H. Moving objects control at a-priory non-formulized environments. “SFedU News. Engineering sciences”. 2008. Vol. 89. # 12. P. 6-19.
13. Kolesnikov A.A. Synergetics control theory. Moscow: Energoatobizdat publ., 1994, 344 p.
14. Kolesnikov A.A. Synergetics control theory. Conceptions, methods, development tends // TSURE News. 2001. Vol. 23. # 5. P. 7-27.



15. Kolesnikov A.A. Synergetic conception of system synthesis: the unity of processes of self-organization and control // TSURE News. 2006. Vol. 61. # 6. P. 10-38.
16. Topchiev B.V. Analytical design of aggregated regulators: multi-wheel mobile robot control // Proc. of XVI Int. scientific conf. "Math. methods in technology and engineering". Rostov-on-Don, May, 26-29, 2003.
17. Topchiev B.V. Synergetic approach to control system design for multi-wheel mobile robots // Proc. of Int. scientific conf. "Problems of synergetics at tribology, triboelectrical chemistry, material study and mechatronics". Novochoerkassk, 2003.
18. Topchiev B.V. Synergetic synthesis of nonlinear kinematic regulators of mobile robots // Synergetics and problems of control theory / Under ed. of Prof. A.A. Kolesnikov, Moscow: FIZMATLIT, 2004. Pages 324 to 324.
19. Kolesnikov A.A., Veselov G.E., Popov A.N., Mushenko A.S., et al. "Synergetics methods of complex systems control: Mechanical and Electromechanical Systems. Moscow: URSS publ., 2006, 304 p.
20. Veselov G.E. Synergetic approach to hierarchical control systems design. // TSURE News. 2006. Vol. 61. # 6. P. 73-84.
21. Veselov G.E. Applied theory of synergetic design of hierarchical control systems. // TSURE News. Special issue: Applied synergetics and system synthesis. –2006. –№5. –P. 66–76.
22. Beji L., Abichou A. Trajectory and Tracking of a Mini-Rotorcraft // Proceedings of the 2005 IEEE Int. Conf. on Robotics and Automation. 2005. P. 2618-2623.
23. Tommaso Bresciani. Modeling, identification and control of a quadrotor helicopter // Master thesis, Lund University. 2008.
24. Luis Rodolfo García Carrillo, Alejandro Enrique Dzul López, Rogelio Lozano, Claude Pégard. Quad Rotorcraft Control // Springer London Heidelberg New York Dordrecht. 2012.





Difficulties on the Study of the Exponentially changed Plasma Quantities. Models for confronting the Mathematical Inabilities

C. L. Xaplanteris^(1,2), L. C. Xaplanteris⁽³⁾ and D.P. Leousis⁽⁴⁾

(1) Plasma Physics Laboratory, IMS, NCSR “Demokritos”, Athens, Greece

(2) Hellenic Army Academy, Vari Attica, Greece .

(3) School of Physics, National and Kapodistrian University of Athens, Greece

(4) Technical High School of Athens, Greece

E-mail: cxaplanteris@yahoo.com

Abstract: It is well known among the plasma physics specialists that the plasmatic state is very unstable and in many instances the instability can turn into a wavy form. So, the development or not of the plasma wave depends on the wave growth rate or damping, the two terms which describe the transitive state of the dynamic system. These wavy terms appear on the exponent of the Neperian logarithms base e , as the change of the plasmatic quantities (plasma density, wave amplitude e.t.c.) are presented with sine wave function of the time ($\propto e^{-j\omega t}$). The quest of an imaginary part as a circular frequency consistent ω leads to the answer of whether the plasma wave will increase or decrease according to ω_i sign. Almost always, the above quantities (growth and damping), are multi-parametric and very sensitive from the initial conditions and the analytical solution of the mathematical elaboration is very difficult or sometimes impossible to be carried out. Due to these difficulties, the modeling of these exponential constants is suggested in the present work. In two previous studies, which were carried out at the plasma laboratory of “Demokritos” and have been already published, similar exponential terms have been found and the wave rising or damping has been justified.

Keywords: Nonlinear dynamics, Neperian logarithms, wavy form, exponential changes, sub-doubling time, conversion rate.

1. Introduction

Physical phenomena, during which the implicated (involved) physical quantities are changed exponentially, have become known in many cases of the Classical Physics. By starting with the decrease of the amplitude in a mechanical oscillation [1,2], we may continue with the charge and discharge law of the capacitor from a d.c. generator and through an electrical resistance, or the establishment or the interruption of the d.c. current on a wrapper (the well known time-circuits).

During last century, with the discovery of physical radio-activity and the invention of the artificial atomic and nuclear fission [3], new cases of the exponential changes have appeared. During the second half of the last century, along with the plasma physics study, many plasmatic quantities were found to change exponentially, as well. Quantities, such as the plasma density, plasma pressure, plasma potential and the plasma waves especially, have enough



exponential influence from the place and time [4-8] for the usefulness of the present study to be justified. The issue of the drift, electrostatic and other kinds of low frequency plasma waves continues to be under the research scrutiny these days as well. Many publications are occupied with the dispersion relation, the growth or damping of the plasma waves, and their identification, consequently [9-13]. As the waves are represented by exponential functions of the place and time, finding the wave growth rate or the damping is the foremost point for a relative researcher [14-18]. So, in reference [14] the growth rate of the waves caused by the rf-field gradient is found, and in reference [17] the growth of the waves caused by the particle collisions is presented, as well; in these functions the involved quantities are so complicated that it is impossible to be studied mathematically. If the chaotic nature and behaviour of the plasma [19-21] is taken into consideration, the research for mathematical models, which may approach the solution and interpret the data, is getting indispensable.

The paper is organized as following: in Sec. 2 the experimental set-up, the plasma production and plasma waves, as well as the growth description are presented. In Sec.3 the simple problem is given in detail. Two characteristic models are studied in Sec.4, whereas the discussions and conclusions are made in Sec.5. Finally, in the two Appendix sections more details of the mathematical elaboration are given.

1. Plasma production – Theoretical Results

A. Experimental Set-Up Description

A nearly 4m long semi-Q machine has been installed in the Plasma Physics Laboratory of the NCSR ‘Demokritos’ since four decades ago and many studies on the rf produced plasma have been carried out [14,15, 17-19]. A steady steel cylindrical cavity of 6 cm internal diameter, with its’ length adaptable to any purpose, is used almost always, as it is preferred due to its’ cylindrical symmetry simplicity. The argon-plasma is usually produced due to the argon atoms inertia and its’ low penetration. A d.c. generator supplies the Q-machine with constant current into a wide value region and with high accuracy. So, the produced magnetic field along the cylindrical cavity axis has an inclination from the constant value smaller than 4% if the Q-machine electro-magnets are placed correctly.

A low power Magnetron generator operates at constant value of the signal frequency (2.45GHz) and supplies the plasma production with the indispensable energy into a wide region of the external magnetic field values (Table 1).

Electrical probes, disk probes, double probes and probe arrays, which can be moved accordingly or not, provide the possibility of measuring the plasma quantities (plasma density, plasma temperature, plasma potential, plasma wave form, e.t.c.) in every point of the plasma column. Figure 1(a) shows a photograph of a similar experimental device and Fig.1 (b) presents a drawing of the Set-Up for better understanding.

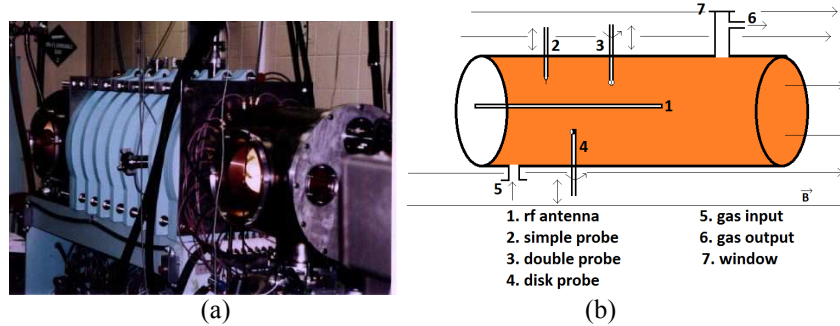


Fig. 1. The photo of the experimental device is shown in (a), whereas the plasma cavity with probes is presented in (b).

B. Plasma production-Plasma Waves

By using a combination of a rotary and a diffusion pump (Balzers type) connected with the cylindrical cavity, the argon pressure can be adjusted in order for the plasma to light within a wide region of values. In a previous publication [18], a complete study of the plasma external parameters, such as gas pressure, rf wave power and magnetic field strength (stress, intensity), has been given. In the present paper, the external parameters and the plasma quantities are summarized in Table 1.

Table 1. The plasma parameters and plasma quantities ranging values

Parameters	Minimum value	Maximum value
Argon pressure p	0.001 Pa	0.1 Pa
Argon number density, n_g	$2 \times 10^{15} m^{-3}$	$2 \times 10^{17} m^{-3}$
Magnetic field intensity, B	10 mT	200 mT
Microwaves' power, P	20 Watt	120 Watt
Frequency of the rf power (standard value)	2.45 GHz	
Electron density, n_0	$2 \times 10^{15} m^{-3}$	$4.6 \times 10^{15} m^{-3}$
Electron temperature, T_e	1.5 eV	10 eV
Ion temperature, T_i	0.025 eV	0.048 eV
Ionization rate	0.1%	90%
Electron-neutral collision frequency, ν_e	$1.2 \times 10^7 s^{-1}$	$3 \times 10^9 s^{-1}$

Among the other noteworthy findings of the thus produced plasma, are its' stability, repetition, and the persistently rising low frequency electrostatic waves, many of which have become audible through the suitable conversion. The waves may have wave-vector component along the three axis originally, but, as the steady state is established, standing waves are sought at the radial and cylinder axis direction, and the waves propagate only azimuthally.



The study of these waves has been done theoretically [14,15,17] by using the fluid mechanics equations and its' dispersion relation, whereas the growth rate and damping have been also found. So, two types of dispersion relations and their growth rate are mentioned here; the first dispersion relation is the following,

$$\omega_l \cong l\Omega_i + \frac{l}{2}(\Omega_R - \Omega_D) - j\frac{v_i}{2} + j|s|C_s\sqrt{\frac{U_R}{U_D} - 1}$$

with the growth rate,

$$\omega_i = |s|C_s\sqrt{\frac{U_R}{U_D} - 1} - \frac{v_i}{2} \quad (2-1)$$

where, $\Omega_i, \Omega_R, \Omega_D$ are the angular (circular) velocities for ions due to d.c. potential gradient, the rf field and the plasma density gradient, respectively. In

addition, there is $C_s^2 \equiv \frac{K_B T_e}{m_i}$ and $s \equiv \frac{1}{n_0} \cdot \frac{dn_0}{d\rho}$.

And the second one is,

$$\omega \cong ku_e + jv_e \frac{\omega_{pe}^2}{\omega_{pi}^2} \cdot \frac{k^2(u^2 - C_s^2) - \omega_{ci}^2}{\omega_{ce}^2}$$

with the growth rate,

$$\omega_i = v_e \frac{\omega_{pe}^2}{\omega_{pi}^2} \cdot \frac{k^2(u^2 - C_s^2) - \omega_{ci}^2}{\omega_{ce}^2} \quad (2-2)$$

where, v_e are the electron-neutral collisions, $\frac{\omega_{pe}^2}{\omega_{pi}^2} = \frac{m_i}{m_e}$, and $u = |u_i - u_e|$.

The first kind of waves is caused by the radial rf -field gradient [14,18], since the second kind is identified as electron-neutral collisional waves [17].

Figure 2 shows a wave form and the frequency spectra of two electrical plasma waves; each spectrum consists of the fundamental frequency and its' upper harmonics, in full accordance with the dispersion relations (2-1) and (2-2). Figure 2 (a) is the waveform, Spectrum (b) for the wave caused by the rf-field radial gradient and spectrum (c) for the collisional wave.

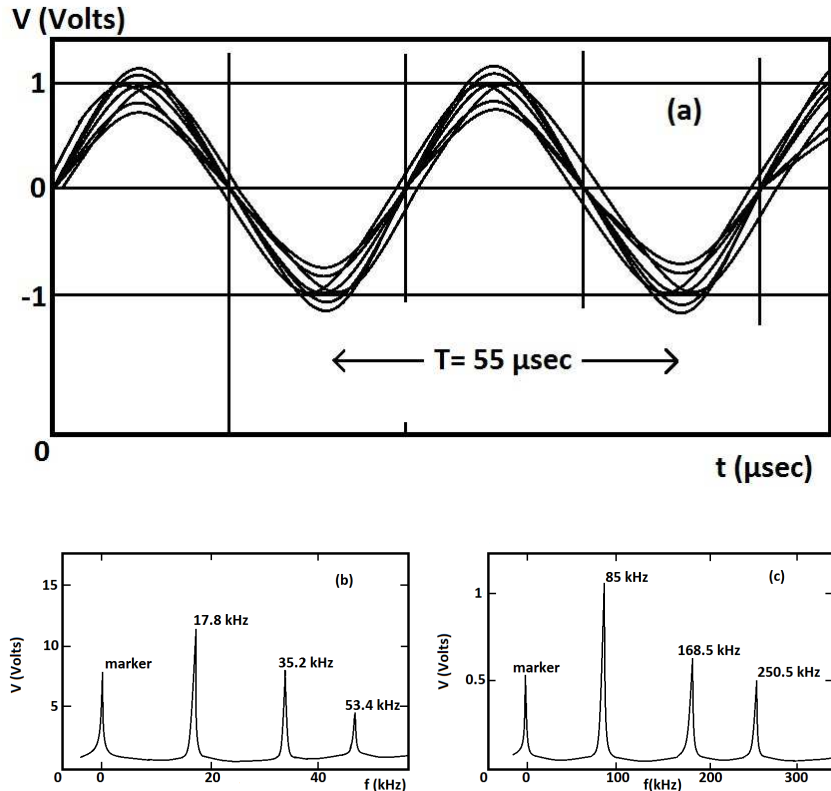


Fig. 2. The wave form is shown in (a), whereas the wave spectra are presented in (b) and (c) for rf-drift and collisional wave, respectively.

C. The ω_i meaning and configuration

An electrostatic wave is described by the following relation;

$$V = V_0 \cdot e^{-j(\omega t - k \cdot r)} \quad (2-3)$$

When the wave frequency ω also has an imaginary part ω_i , then $\omega = \omega_r + \omega_i \cdot j$ or $\omega + \omega_i \cdot j$ substitutes the ω in the relation (2-3), where ω is taken as ω_r , the real part of the wave frequency.

So, the (2-3) is formed as following,

$$V = V_0 \cdot e^{-j(\omega_r + \omega_i \cdot j)t} \cdot e^{+jk \cdot r} \text{ or } V = V_0 \cdot e^{\omega_i t} \cdot e^{-j(\omega_r t - k \cdot r)} \quad (2-4)$$

It is evident from the relation (2-4) that the wave evolution consists of two factors: firstly, the exponentially changed quantity $V = V_0 \cdot e^{\omega_i t}$, which shapes the wave amplitude, and, secondly, the harmonic wave form $e^{-j(\omega_r t - k \cdot r)}$. So, the



significance of the exponentially changed quantities study has become obvious. The imaginary part ω_i , as the relations (2-3) and (2-4) reveal, is expressed by the plasma physical quantities, which depend on the time and on one another. It is perceptible that the imaginary part ω_i of the wave frequency forms the wave amplitude within the transitive state. When the steady state is established, it must be $\omega_i = 0$, or $\omega_i \rightarrow 0_+$, for more accuracy. It is evident that the ω_i takes various values from negative (when there is a damping) to positive (when there is growth).

In any case, two antagonism factors shape the form of the ω_i : firstly, the factor on which the wave is rising, and, secondly, the collisions between ions and atoms. The first strengthens the wave growth, while the second is responsible for the wave damping. The two factors are added in the example of the relation (2-1), while they are multiplied in the example (2-2).

At all events, in any case ω_i is a multi-parametric magnitude and the involved physical quantities depend on each other and are difficult to find. For this reason the modeling of the exponentially changed plasma quantities is useful, if not indispensable, for the wave evolution understanding.

3. Physical Quantities with Exponential Changing-Models

Many examples have been taken from other areas of Physics and not only to state the models for the exponentially changed quantities, which is the topic of the present study; the known Radioactive Conversion (Change) Law is taken from the Physics and the mortality problem is a clearly statistical subject.

The simple solution of the transitive problems

An easily perceptible example is the solution of the radioactively-law problem. Although the solution of this problem is known since the early university lessons, let us repeat its' solution here, for two basic reasons: i) to give the physical interpretation of every mathematical hypothesis or operation (action) and ii) to study the terms of this simple problem, such as the conversion rate, sub-duplication time, semi-life time e.t.c.

The problem situation: At the time $t=0$, the unbroken radioactive nucleus are N_0 . How many unbroken nucleus N will still exist after the passing of the time t ?

Starting by the given fact that at time instant t the remaining unbroken nucleuses are N , an infinitesimal increase of the time by dt is considered. A consequence of this is the breaking off dN from the unbroken nucleuses (the infinitesimal increase of the time causes, infinitesimal decrease of the unbroken nucleuses).

The next step is the seeking of the dependences of the dN change of the unbroken nucleuses on the other physical quantities. (the whole physical interest



of the issue is concentrated on this point of the solution proceedings). These influences are the following: i) the dN change is proportional to the time increase dt (why?), ii) the dN change is proportional to the available quantity of the unbroken nucleuses N . The change dN is proportional to the product of these two factors consequently, and in accordance with the following relation,

$$dN \propto N \cdot dt \quad (3-1)$$

If it is considered that there are no other changeable physical quantities that influence the dN , an analogy constant λ (for the quantities units equalization) must be introduced to the above relation (3-1). So, the following differential equation is resulted, which fits the problem,

$$dN = -\lambda \cdot N \cdot dt \quad (3-2)$$

The constant λ , is named breaking off constant, depends on the breaking nuclear material, and its' unit is the sec^{-1} . To sign (-) is simply put due to the decrease of the remained unbroken nucleuses.

Although the differential equation (3-2) is solved very easily, at the end of the paper Appendix A gives more details; its' solution is the known relation,

$$N = N_0 \cdot e^{-\lambda \cdot t} \quad (3-3)$$

The Law's (3-3) study

a) sub-doubling time: as sub-duplication time is defined the time $t = t_{1/2}$ at which the remaining unbroken nucleuses are half of the original ones, $N = \frac{N_0}{2}$.

With the replacement of the pair of the values $(t_{1/2}, \frac{N_0}{2})$ on the relation (3-3) it is found that,

$$\frac{N_0}{2} = N_0 \cdot e^{-\lambda \cdot t_{1/2}} \quad \text{or} \quad 2 = e^{\lambda \cdot t_{1/2}}$$

and finally,

$$t_{1/2} = \frac{\ln 2}{\lambda} \quad (3-4)$$



In the same way the time of the sub-quadruplication $t_{1/4}$, for which the remaining unbroken nucleuses are $N = \frac{N_0}{4}$, can be found. With the same mathematical thoughts, the following is resulted,

$$t_{1/4} = \frac{\ln 4}{\lambda} = \frac{2 \ln 2}{\lambda} = 2.t_{1/2} \quad (3-5)$$

For the sub-eight time $t_{1/8}$ it is found that,

$$t_{1/8} = \frac{\ln 8}{\lambda} = \frac{3 \ln 2}{\lambda} = 3.t_{1/2} \quad (3-6)$$

Thinking that going from $\frac{N_0}{4}$ unbroken nucleuses to $\frac{N_0}{8}$ is actually a sub-doubling, it is valid that,

$$t_{1/8} - t_{1/4} = 3.t_{1/2} - 2.t_{1/2} = t_{1/2} \quad (3-7)$$

b) Broken nucleuses

The broken nucleuses N' are: $N' = N_0 - N = N_0 - N_0.e^{-\lambda.t} = N_0.(1 - e^{-\lambda.t})$
or

$$N' = N_0.(1 - e^{-\lambda.t}) \quad (3-8)$$

The drawing of the relations $N = N(t)$ (3-3) and $N' = N'(t)$ (3-8) is presented in Fig.3.

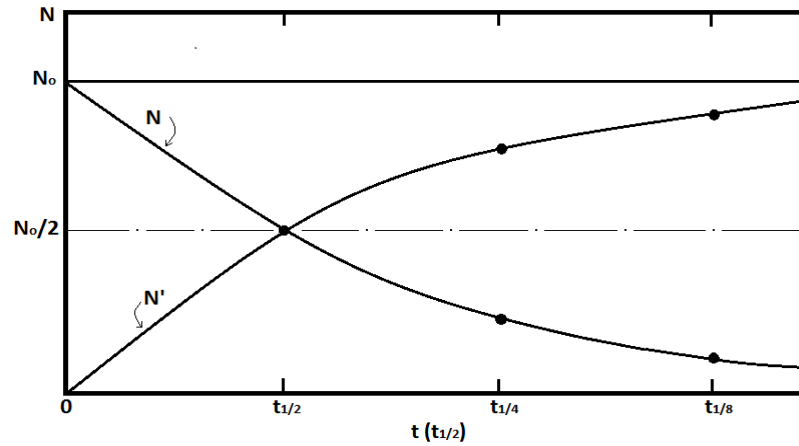


Fig. 3. The $N = N(t)$ and $N' = N'(t)$ drawing is presented

c) Conversion rate

The quotient $\frac{dN}{dt}$ is defined as conversion rate. Consequently, the derivation of the relation (3-3) gives the conversion rate as following,

$$\frac{dN}{dt} = N_0 \cdot (-\lambda) \cdot e^{-\lambda \cdot t} = -\lambda \cdot N$$

$$\text{or } \frac{dN}{dt} = -\lambda \cdot N \quad (3-9)$$

In Fig.4 the conversion rate versus the time is presented graphically.

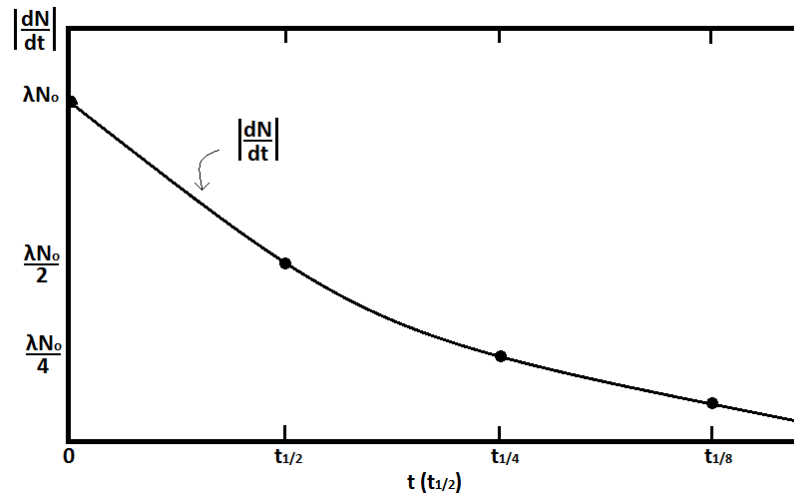


Fig. 4. The conversion rate $\frac{dN}{dt}$ versus the time t is shown.

Observations-Comments:

1. The sub-doubling time remains constant, apart from the quantity of the unbroken radioactive nucleuses.
2. In accordance with the radioactively law (relation 3-3), when $t = \infty$, the remaining unbroken nucleuses are nullified.
3. The drawings of the remaining nucleuses $N = N_0 \cdot e^{-\lambda \cdot t}$ and the already broken ones $N' = N_0(1 - e^{-\lambda \cdot t})$ are symmetrical to the straight line $\psi = \frac{N_0}{2}$ (Fig.3).

4. Cases-Models with no constant λ

In most cases the λ is not constant, but changeable by the time (quantities changeable by the time), sometimes in a small rate and other times in a big one. Let us consider the radioactively conversion again: two disputes of the results found from the previous solution can be placed here: i) the stability of the sub-life time $t_{1/2}$, apart from the available number of the unbroken nucleuses N , and ii) the total breaking off all the available nucleuses.

The physical perception obtained from the observation of related physical phenomena expects the sub-life time to decrease as the available unbroken nucleuses diminish, while the conversion proceedings have to stop leaving a small quantity of unbroken nucleuses.



Nuclear breaking off with decreased factor λ

I. Case

Let us now consider that the factor λ is not constant, but it has the following influence from the time,

$$\lambda = \lambda_0 - \mu t \quad (4-1)$$

where μ is a constant measured in sec^{-2} .

Repeating the formulation of the previous problem, where λ is considered as a constant, and, if at the moment t the remaining unbroken nucleuses are N , then, within the infinitesimal time dt , the change of the unbroken nucleuses dN is given from the following relation,

$$dN = -\lambda.N.dt \quad \text{or} \quad dN = -(\lambda_0 - \mu t).N.dt \quad \text{or}$$

$$\frac{dN}{N} = -(\lambda_0 - \mu t).dt \quad (4-2)$$

The integration of the relation (4-2) gives the influence of time for the unbroken nucleuses evolution,

$$N = N_0.e^{-\lambda_0 t + \frac{\mu}{2}.t^2} \quad (4-3)$$

The law's (4-3) study

a) Semi-life time: by putting $t = t_{1/2}$ when $N = \frac{N_0}{2}$, the equation $\mu.t_{1/2}^2 - 2\lambda_0.t_{1/2} + 2 \ln 2 = 0$ is obtained and its' solution gives the semi-life time,

$$t_{1/2} = \frac{\lambda_0 - \sqrt{\lambda_0^2 - 2\mu \ln 2}}{\mu} \quad (4-4)$$

If it is put that $t = t_{1/4}$ when $N = \frac{N_0}{4}$, in the same way as above the sub-quadruplication time is obtained,



$$t_{1/4} = \frac{\lambda_0 - \sqrt{\lambda_0^2 - 4\mu \ln 2}}{\mu} \quad (4-5)$$

From the last two relations (4-4) and (4-5) and by using the mathematical inducement method, it is easily proved that,

$$t_{1/4} \phi 2.t_{1/2}$$

b) Broken nucleuses: The broken nucleuses N' are calculated from the difference $N' = N_0 - N$ or

$$N' = N_0(1 - e^{-\lambda_0 t + \frac{\mu}{2} t^2}) \quad (4-7)$$

The drawing of the relations $N = N(t)$ (4-3) and the $N' = N'(t)$ (4-7) is presented in Fig 5.

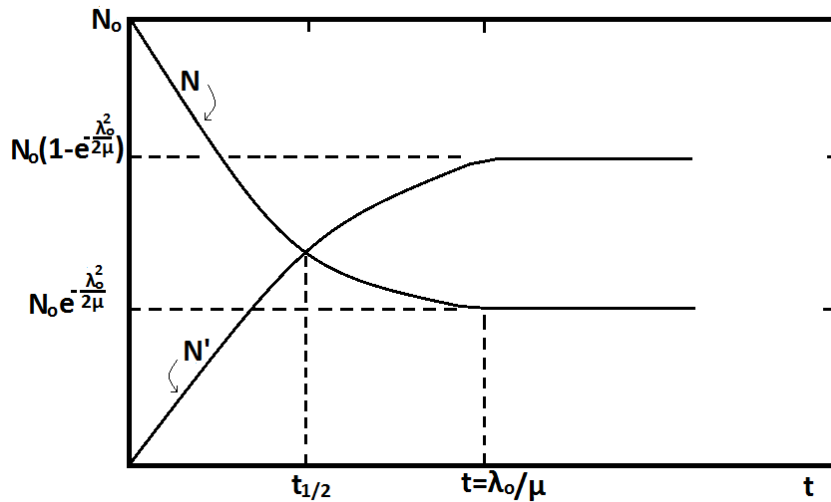


Fig.5. The $N = N(t)$ (relation 4-3) and $N' = N'(t)$ (relation 4-7) drawings are presented.

c) Conversion rate: The conversion rate $\frac{dN}{dt}$ is defined from the derivative of the relation (4-3). This derivative of the time is,

$$\frac{dN}{dt} = N_0(-\lambda_0 + \mu.t).e^{-\lambda_0.t + \frac{\mu}{2}.t^2} \quad \text{or} \quad \frac{dN}{dt} = -(\lambda_0 - \mu.t).N \quad (4-8)$$



d) The relation (4-3) study

The derivative of the relation (4-3) gives the conversion rate, which is,

$$\frac{dN}{dt} = N_0(-\lambda_0 + \mu t).e^{-\lambda_0 t + \frac{\mu}{2} t^2}$$

If it is put that $\frac{dN}{dt} = 0$, when $t = \lambda_0 / \mu$, which is the duration time of the phenomenon, the relation (4-3) has an extremity value as well. The kind of the extremity value is found from the relation $\left(\frac{d^2 N}{dt^2}\right)_{t=\lambda_0/\mu}$, and its' value from the relation $N(\lambda_0 / \mu)$.

For the second derivative it is concluded that,

$$\frac{d^2 N}{dt^2} = N_0 \mu e^{\frac{\mu}{2} t^2 - \lambda_0 t} + N_0 (\mu t - \lambda_0) (\mu t - \lambda_0) e^{\frac{\mu}{2} t^2 - \lambda_0 t} \quad \text{or}$$

$$\frac{d^2 N}{dt^2} = N_0 [\mu + (\mu t - \lambda_0)^2] e^{\frac{\mu}{2} t^2 - \lambda_0 t} \quad (4-9)$$

By setting $t = \lambda_0 / \mu$ the relation (4-9) gives,

$$\frac{d^2 N}{dt^2} (t = \lambda_0 / \mu) = N_0 [\mu + (\lambda_0 - \lambda_0)^2] e^{\frac{\mu}{2} \frac{\lambda_0^2}{\mu^2} - \lambda_0 \frac{\lambda_0}{\mu}} \quad \text{and, finally,}$$

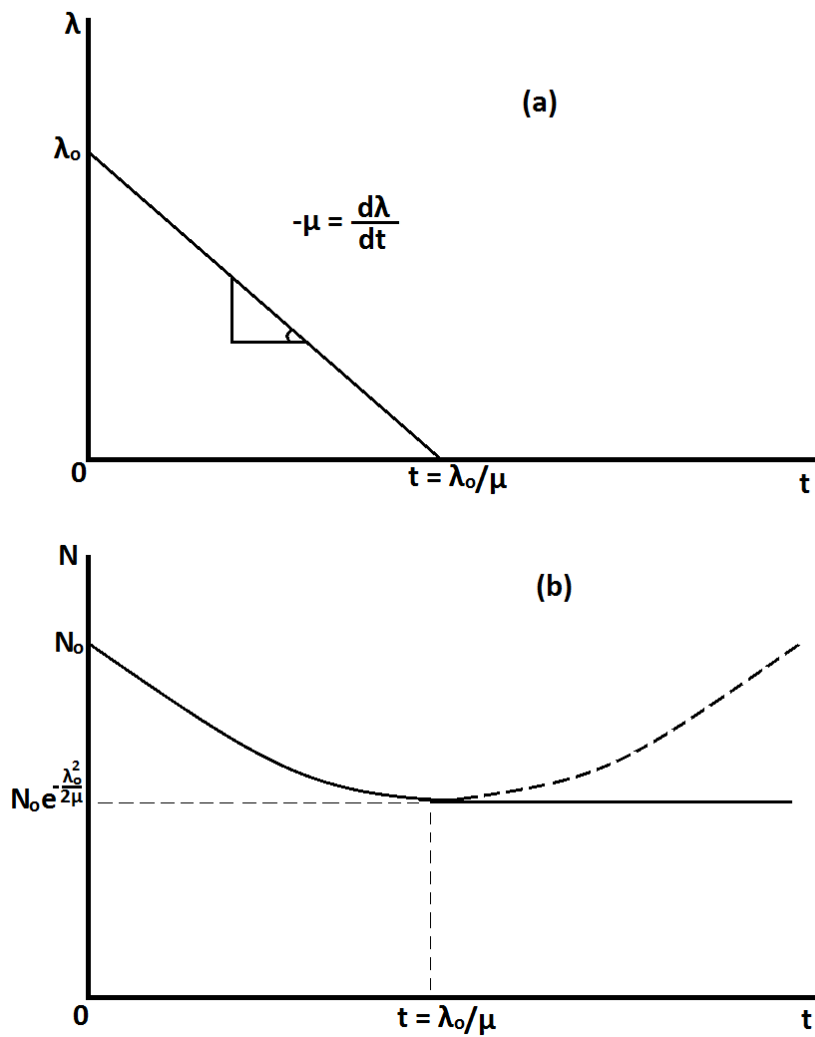
$$\frac{d^2 N}{dt^2} (t = \lambda_0 / \mu) = N_0 \cdot \mu \cdot e^{-\frac{\lambda_0^2}{2\mu}} \neq 0 \quad (4-10)$$

It is resulted from the relation (4-10) that the remaining unbroken nucleuses N have a minimum value, which is,



$$N(t = \lambda_0/\mu) = N_0 \cdot e^{-\frac{\lambda_0^2}{2\mu}} \quad (4-11)$$

In Fig.6 the change by the time of the factor $\lambda(t)$, the unbroken nuclei $N(t)$ and the conversion rate $\frac{dN}{dt}$ is presented.



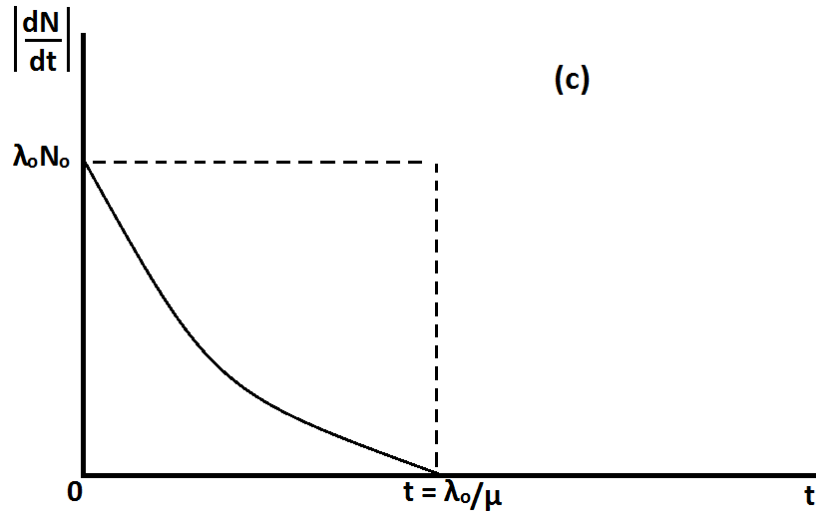


Fig. 6. The factor $\lambda(t)$, the unbroken nucleuses $N(t)$ and the conversion rate $\frac{dN}{dt}$ versus the time t is shown.

e) Comments: By considering the conversion factor λ not constant but changeable by the time, the following advantages arise from the solution of the problem:

1. The sub-doubling time $t_{1/2}$ does not remain constant, but it increases as the unbroken nucleuses diminish.

2. The initially available nucleuses N_0 are not broken in total, but there is a remaining quantity $N_0 \cdot e^{-\lambda_0^2 / 2\mu}$.

3. The solution of the problem and its' results are general and include the results of the solution with $\lambda = \text{cons} \tan t$, if it is set on the solution, where $\mu = 0$.

4. The suggested change of the factor λ is linear, which results to the solution being relatively simple, although slightly more complicated from what it is considered to be $\lambda = \text{cons} \tan t$.

5. In the problem the change factor μ appears, which is experimentally determinable.



II. Case

Now, let us consider that the constant λ is influenced by the remaining unbroken nucleuses N (and consequently, indirectly from the time t), in accordance with the relation,

$$\lambda = \lambda_0 + \mu N \quad (4-12)$$

Then the differential equation is written as following:

$$dN = -(\lambda_0 + \mu N).N.dt \quad \text{or} \quad \frac{dN}{(\lambda_0 + \mu N).N} = -dt$$

Integrating the last one, it is obtained that,

$$\int \frac{dN}{(\lambda_0 + \mu N).N} = -\int dt + C \quad (4-13)$$

The above relation (4-13) has the solution:

$$N = \frac{N_0 \cdot \Psi}{\Psi + \mu(1 - e^{-\lambda_0 t})} \cdot e^{-\lambda_0 t} \quad (4-14)$$

where is,

$$\Psi = \lambda_0 / N_0$$

The law's (4-14) study

a) sub-doubling time: By setting into the (4-14) $t = t_{1/2}$ when $N = \frac{N_0}{2}$, the

next equation is obtained, $2 = \frac{\Psi + \mu(1 - e^{-\lambda_0 t_{1/2}})}{\Psi} \cdot e^{\lambda_0 t_{1/2}}$

the solution of which gives the sub-doubling time,

$$t_{1/2} = \frac{1}{\lambda_0} \ln \frac{2\lambda_0 + \mu N_0}{\lambda_0 + \mu N_0} \quad (4-15)$$

If it is set that $t = t_{1/4}$ when $N = \frac{N_0}{4}$, in the same way as above the following result is obtained again



$$t_{1/4} = \frac{1}{\lambda_0} \ln \frac{4\lambda_0 + \mu N_0}{\lambda_0 + \mu N_0} \quad (4-16)$$

From the last two relations (4-15) and (4-16) and by using the mathematical inducement method it is easily proved that,

$$t_{1/4} \phi 2.t_{1/2}$$

b) Broken nucleuses: The broken nucleuses N' are found from the difference

$$N' = N_0 - N \text{ or}$$

$$N' = N_0 \left(1 - \frac{\Psi}{\Psi + \mu(1 - e^{-\lambda_0 t})} e^{-\lambda_0 t} \right) \quad (4-17)$$

c) Conversion rate: The conversion rate $\frac{dN}{dt}$ is calculated from the derivative of the relation (4-14). This derivative on the time is,

$$\frac{dN}{dt} = -\lambda_0^2 \cdot \frac{\Psi + \mu}{[\Psi - \mu(1 - e^{-\lambda_0 t})]^2} \cdot e^{-\lambda_0 t} \quad (4-18)$$

d) The study of the relation (4-14). The derivation on time of the relation (4-14) is the relation (4-18), which is not zero at any moment except the point $t = \infty$. The $N(t)$ does not have extreme values consequently.

5. Discussion and Conclusions

Although the experimental confirmation of the present study's usefulness is feeble now, the effort for the models' development must continue and a list of those models must be composed. This means that the 'Demokritos' team have to do theoretical future work on the same topic and experimental confirmation of the mathematic models.

In any case, the experimental measurements are very difficult to be carried out; firstly, because of the very little time required for the establishment of the steady state of the plasma waves, and, secondly, due to the great amount of time required for a perceptible physical nuclear decay.

If the thoughts were limited on the plasma waves rising only, the following syllogism may be useful for the understanding of the growth rate or damping role.

It is known that the plasma wave appearance becomes evident by the plasma potential fluctuation, in accordance with the relation,

$$V = V_0 \cdot e^{-j(\omega t - k \cdot \vec{r})} \quad (5-1)$$

When the circular frequency ω includes an imaginary part ω_i , the above wavy



expression becomes,

$$V = V_0 \cdot e^{-j(\omega + \omega_i)t} \cdot e^{+jk \cdot P} \text{ or } V = V_0 \cdot e^{\omega_i t} \cdot e^{-j(\omega t - k \cdot P)} \quad (5-2)$$

where ω is now the real part ω_r of the circular frequency.

It is evident from the relation (5-2), that the wave amplitude is described by the factor $V = V_0 \cdot e^{\omega_i t}$, is an exponentially changed quantity by the time ; furthermore, the sign of the ω_i defines the wave rising (growth), the wave extinguishing (damping), or the wave stability. The wave growth rate occurs by positive ω_i , the wave damping by negative value, whereas, the ω_i nihilism gives the wave stability. The imaginary part of the wave circular frequency has been actually calculated via the steady state hydrodynamic equations [14, 17]. On the other hand, the wave stability on the steady state demands ω_i to be near zero, whence it must be considered that the extinguishing factors press for $\omega_i \rightarrow 0$.

When a steady plasma wave appears, the final amplitude becomes constant by starting from one initial value V_{\oplus} , and completed at V_0 , at the time t_0 (transit).

There is always the transition time t_0 , which is the required time for the wave establishment. If the ω_i remains variable but is positive within this time, the inequality $e^{\omega_i t_0} \phi 1$, is valid and the wave amplitude increases at the value $V_0 \cdot e^{\omega_i t_0}$. By thinking, for example, that the ω_i is varied as $\omega_i = \omega_{i0} - \mu t$, the

t_0 is defined by the form $t_0 = \frac{\omega_{i0}}{\mu}$.

Figure 7 represents the wave amplitude establishment for different values of the ω_i

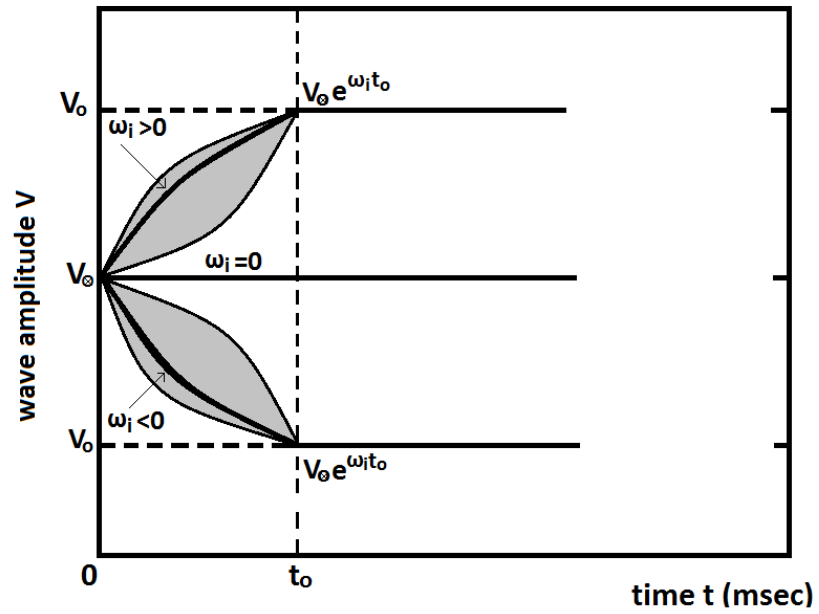


Fig. 7. The wave amplitude $V_0(t)$ versus the time t is presented for different values of the ω_i .

Appendix A



Solution of the differential equation (3-2)

The equation (3-2) is the simplest form of a differential equation with two changeable quantities (N, t) , which can be divided into its' two parts. So, the following is resulted,

$$\frac{dN}{N} = -\lambda dt \quad (A1)$$

The relation (A1) is integrated by parts in two ways: i) by defined integrals, if the changeable quantities' limits are known, or ii) by indefinite integrals, adding the integration constant C . If the second method is preferred, the following is resulted,

$$\int \frac{dN}{N} = -\lambda \int dt + C$$

$$\text{or} \quad \ln N = -\lambda t + C \quad (A2)$$

For the finding of the integration constant C , one values pair of the changeable quantities N and t is enough to be known. One known pair of values in this problem is the original conditions, where, for $t=0$, it is $N = N_0$. The replacement of the quantities t and N on the equation (A2) with the above known values, gives the value of the constant as,

$$C = \ln N_0 \quad (A3)$$

By the substitution on the relation (A2), the following relation is resulted,

$$\begin{aligned} \ln N &= -\lambda t + \ln N_0 \quad \text{or} \\ \ln \frac{N}{N_0} &= -\lambda t \quad (A4) \end{aligned}$$

And, finally, the known law of the radioactivity is obtained,

$$N = N_0 \cdot e^{-\lambda t} \quad (A5)$$

Appendix B

Solution of the differential equation (4-13)

By dividing the integral function of the first part of the (4-13) into smaller additives, two factors α and β are seeking for the following equality to be valid,



$$\frac{1}{(\lambda_0 + \mu.N).N} = \frac{\alpha}{N} + \frac{\beta}{\lambda_0 + \mu.N} \quad (\text{B1})$$

Finally, the two factors have the values, $\alpha = 1/\lambda_0$ and $\beta = -\mu/\lambda_0$, and the last relation is written,

$$\frac{1}{(\lambda_0 + \mu.N).N} = \frac{1}{\lambda_0 N} - \frac{\mu}{\lambda_0(\lambda_0 + \mu.N)} \quad (\text{B2})$$

With the substitution of the relation (B2) into the (B1) one, it is obtained that,

$$\int \frac{dN}{(\lambda_0 + \mu.N).N} = \frac{1}{\lambda_0} \int \frac{dN}{N} - \frac{\mu}{\lambda_0} \int \frac{dN}{\lambda_0 + \mu.N} = -\int dt + C$$

$$\text{or} \quad \ln N - \ln(\lambda_0 + \mu.N) = -\lambda_0 t + C' \quad (\text{B3})$$

The initial condition ($t = 0, N = N_0$) determines the integration constant C' , which takes the value, $C' = \ln N_0 - \ln(\lambda_0 + \mu.N_0)$

With substitution into the relation (B3) and by using suitable mathematical elaboration the following is obtained,

$$N = \frac{N_0 \cdot \Psi}{\Psi + \mu(1 - e^{-\lambda_0 t})} \cdot e^{-\lambda_0 t} \quad (\text{B4})$$

where is,

$$\Psi = \lambda_0 / N_0$$

References

1. L Landau and E. Lifschitz. *Mechanics*. Pergamon Press, Oxford, 2nd edition, 1969.
2. H. Goldstein, C. P. Poole Jr. and J. L. Safko "Classical Mechanics" 3rd edition, Addison Wesley, 2000.
3. K. S. Krane "Introductory Nuclear Physics" 3rd Edition, John Wiley & Sons, 1987.
4. N.D'Angelo . Phys. Fluids 4, 1054 (1961).
5. N.D'Angelo and R.W. Motley, Phys. Fluids 6, 423 (1963).
6. L. Spitzer, Physics of Fully Ionized Gases, 2nd edn. New York: John Wiley & Sons, 1967.
7. K Hendel H. W., Coppi B., Perkins F. and Politzer P.A. Phys. Rev. Lett. 18. 439 (1967).
8. N.Krall and A.Trivelpiece, Principles of Plasma Physics, McGraw-Hill Kogakusha,LTD, 1973.
9. D. Petrovic, J. Vranjes and S. Poedts, Physics Plasmas 12, 112103, 2005.
10. P.K. Shukla, G. Sorasio and L. Stenflo, Phys. Rev E, 66, 067401, 2002.



11. J.Vranjes, H. Saleem and S. Poedts, *phys.rev. E* 69, 056404, 2004.
12. C. Schröder, O. Grulke and T. Klinger, *Physics Plasmas* 12, 042103, 2005.
13. A. Mikhailovskii, et al, *Physics Plasmas*, 14, 1121108, 2007.
14. A. Anastassiades, and C.L. Xaplanteris, *J. Phys.Soc. of Jpn* 52, 492, 1983
15. C.L. Xaplanteris, *Astrophys. Space Science* 139, 233-242, 1987.
16. J. Wesson, *Tokamaks*, 2nd edn.Oxford: Clarendon Press, 1997.
17. C.L. Xaplanteris, *J. Plasma Physics*, Vol. 75, part 3 pp 395-406, 2009.
18. C.L. Xaplanteris et al, *J. Plasma Physics*, Vol. 78, part 2 pp165-174, 2012.
19. C.L. Xaplanteris and E. Filippaki *CHAOS 2010*, International Conference Proceedings Chania, 2010.
20. T. Klinger, in *Handbook of Chaos Control*, edited by H.G.Schuster (Wiley VCH, Weinheim, 1998) pp 513-562.
21. D.Block et al, *Phys. Rev. E* 63, 056401, 2001.

Captions

Fig. 1. The photo of the experimental device is shown in (a), whereas the plasma cavity with probes is presented in (b).

Fig. 2. The wave form is shown in (a), whereas the wave spectra are presented in (b) and (c) for rf-drift and collisional wave, respectively.

Fig. 3. The $N = N(t)$ and $N' = N'(t)$ drawing is presented.

Fig. 4. The conversion rate $\frac{dN}{dt}$ versus the time t is shown.

Fig.5. The $N = N(t)$ (relation 4-3) and $N' = N'(t)$ (relation 4-7) drawings are presented.

Fig. 6. The factor $\lambda(t)$, the unbroken nucleuses $N(t)$ and the conversion rate $\frac{dN}{dt}$ versus the time t is shown.

Fig. 7. The wave amplitude $V_0(t)$ versus the time t , for different values of the ω_i , is presented.



Maxwell-Bloch Equations, a Lorenz Type Chaotic System in Lagrangian Form

H. Ahmet Yıldırım¹ E.Eray Akkaya² Avadis S. Hacınlıyan^{2,3} Gökhan Şahin³

¹ Sakarya University ,Department of Physics, Adapazarı, Turkey
(E-mail: yildirim.ha@gmail.com)

² Yeditepe University,Department of Physics,Istanbul, Turkey
(E-mail: eeakkaya@gmail.com)

³ Yeditepe University,Department of Information Systems and Technologies,
Istanbul,Turkey

Abstract. Maxwell-Bloch equations, also known as Lorenz-Haken equations, represent the laser working mechanism and can be derived from the classical equations for the electromagnetic field and quantum mechanical equations for the particles under special conditions. For special conditions on the parameters, it is related to the Lorenz model and behave similarly. Maxwell-Bloch equations exhibit various types of routes to chaos for different parameter ranges. In this study, a constrained lagrangian form that lead to the Maxwell-Bloch equations has been obtained from the equivalent treatment of the Lorenz model. This allows us to analyze the long term behaviour of its attractor.

Keywords: Maxwell-Bloch equations,constrained lagrangian form, attractor.

1 Introduction

The Bloch model is known to be a linear model so that chaotic behavior is not ordinarily expected. However, the trajectories fill the phase space for strong coupling of the AC field. Adding nonlinearity to the model can be done by coupling the Bloch system to the Maxwell equations. So, the resulting model called Maxwell-Bloch equations.

The chaotic behavior observed in laser light dynamics can be modeled by the Maxwell-Bloch equations in terms of their parameters [2] [5].

$$\begin{aligned}\dot{\mathbf{E}} &= -k\mathbf{E} + g\mathbf{P} \\ \dot{\mathbf{P}} &= -\gamma_{\perp}\mathbf{P} + g\mathbf{E}\mathbf{\Delta} \\ \dot{\mathbf{\Delta}} &= -\gamma_{\parallel}(\mathbf{\Delta} - \mathbf{\Delta}_0) - 4g\mathbf{P}\mathbf{E}\end{aligned}\quad (1)$$

Regions of chaotic behavior can be studied where \mathbf{E} is the electric field, \mathbf{P} is the polarization and $\mathbf{\Delta}$ is the population inversion. Also, $\mathbf{\Delta}_0$ is the population inversion which would be established by the pump mechanism and the remaining parameters, $\gamma_{\perp}, \gamma_{\parallel}, k$ are loss rates of the fields and g is the coupling constant.

Actually, these equations can be formally related to the Lorenz equations found by Edward Lorenz in an unrelated context. The original Lorenz equations

are

$$\begin{aligned} x' &= -\sigma x + \sigma y \\ y' &= Rx - y - xz \\ z' &= -Bz + xy \end{aligned} \quad (2)$$

Chaos can be observed in many regions, such as $\sigma=10, B=8/3, R=28$ and these can be transformed into corresponding regions for the Maxwell Bloch system.

The Lorenz and Maxwell-Bloch systems are not in Hamiltonian form. However, just as in the case of the Lorenz model, [1] it can be reexpressed as a constrained, velocity dependent Lagrangian system.

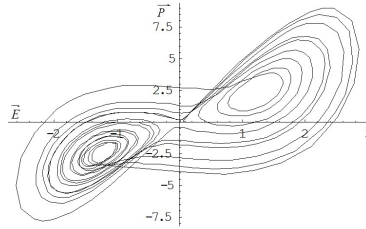


Fig. 1. The basic operating point shows "Throw and catch" chaotic behavior similar to Lorenz system.

As seen in Figure 1, Lorenz type throw and catch mechanism at given parameters where $k=11.75, g=6.06, g_{\perp}=2.66, g_{\parallel}=2.75, \Delta_0=28$.

2 The Maxwell-Bloch system in constrained Lagrangian form

The Lorenz system can be written in Lagrangian form and can be made mechanical analog inspite of it is thermodynamical system. The Maxwell-Bloch equations have more parameters than the Lorenz system but this system can be transformed into the Lorenz system, if $x=\mathbf{E}, y=g\mathbf{P}/k$ and $z=\Delta_0-\Delta$ changes are made. Then, following parametric identifications also need to be made $k=\sigma, \gamma_{\perp}=g^2/k, R=g^2\Delta_0/k, \gamma_{\parallel}=B$.

Consider a one-particle system with a velocity dependent Lagrangian of the form.

$$L = \frac{1}{2m}(m\mathbf{v} - \lambda\mathbf{A})^2 = \frac{1}{2}m\mathbf{v}^2 - \lambda\mathbf{v} \cdot \mathbf{A} + \frac{\lambda^2}{2m}\mathbf{A}^2 \quad (3)$$

\mathbf{A} is vector potential and $V=(\lambda^2\mathbf{A}^2)/2m$ is scalar potential. The explicit form of our nonlinear potential can be written;

$$\frac{\lambda}{m}\mathbf{A}(\mathbf{E}, \frac{g\mathbf{P}}{k}, (\Delta_0 - \Delta)) = \frac{1}{\tau} \begin{bmatrix} k(-\mathbf{E} + \frac{g\mathbf{P}}{k}) \\ \mathbf{E}(\frac{g^2\Delta_0}{k} - (\Delta_0 - \Delta)) \\ \frac{g(\mathbf{E} \cdot \mathbf{P})}{k} - \gamma_{\parallel}(\Delta_0 - \Delta) \end{bmatrix} \quad (4)$$



We now proceed to determine the constrained form;

$$\frac{d}{dt} \frac{\partial L}{\partial \dot{x}} - \frac{\partial L}{\partial x} = 0 \quad (5)$$

Using (3) constrained form can be written and equation of motion can be observed

3 Equations of motion and regions of chaotic behavior

After determining constrained form, equation of motion can be written as;

$$m\dot{v} = \frac{\dot{p}}{m} + \frac{\lambda}{m} \dot{A} \quad (6)$$

The generalized butterfly equation of motion is given for $p=0$, which leads to chaotic behavior for certain choices of parameters in Figure 1

4 Result and conclusion

In this paper, Maxwell-Bloch equations which is related to Lorenz type systems was transformed into Lagrangian form and equations of motions are constructed in this formalism. The equations of motion can be used to analyze circumferences under which this system is going to chaos.

On the other hand, Hamiltonian systems conserve the phase space volume so that a butterfly type attractor can not be directly expressed in this notation. The advantage of using the present formalism enables one to try the wide variety of mechanisms available for constructing approximate solutions of Hamiltonian systems.

References

- 1.J.Micheal Finn.Classical Mechanics. Infinity Science press LLC 2008
- 2.A.S.Hacinliyan, I.Kusbeyzi, O.O. Aybar. Approximate solutions of Maxwell Bloch equations and possible Lotka Voltera type behavior. Nonlinear Dyn (2010) 62:17-26
- 3.F.T.Arecchi.Generalized multistability and chaos in quantum optics. Phil.Trans.R.Soc.Land.A313,307-310(1984)
- 4.H.Haken.Laser Light Dynamics.Volume 2.1985
- 5.Hacinliyan, A. S., Akkaya, E. E., Kusbeyzi, I., Aybar, O. O. Maxwell-Bloch Equations as Predator-Prey System 2nd Chaotic Modeling and Simulation International Conference , Chania, Crete (2009).





Behavioral Modeling of Microtweezer Integrated with Capacitive Touch Sensor

Nayyer Abbas Zaidi^{#1}, Shafaat A. Bazaz^{#2}, Nisar Ahmed^{#3}, Rahim Umar^{#4}

^{#1#3} Faculty of Electronic Engineering, Ghulam Ishaq Khan Institute of Engineering Sciences and Technology, Pakistan.

^{#2} Department of Computer Science, Centre for Advance Studies in Engineering (CASE), 19 Ataturk Avenue, G-5/1, Islamabad, Pakistan.

^{#4} Faculty of Engineering Sciences, Ghulam Ishaq Khan Institute of Engineering Sciences and Technology, Pakistan.

E-mail: nayyergiki@gmail.com

Abstract: This paper presents behavioral modeling of an electrostatic microtweezer integrated with capacitive touch sensor. The design of the microtweezer is optimized using standard SOIMUMPS process. Microtweezer performance is forecasted using system level simulation. The results of the system level simulation obtained from behavioral modeling shows total displacement of 7.039 μm and 37.5 μm is obtained at central beam and tweezer jaw respectively, when a voltage of 55 V is applied. Behavioural modeling of the sensor part of microtweezer is performed and system level simulation results shows that minimum and maximum capacitance is 0.45 pF and 0.65 pF respectively. Pull-in voltage analysis through behavioral modeling shows that actuator works with maximum performance, at applied voltage of 55 V. The results of displacement, sense capacitance and pull-in voltage analysis are nearly identical to analytical results when compared.

Keywords: MEMS, Behavioural model, SOIMUMPS, System level simulation, Microtweezer..

1. Introduction

In the last ten years, new customized as well as standard micromachining processes have been emerged, making it possible to develop complex type of Microelectromechanical systems (MEMS). Due to such innovations, MEMS have found its place in many practical applications where one of the areas is micromanipulation of micro-objects. Micromanipulation has become important in the applications, like microassembly, to assemble parts of micron size that are generally fabricated on a substrate. One such micromanipulator was developed in 2004, that uses MEMS microtweezer as an end-effector attached to the robotic workstation [1]. The microtweezer performs the task of grasping the micropart and then the robotic arm performs the manipulation operation. A passive microtweezer is designed to grasp the micro-object with a specific size. Another important application of micromanipulator is in the area of biological and biomedical research [2]. Design of three degree-of-freedom Micromanipulator based on MEMS heat actuators have been developed that can be used to probe or position biological object [3]. Another three degree-of-freedom micromanipulator based on comb drive actuators were developed for precise positioning of probing instruments like Atomic Force Microscopy (AFM), or tools to provide energy beam like e-beam, X-ray etc. [4]. These



systems cannot safely grasp the micro-objects. Moreover, all such systems do not provide integrated sensing mechanism that makes their use to limited applications.

Many MEMS based microtweezers have been proposed in recent years for different micromanipulation applications [2, 5, 6]. Most of these microtweezers were based on electrostatic or piezoelectric actuation principle. These microtweezers comprised of the jaws mechanism with the dimensions of the size of the cell that are generally of diameter of tens of microns. Moreover, these jaws should be able to grasp the cells with different and irregular shapes. In order to grasp more precisely, not only the jaw mechanism but also the integration of touch sensor, makes microtweezer design more effective. As this addition excludes the fracture of microobject due to the uncontrolled excessive force, which is not found in to the microtweezers design proposed by Kim and Volland [5, 6]. Finally, batch production of such system requires the use of standard MEMS based micromachining technology thus making it cost effective, have good repeatability and also reliability from the point of view of the fabrication and production of the microstructures.

To fabricate microtweezer, Modeling and Simulation plays vital role in predicting the dynamics of the device. These analytical and simulation results minimizes iterative fabrication that is costly and time consuming. Previously microtweezers were simulated using Finite Element Methods [2, 3, 19, 20]. Beside the fact that, these methods gave high accurate solution but a compromise is made in terms of times, memory requirement and the restriction of integration of electronics with the device, bounded the user to limited type of simulations.

On the other hand, Behavioral Modeling and system level simulation tool performs MEMS analysis efficiently both in terms of time, memory requirement and integration of electronics with the MEMS makes Microsystem to be analyzed in a single simulation environment. In mid-nineties, simulation tools such as SUGAR and NODAS that comprise basic MEMS elements library were developed at UC Berkeley and Carnegie Mellon University respectively, in which Matlab and Cadence are used as system level simulator [7, 8, 9]. Now days, very specialized MEMS modeling and simulation such as CoventorWare Architect [17] with large MEMS library is available to simulate MEMS devices. Various MEMS devices including Gas Sensors [10], Accelerometers [11] and Gyroscope [12] were first simulated in CoventorWare Architect and then they are fabricated.

This paper presents the analytical analysis of microtweezer with its novel behavioral modeling and simulation of both the actuator and the sensor part. In Section II, SOIMUMPs process is explained, in which sample model of the microtweezer is designed. In section III, design details of microtweezer are explained. The theory of operation of microtweezer is explained in section IV. The parameters related to design such as displacement, change in capacitance and pull in voltage are discussed in section V. The behavioral modeling is illuminated in section VI and then results and discussion in section VII. Finally section VIII illustrates conclusion.

2. SOI-MUMPS Process

The standard SOI-MUMPS [13] process is selected for the development of sample model of microtweezer. The reason for choosing this process is, it is easily available with reliable design instructions. SOIMUMPs process offers, 2 μm minimum feature size and spacing between structure layers. This can be used to construct a high capacitance com drive. In order to grasp a microobject through microtweezer the grasping area should be equal or larger then the thickness of the micro-object. This process proposes quite high grasping area of 25 μm , which is enough to grasp a microobject. The fabrication sequence of the microtweezer using SOIMUMPs process is shown in Fig. 1.

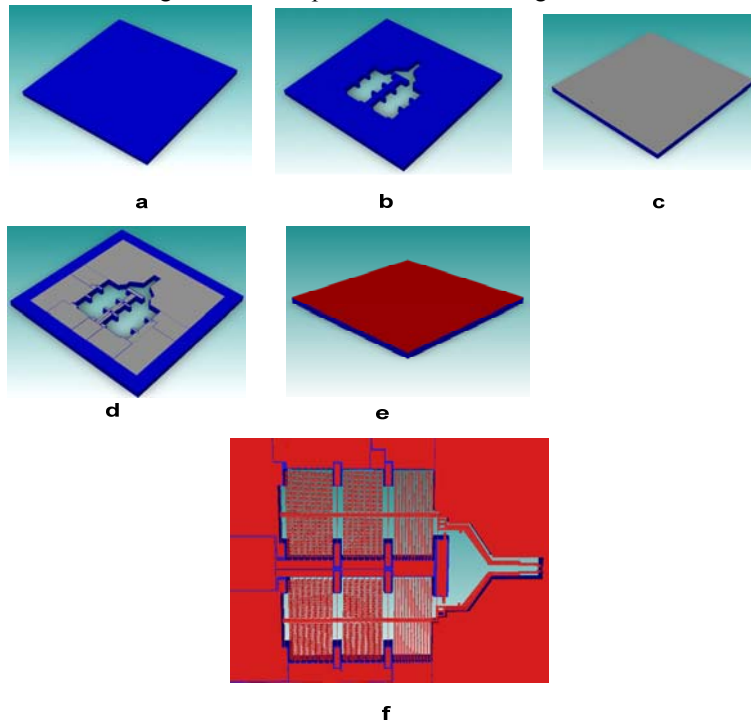


Fig. 1: Process flow for the fabrication of microtweezer using SOI-MUMPS in CoventorWare. (a) Silicon-on-insulator (SOI) wafer as starting substrate (b) DRIE silicon etch is used to etch substrate completely (c) Thermal oxidation is done to built insulator layer on substrate (d) DRIE etch completely etch the substrate and oxide layer (e) Single crystal silicon layer is deposited having thickness of 25 μm (f) Deep reactive ion etch is used to etch the silicon to the oxide layer and after that finally DRIE is used to etch down to the oxide layer.

3. Microtweezer design

The designed microtweezer 2-D layout, developed in MEMSPro is shown in Fig. 2. It consists of three parts a) actuator b) sensor and c) jaws.

3.1 Actuator Design

The actuator part of the microtweezer is comprised of comb drive mechanism which is Lateral. This technique consists of interdigitated finger, in which fixed and moveable parts are called stator and rotor combs. The length of the fingers is set to $50\ \mu\text{m}$ and overlap length is set to $30\ \mu\text{m}$. The spacing between the two fingers is designed to $3\ \mu\text{m}$ to avoid the collapse of the fingers as shown in Fig. 3. The three clamped-clamped beams are used to suspend the structure and moves back the central mass movement to its free position.

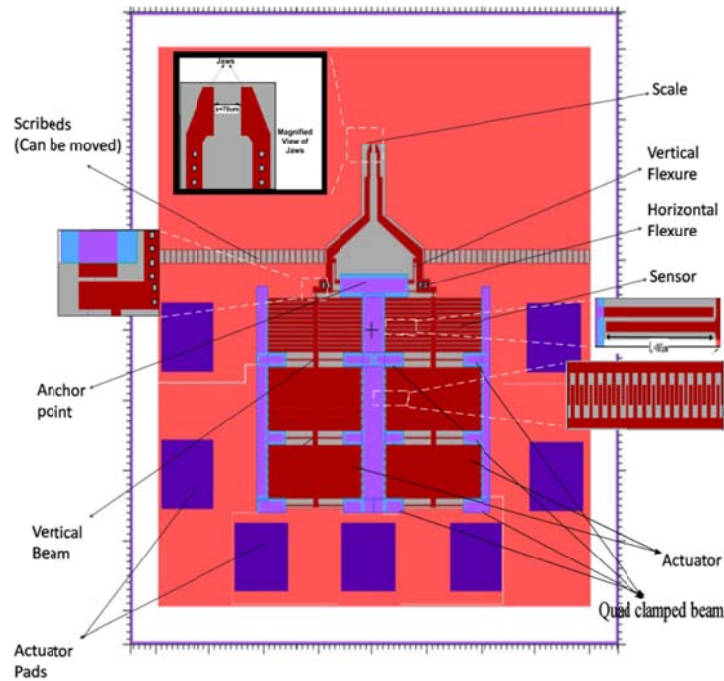


Fig. 2: Complete microtweezer design with integrated touch sensor.

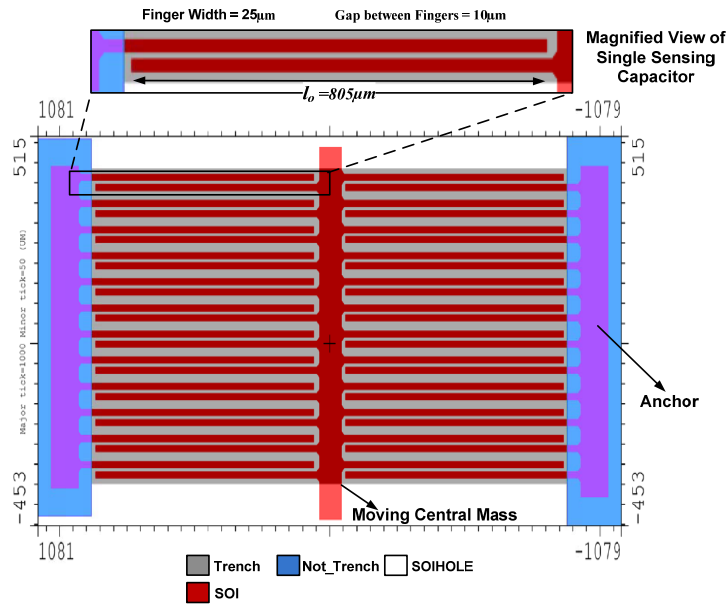


Fig. 4: Complete sensor combs design.

3.3 Jaw Design

A novel tweezer arm and jaw with the compliant structure has been designed as shown in Fig. 5 for grasping the micro-sized objects. The design includes a horizontal and a vertical beam to produce elastic restoring force in horizontal and vertical direction simultaneously. The vertical beam additionally provides support against the out of plane movement of the tweezer arms. The structure is designed in such a way that it will maintain an angle of 90^0 between the tweezer arm and the horizontal beam. Additionally, the jaw moves a little distance forward along y -axis during grasping due to direction of applied force. This action ensures that object completely comes between the jaws while grasping. Two stoppers have been placed near the point of application of force in order to stop any extra movement of central beam after the object has been fully grasped. In the proposed tweezer arm design, the vertical displacement produced in central beam is amplified by constant times the displacement produced at the tips of tweezer jaws.

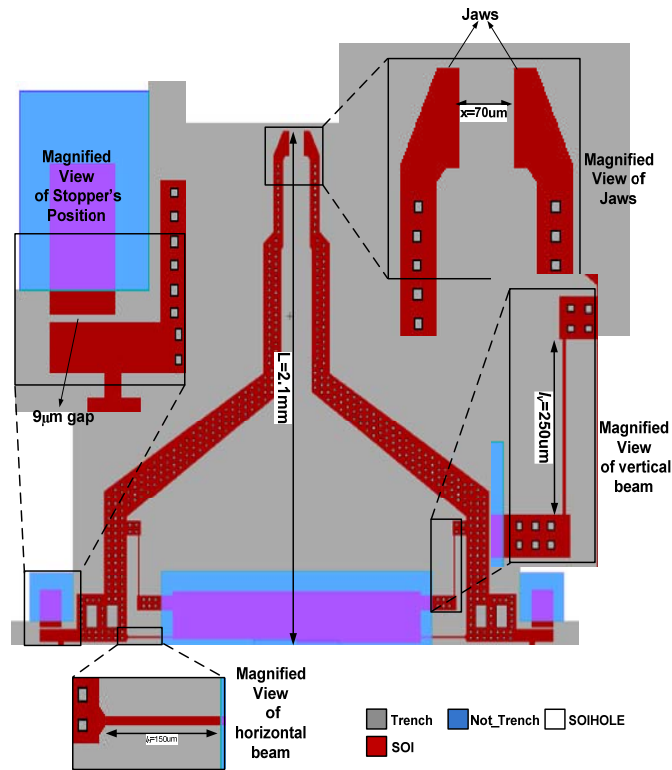


Fig. 5: Complete design of tweezer arms.

4. Theory of operation

The proposed microtweezer design uses novel dual electrostatic actuation system i.e. there are two separate electrostatic actuators for the simultaneous movement of two jaws. Each actuator consists of a set of stator combs interdigitated with a set of rotor combs. DC voltage is applied to both the actuators simultaneously such that the stator combs are at positive potential with respect to rotor combs. Hence electrostatic force is produced which pulls the two comb drives. This electrostatic attraction produces elastic restoring force in the quad clamped flexure springs which is equal in magnitude to the applied force. The central beam of each actuator is attached to the respective tweezer arm. Each tweezer arm is further supported by two cantilever beams namely horizontal and vertical beam. Hence total elastic restoring force is a combination of force due to the quad-clamped flexure springs and the two cantilever beams. Any vertical movement of the central beam in upward direction is amplified at the tweezer jaws due to the integrated action of the tweezer arm and the beam



system. One transverse comb drive based capacitive touch sensor is included along each of the two central beams in between the tweezer arm and actuator explain in Fig. 2. The overlap length varies in the sensor combs result in the change in capacitance. When there is no capacitance change it indicates that the object has been gripped and thus to avoid any damage to the object no further actuation voltage is applied.

5. Design parameters

5.1 Displacement of central beam

An applied voltage to actuator generates electrostatic force between the comb drives. This electrostatic force is conveyed to the jaw via quad-clamped, horizontal and vertical flexures. The spring constant of flexures added because of parallel connection [15].

$$K = k_h + k_f + k_v \quad (1)$$

$$K = Et \left(\frac{8bf^3}{l_f^3} + \frac{bh^3}{4lh^3} + \frac{bv^3}{4lv^3} \right) \quad (2)$$

Using Hook's law force in terms of displacement is given as:

$$F = Et \left(\frac{8bf^3}{l_f^3} + \frac{bh^3}{4lh^3} + \frac{bv^3}{4lv^3} \right) \times y \quad (3)$$

The electrostatic F produced by actuator is given as:

$$F = \frac{N.n}{2} \epsilon \frac{tV^2}{d} \quad (4)$$

Where nN is the entire number of comb drives connected in parallel, t is the thickness, d is the gap between the comb drives and V is the applied voltage. Eq. (3) and (4) are equated, the central mass displacement is given as:

$$y = \frac{\frac{N.n}{2} \epsilon_0 \frac{tV^2}{d}}{Et \left(\frac{8bf^3}{l_f^3} + \frac{bh^3}{4lh^3} + \frac{bv^3}{4lv^3} \right)} \quad (5)$$

5.2 Displacement of single Jaw

The horizontal flexure and the length of the jaw are responsible for the amplification at the jaws. Thus central beam movement is amplified by L/L_Q . The total movement at single jaw is calculated as:



$$X = \frac{L}{l_Q} \times \frac{\frac{N.n}{2} \frac{\epsilon t V^2}{d}}{Et \left(\frac{8b f^3}{l_f^3} + \frac{bh^3}{4lh^3} + \frac{bv^3}{4lv^3} \right)} \quad (6)$$

Where $L=2.1mm$ is the length of the microtweezer jaws and $l_Q = 150 \mu m$ horizontal flexure length as shown in Fig. 5.

5.3 Sensor

In the sensor, the capacitance increases and decreases by same proportion on the two sides of the comb drives. These capacitances are given as:

$$\left. \begin{aligned} C_{s1} &= Nn \frac{\epsilon(t \times l)}{d_0 + \left(\frac{L}{l_Q}\right)X} + C_{fringe} \\ C_{s2} &= Nn \frac{\epsilon(t \times l)}{d_0 - \left(\frac{L}{l_Q}\right)X} + C_{fringe} \end{aligned} \right\} \quad (7)$$

where d_0 is the initial gap between the transverse combs, C_{s1} is the decreased capacitance and C_{s2} is the increased capacitance in the transverse comb sensor corresponding to the gap change $y = \left(\frac{L}{l_Q}\right)X$ and C_{fringe} is the capacitance produced due to the fringe fields.

5.4 Pull-in Voltage

In the proposed microtweezer design, the comb drive actuator one of which, typically called as rotor finger, is suspended and connected to the compliant springs while other, usually called as stator finger, is fixed. The pull in voltage is defined as the voltage at which the two fingers come in touch with each other. The pull-in voltage $V_{pull-in}$ is given [16]:

$$V_{pull-in}^2 = \frac{d^2 k_y}{2\epsilon_0 b n} \sqrt{2 \frac{k_x}{k_y} + \frac{y_0^2}{d^2}} - \frac{y_0}{d} \quad (8)$$

Where d is the gap spacing between the fingers, ϵ_0 is the dielectric constant in air, $\frac{k_x}{k_y}$ is the spring stiffness ratio.

6. Behavioural model development

The reduced order equations are used to perform behavioral modeling and simulation. In this modeling technique complete model is simulated rather than simulating number of finite components that constitute the model. Thus the efficiency in time is achieved in this method rather than finite element analysis. The components that are used to develop behavioral model are presents in its libraries. The core code inside these libraries tells the individual components how to behave when exposed to stimuli in terms of electrical and mechanical [17]. The main components that develop behavioral model design are Beams, Comb drives and rigid plates. Fig. 6 shows the behavioral schematic of the

actuator, sensor and jaw. Mechanical bus is used for connecting the components. This bus consists of array of six wires in which three are translational and other rotational. These wires contain information about rotational and translational motion of the mechanical components in space. The mechanical bus connector is connected at the tip of the jaw and with central beam in order to find their displacement. The 3-D model shown in Fig. 7 is generated after net listing and importing the schematic design in to scene 3D of the architect. In the 3D model half portion of the microtweezer is modeled because of geometrical evenness.

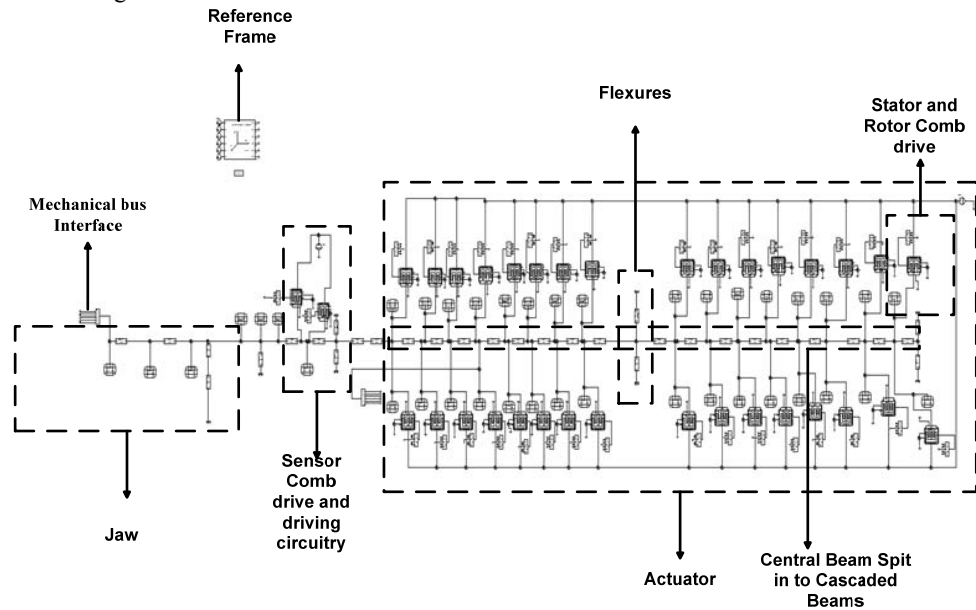


Fig. 6: Behavioural schematic of the microtweezer.

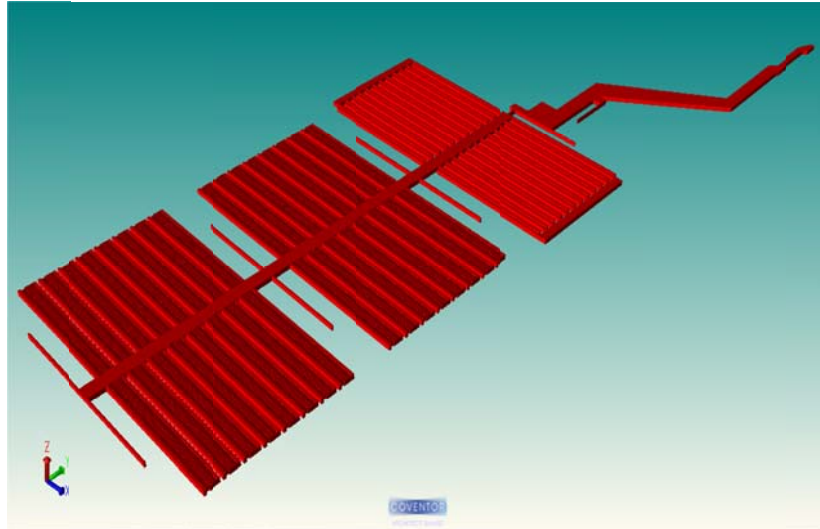


Fig. 7: Microtweezer 3-D model in CoventorWare architect.

7. Result & discussion

The graph shown in Fig. 8 obtained analytically (by Eq. (5)) for a displacement of central beam when a voltage is sweep form 0 - 55 V. At 50 V the displacement is found to be $6.3 \mu\text{m}$. The behavioral model simulation, between voltage and central beam displacement is shown in Fig. 9. Both the results are approximately same as analytically predicted. The simulation results are shown in Fig. 10, the color of the contours plot shows the displacement of every component of the microtweezer in y -axis direction. It is observed that stator combs are stationary while rotor combs moves the central beam in y -axis.

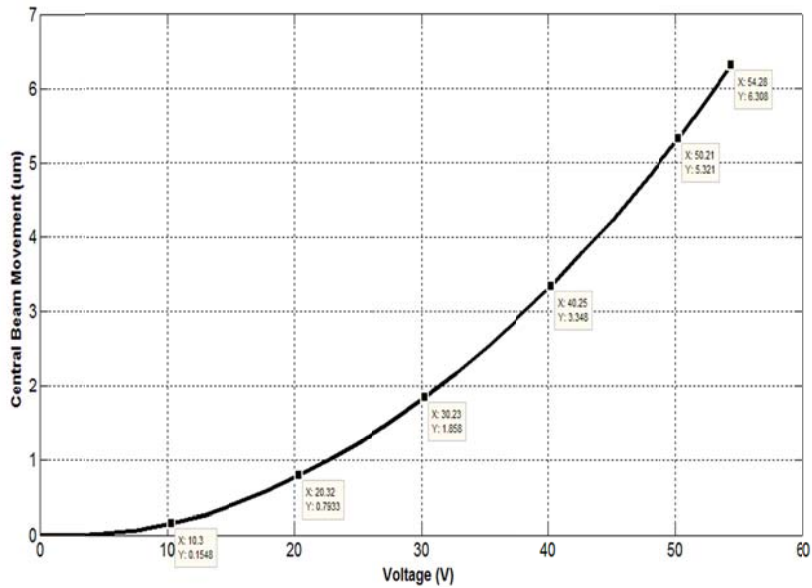


Fig. 8: Analytical relation between voltage (V) and central beam displacement (μm).

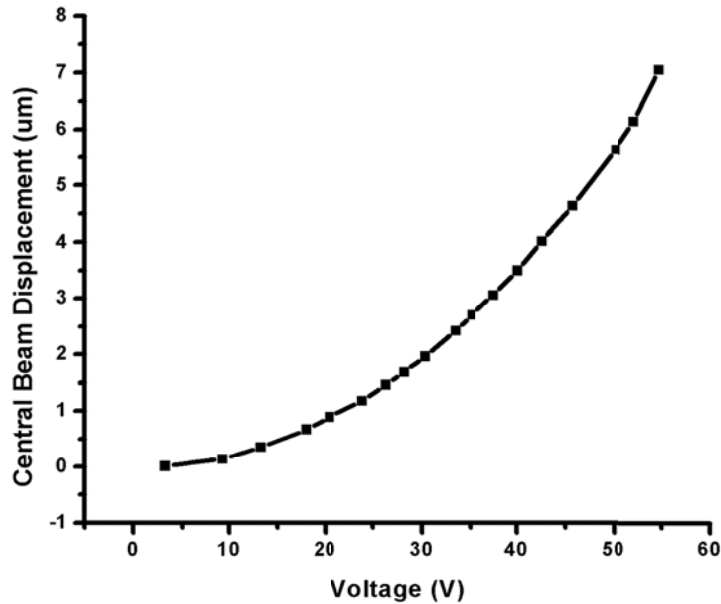


Fig. 9: Graph between voltage (V) and central beam displacement (μm) acquired by behavioral modeling.

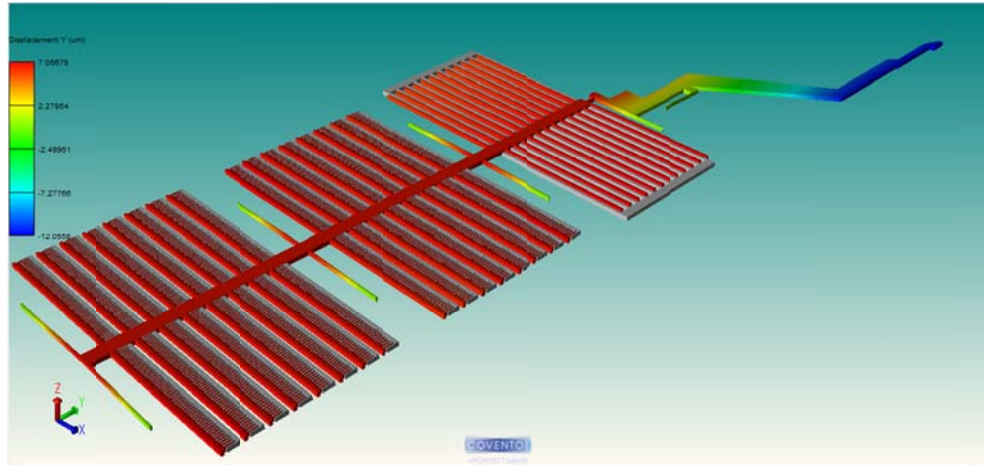


Fig.10: Displacement visualization in a color contours for microtweezer.

The graph shown in Fig. 11 is the analytically calculated result that is obtained from Eq. 6, between voltage (V) and the jaw displacement (μm). The maximum displacement obtained is at the tip of the jaw which is $34.3 \mu\text{m}$ at 55 V . The jaw displacement obtained through system level simulation is $38 \mu\text{m}$ at 55 V which is nearly same as analytically calculated. From analytically and simulation outcomes show that the microtweezer can easily grasp microobjects in diameter from $0 - 70 \mu\text{m}$ when it's both jaws are in motion. This can avoid the fabrication of 2 stage jaws [18].

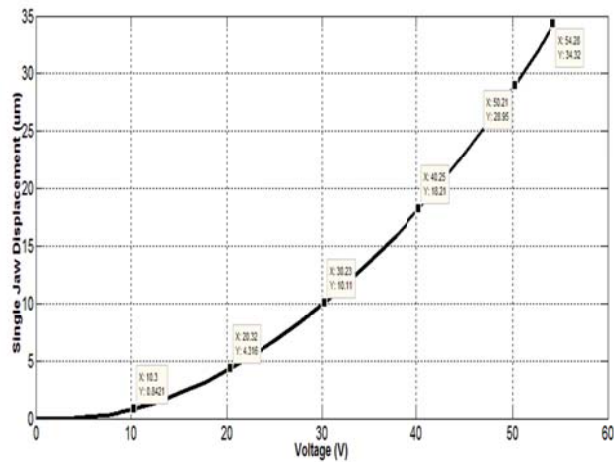


Fig. 11: Analytical relationship between voltage (V) and jaw displacement (μm).

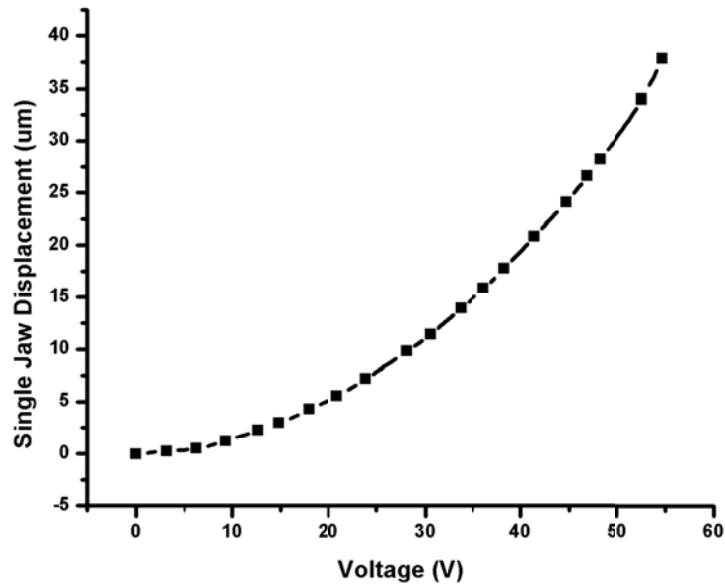


Fig. 12: Graph between voltage (V) and jaw displacement (μm) obtained by behavioral modeling.

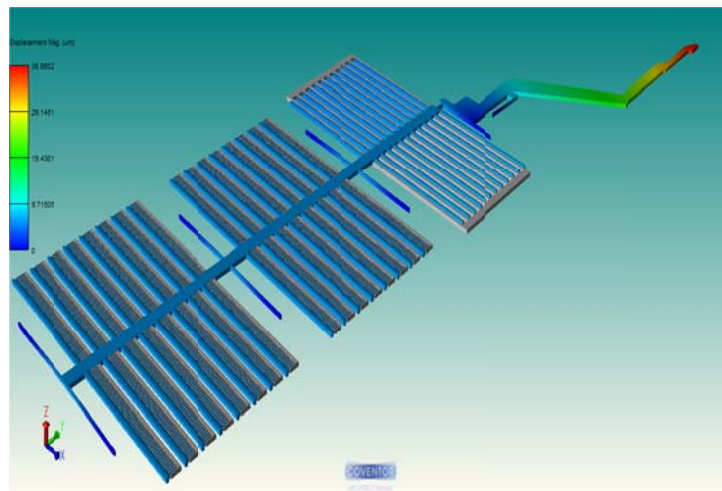


Fig. 13: Displacement visualization in a color contours for microtweezer.

The graph shown in Fig. 14 and Fig. 15 shows the change in capacitance vs displacement of transverse comb drive calculated both analytically by Eq. (7),



and over behavioral modeling respectively. From the result it is clear the capacitance on one side of the transverse C_{S1} increases while the capacitance on the other end C_{S2} decreases. The behavioral model result shows the same capacitance increase and decrease. These results are approximately the same. The integration of the capacitive touch sensor informs that the range of capacitance (0.45 fF - 0.65 fF) that is obtained in gripping microobject. This range of capacitance is significant in programming the capacitive read out circuitry MS3110 [14].

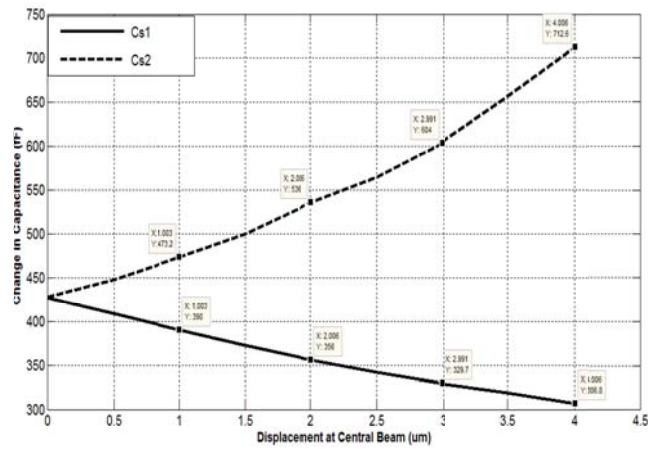


Fig. 14: Analytical relationship between displacement at central beam and change in capacitance (fF).

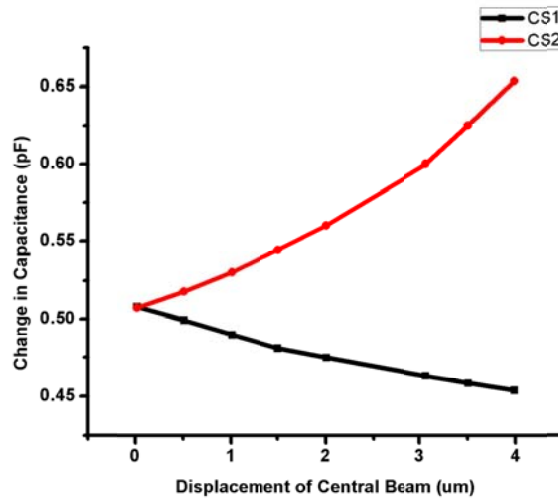




Fig. 15: Graph between displacement at central beam and change in capacitance (fF) obtained by behavioral modeling.

The pull in voltage analysis is carried out to predict the maximum operating voltage of the actuator of the microtweezer. Analytically the maximum pull in voltage calculated through Eq. 8 is 55 V while through system level simulation 58 V is obtained. These results are approximately same.

The above defined parameters are summarized in Table:1, which reveals that the possibility of developing a prosperous device are higher because of the fact that the analytical and behavioral models results are nearly equal.

Parameter	Analytical results		Behavioral model results	
Maximum Central Beam moment (μm)	6.3		7.039	
Maximum Jaw Displacement (μm)	34.3		38	
Capacitance (fF)	C_{s1}	306fF	C_{s1}	0.45pF
	C_{s2}	712fF	C_{s2}	0.65pF
Pull-in voltage (V)	0 - 55		0 - 58	

Table 1: Comparison between analytical and behavioral model results.

8. Conclusions

A MEMS based microtweezer integrated with capacitive touch sensor has been designed using SOI-MUMPS process. The layout model of the device is developed in MEMSPro CAD tool environment. The designed microtweezer gives analytically central beam displacement of $6.3 \mu\text{m}$, single jaw displacement of $7.03 \mu\text{m}$, capacitance change of $C_{s1}=306 \text{ fF}$ and $C_{s2}=712 \text{ fF}$ and result of pull-in voltage is 55 V.

Extensive simulation through behavioral modeling using the architect module of the CoventorWare verifies the maximum central beam movement of $7.03 \mu\text{m}$ and jaw displacement of $38 \mu\text{m}$ with change in capacitance of 0.45 pF to 0.65 pF . Pull-in voltage analysis shows that at 58 V, actuator gives maximum performance. The use of analytical and simulation approach avoids iterative fabrication that is expensive. The microtweezer is now ready to send for fabrication with higher chances of its success.

References

- [1] N. Dechev, W.L. Cleghorn, and J.K. Mills, "Microassembly of 3D microstructures using a compliant, passive microgripper", *Journal of Microelectromechanical Systems*, Vol. 13, No. 2, pp. 176-189, 2004.



- [2] T. Chen, L. Chen, and L. Sun, "Piezoelectrically driven silicon microgripper integrated with sidewall piezoresistive sensor", *Proceedings of the IEEE International Conference on Robotics and Automation*, Kobe, Japan, pp. 2989-2994, 2009.
- [3] S. Venugopal, L.C. Jsu, S.M.N. Rao, B.P.Wang, M. Chiao, and J.C. Chiao, "Design and modeling of a high accuracy, three degree of freedom MEMS manipulator", *Conference on MEMS and Photonics*, Brisbane, Australia, 2005.
- [4] B. R. Jong, D. M. Brouwer, M. J. Boer, H. V. Jansen, H. M. J. Soemers, and G. J. M. Krijnen, "Design and fabrication of a planar three-DOFs MEMS-based manipulator", *Journal of Microelectromechanical System*, Vol. 19, No. 5, pp. 1116-1130, 2010.
- [5] C. J. Kim, A. P. Pissano, and R. S. Muller "Silicon-processed overhanging microgripper", *Journal of Microelectromechanical System*, Vol. 1, No. 1, pp. 31-36, 1992.
- [6] B. V. Volland, H. Heerlein, and I. W. Rangelow, "Electrostatically driven microgripper", *Journal of Microelectronic Engineering*, Vol. 61, pp. 1015-1023, 2002.
- [7] J. V. Clark, N. Zhou, S. Brown and K. S. J. Pister, "MEMS Simulation Using SUGAR v0.5", *Solid-State Sensors and Actuators* pp. 191-196, 1998.
- [8] Q. Jing, T. Mukherjee and G. K. Fedder, "Schematic-Based Lumped Parameterized Behavioral Modeling for Suspended MEMS", *International Conference on Computer Aided Design*, San Jose, CA, Nov. 10-14, 2002.
- [9] G. C. Wong, G. K. Tse, Q. Jing, T. Mukherjee, G. K. Fedder, "Accuracy and Composability in NODAS", IEEE Int. Workshop on Behavioral Modeling and Simulation, San Jose, CA, 2003.
- [10] G. Uma, M. Umapathy, L. Baby Vidhya, M. Maya, T. Sophia and K. Tamilarasi, "Design and Analysis of Resonant Based Gas Sensor", *Sensors Applications Symposium*, Atlanta, pp. 119-121, 2008.
- [11] A. Manut and M. I. Syono "Effects of Mechanical Geometries on resonance Sensitivity of MEMS Out-of-Plane Accelerometer", *IEEE International Conference on Semiconductor Electronics*, Kuala Lumpur, 2006.
- [12] Kashif Riaz, Shafaat A. Bazaz, M. Mubasher Saleem and Rana I. Shakoor, "Design, Damping Estimation and Experimental Characterization of Decoupled 3-DoF Robust MEMS Gyroscope", *Journal of Sensors and Actuators A*, Vol. 172, No. 2, pp. 523-532, 2011.
- [13] K. Miller, A. Cowen, G. Hames, B. Hardy, SOIMUMPs Design Handbook, Version 4, MEMSCAP Inc., 2004. Available at: <http://www.memscap.com/products/mumps/soimumps/reference-material>
- [14] Universal Capacitive Readout™ IC (MS3110) manual Irvine Sensor Corporation. Available at: <http://www.irvine-sensors>.
- [15] M. Bao, "Analysis and design principles of MEMS devices" 1st edition Elsevier, 2005.
- [16] R. Legtenberg, A. W. Groeneveld and M. Elwenspoek, "Comb-drive actuators for large displacements", *Journal of Micromechanics Microengineering*, Vol. 6, No. 3 pp. 320-329, 1996.
- [17] CoventorWare ARCHITECT, version 2008, Reference: MEMS and Microsystems System-Level Design Coventor, Inc.
- [18] K. Amjad, S. A. Bazaz and Y. Lai, "Design of an electrostatic MEMS microgripper system integrated with force sensor", *The 20th IEEE international conference on microelectronics*, Sharjah, 2008, pp 275-278, 2008.
- [19] F. Krecinic, T.C. Duc, G.K. Lau and P.M. Sarro "Finite element modeling and experimental characterization of an electro-thermally actuated silicon-polymer microgripper", *Journal of micromechanics and Microengineering*, Vol. 18, pp., 2008.
- [20] E.V. Bordatchev and S.K. Nikumb, "Microgripper: Design, finite element analysis and laser microfabrication", proceeding of the international conference on MEMS, NANO and Smart Systems, Canada, pp. 308-313, 2003.





Control of the movement of mechanic system, interacting with surroundings. Problems of evolution and self organization

Vilor L. Zakovorothnii (Prof.)

Don State Technological University
344000, Rostov-on-Don, Gagarin Square, Russia
E-mail: vzakovorotny@dstu.edu.ru

Abstract: The problem of the control of the dynamic system interacting with the processing of cutting is considered in the report. In this report the system is represented as the evolution system compared to the previous approaches. In this system the parameters are represented as the integral operators of Voltaire of the second type related to the trajectory of power of the irreversible transformations of the accomplished work. As a result the system gets the features of the evolution and self organization in the process of its functioning. The example of the dynamic self organization of such system in the process of evolution is given. The problems of the control of such system are discussed

The Problem

During the last decades the synergetic theory of control has been rapidly developed in Russia. The method of coordination of outer control with the inner dynamics of the system forms the basis of this theory [1, 2].

Besides, the method of “expansion-compression” of the space of state forms also the basis of this theory. The principle of expansion of the space of state includes the introduction of the extra coordinates and connections into the controlled system. These coordinates form the transformation of the controlled coordinates to the coordinates that create the interactions between the system and the dynamic connection with the surroundings. The principle of the compression of the space of state is based on the always existing attractors in the dissipative systems that attract the multiplicities and all the trajectories of the space of state. In this case it is necessary to project the desirable multiplicities during the process of the synthesis of control. Besides, it is necessary to ensure the asymptotic stability of the projected multiplicities in the sphere of their attractions with the help of the outer control.

The realization of this principle of “expansion-compression”, that demands rather complex algorithms of control, does not create any contradictions using the computer control, that is, using the mechatronic system.

In this paper the example of using this principle of expansion-compression in control of the processes of machine tool processing is given. In this case the mathematical models of the controlled drives of the working elements of machine tools (the models for controlled movements of supports of the lathes and the frequency of the spindle rotations) are given.



Besides, the coordinates of the resilient deformation shifts of the top of the instrument relatively to supports; the resilient deformation shifts of making the points of the upper side of the instruments; the dynamic connection formed by the process of cutting in the trajectories of movements of the upper side of the instrument relatively to the work piece are given.

These trajectories are called the trajectories of the form creating movements. Such presentation, first of all, transforms the relatively autonomous systems of control of the making elements to the systems of connected (vector) control. Secondly, the systems become non linear and evolutionary changeable with the help of the dynamic connection. Thirdly, the correlation between the outer controls with the inner dynamics of the system according to the goal is provided, for example, the providing of the parameters of the quality of the details producing. The principles of the construction of such systems are explained in the following monographs [3, 4]. Nevertheless, this research explains the dynamic connection that is formed by cutting explained in vector parameters, but it does not explain its evolution changes. Our research is aimed to explain these evolution changes.

Mathematical model of the system and the methods of analysis of the evolution change of the system

Let us describe the controlled sub system in which the resilient deformation shifts of the machine tools and work pieces are analyzed [3, 4].

$$m \frac{d^2 X}{dt^2} + h \frac{dX}{dt} + cX = F(X, \frac{dX}{dt}, S_p, t_p, V_p, p) \quad (1)$$

where $X = \{X_1, X_2, \dots, X_n\}^T$ - vector of resilient deformation shifts;

$$F(X, \frac{dX}{dt}, S_p, t_p, V_p, p) = \{F_1(X, \frac{dX}{dt}, S_p, t_p, V_p, p), \dots, F_n(X, \frac{dX}{dt}, S_p, t_p, V_p, p)\}^T$$

- vector – function, that characterize the dynamic connection been formed in the system “system-surroundings”, in which some components of vector – function might be equal to zero; $p = \{p_1, p_2, \dots, p_k\}$ - parameters of the equation of

connection formed by surroundings; $m = \begin{bmatrix} m_{1,1} & m_{2,1} & \dots & m_{n,1} \\ m_{1,2} & m_{2,2} & \dots & m_{n,2} \\ \dots & \dots & \dots & \dots \\ m_{1,n} & m_{2,n} & \dots & m_{n,n} \end{bmatrix}$,

$$h = \begin{bmatrix} h_{1,1} & h_{2,1} & \dots & h_{n,1} \\ h_{1,2} & h_{2,2} & \dots & h_{n,2} \\ \dots & \dots & \dots & \dots \\ h_{1,n} & h_{2,n} & \dots & h_{n,n} \end{bmatrix}, c = \begin{bmatrix} c_{1,1} & c_{2,1} & \dots & c_{n,1} \\ c_{1,2} & c_{2,2} & \dots & c_{n,2} \\ \dots & \dots & \dots & \dots \\ c_{1,n} & c_{2,n} & \dots & c_{n,n} \end{bmatrix} - \text{consequently matrix of}$$

inertial, high – speed and resilient coefficients in the contolled system that interact with the surroundings; S_p, t_p, V_p , - technological regimes made by the controlled trajectories of the producing machine tools movements.



Matrix m , h and c are symmetrical and positive definitions. In $p = \{p_1, p_2, \dots, p_k\} = \text{const}$ and $S_p, t_p, V_p = \text{const}$ system (1) has points of stability X^* , defined by equation

$$cX^* = F(X^*, 0, S_p, t_p, V_p, p). \quad (2)$$

In connection with vector-function $F(X, 0, S_p, t_p, V_p, p)$ and parameters $p = \{p_1, p_2, \dots, p_k\}$ they could have the only decisions or they could have multiple decisions. That is why while varying of control S_p, t_p, V_p or changing parameters $p = \{p_1, p_2, \dots, p_k\}$ the branching of the points of stability could occur that coincide with the branching of the exactness of machine processing. Besides, the system (1), analyzed in the variations relatively X^* , might be stable or un stable asymptotically.

In [5, 6] it was shown that there might be the three main mechanisms of the stability losses.

The first one is connected with the fact that the positively defined symmetrical matrix becomes asymmetrical because of the reaction from the side of the machine processing. Then the loss of stability on the point of stability could happen by forming of skew symmetric parts of matrix of the circulation forces. Moreover the development of fluctuations happens in the form of wobbling. Then the loss of stability will be transformed from the positively defined into the negatively defined in the transformations of symmetrical matrix.

The second mechanism is explained by the transformations of symmetrical matrix high-speed coefficients from the positively defined to the negatively defined. The gyroscopic forces formed by the skew symmetrical parts of matrix could not create the stability of the system. They could transform the stable system according to Lyapunov into the asymptotically stable.

The **third** mechanism is explained by the existence of the periodically changing parameters of the system (1), that are parametrical phenomenon.

In the case when the stability is not achieved, then in the surroundings the different attracting multiplicities are created (the utmost cycles, invariance torus, chaotic attractors). But not all of them cause the worsening of the quality of the cutting surface. This deserves extra research. The control of the system balance (1) and the system's qualities is made by the choice of the parameters S_p, t_p, V_p and the choice of the parameters of the interconnected subsystems.

But the parameters of the dynamic connection formed by the surrounding $p = \{p_1, p_2, \dots, p_k\}$ do not stay unstable. They depend of the trajectory of the power and the work of the non controversial changes in the system "system-surroundings." As long as they change in the connection of the phase trajectory of "power-trajectory" of the unchanged transformations they could be represented as modified integral operators of Voltaire of the second type. The methods of identifications of the parameters and nucleus of the integral operators of evolution could be represented in the paper. The system (1) could be represented in the following way



$$\left\{ \begin{array}{l} m \frac{d^2 X(t)}{dt^2} + h \frac{dX(t)}{dt} + X(t) = F[S_P(t), t_P(t), X, \frac{dX}{dt}, Y, \frac{dY}{dt}, p]; \\ M \frac{d^2 Y(t)}{dt^2} + H \frac{dY(t)}{dt} + CY(t) = F[S_P(t), t_P(t), X, \frac{dX}{dt}, Y, \frac{dY}{dt}, p]; \\ p^{(i)}(A) = p_{i,0} + \alpha_i \int_0^A w_i(A-\zeta) N(\zeta) d\zeta, j=1,2\dots s; \\ A(t) = \int_0^t N(t) dt; \\ N(t) = V(t)F(t), \end{array} \right. \quad (3)$$

where m , M positively defined diagonal matrix of inertial coefficients in the measure of $3 \otimes 3$ that relate to the subsystems of the machine tool, and the work piece; $c = [c_{s,k}]$, $C = [C_{s,k}]$, $h = [h_{s,k}]$, $H = [H_{s,k}]$ - positively defined symmetrical matrix of rigidity and dissipation of the subsystem of the machine tool and the work piece, the measure is $3 \otimes 3$, non changeable to the coordinates relatively to their movements; $F = \{F_1, F_2, F_3\}^T$ - vector-function of the forces of the contact interaction which has sense in (1); $w_i(A-\zeta) = \exp[-\frac{1}{T_{i,1}}(A-\zeta)] + \beta_i \exp[\frac{1}{T_{i,2}}(A-\zeta)]$ - nucleus of the integration operators where $T_{i,1}$, $T_{i,2}$ - constant works that have the dimensionality kGm , these parameters characterize the evolution heredity of the trajectories during the machine work.

It is shown that in the linear understanding the nucleus of the integration operators could be represented in the form of exponent functions; α_i - parameters that form the connection of the fructuous power of the non irreversible changes and the trajectories of power of the done work in accordance with the parameter; $P_{i,0}$ - primary significations of parameters. In the analyzed system the parameters of the dynamic characteristics of cutting

process have the primary significations $P_{i,0}$ and values $p_i(A, N)$, which depend on the trajectory of power in the done work. In their own turn, the trajectory of work and power is the function of coordinates of the system. Then, the system (3) is the functional, integrated – differential system that needs to be analyzed properly. In the frames of this research we take into consideration that all the evolution changes take occur very slowly that the system (3) could be characterized as frozen. Then it is possible to introduce the notion of the stationary evolution trajectory $X^*(A) Y^*(A)$, to which the evolutionary



changeable parameters relate $p_i(A, N)$. It is possible to describe these parameters and the evolutionary trajectory according to the following rule

$$\left\{ \begin{array}{l} cX^*(A) = F[X^*, 0, Y^*, 0, p(A, N), S_p, t_p, V_p]; \\ CY^*(A) = F[X^*, 0, Y^*, 0, p(A, N), S_p, t_p, V_p]; \\ p^{(i)}(A) = p_{i,0} + \alpha_i \int_0^A w_i(A - \zeta) N(\zeta) d\zeta, i = 1, 2, \dots, s; \\ A(t) = \int_0^t N(t) dt; \\ N(t) = V(t)F(t). \end{array} \right. \quad (4)$$

If in (4) $\alpha_i = 0$ and non linear functions $F[X^*, Y^*]$ are monotonous related to X^*, Y^* , then the stationary evolution trajectory is the constant unique point of stability of the system. It shifts slowly in the time and defines the stationary evolution trajectory. This takes place in the dynamic system in which the flexural deformation shifts of machine tool are small values. In the conditions when the flexural deformation shifts are big values, then on the way of the growth of the outer forces the branching of the points of stability could occur. But in this case of the sphere of attraction of points, in the condition of their asymptotic stability the concrete point of stability is (rests) non changeable.

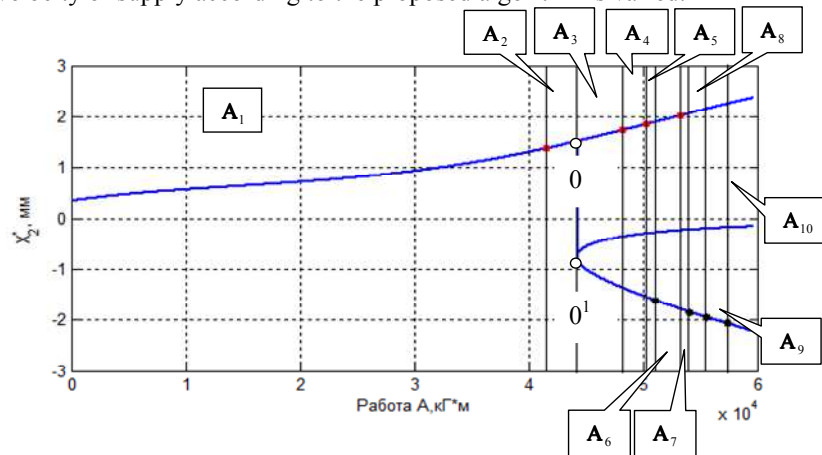
If $\alpha_i \neq 0$, then by the way of extracted power related to the trajectory of changes of power of the done work, the shift of the points of stability could occur. These shifts $X^*(A, N, t), Y^*(A, N, t)$ are caused not by the outer forces (influences), including control, but by the evolutionary changes of the parameters that form the stable relations between the forces and the technological regimes in accordance with the resilient deformation shifts of the machine tools related to the work sample. The trajectories

$X^*(A, N, t), Y^*(A, N, t)$ are the stationary evolution trajectories to which the parameters of the system $p^{(i)}[A(t), N(t)] \in P^{(i)}$ relate. It is important to note that the points $X^*(A, N, t), Y^*(A, N, t)$ and parameters $p_i(A, N)$ are stable in the limits not only of the impulsive reactions of the sub systems but the impulsive reactions of the drives of the executive travels. That is why the analysis of the features of the evolutionary changeable system is taken place during the two stages. The first stage deals with the stationary evolution

trajectory. The second stage deals with the analysis of the system behavior in the variations related the stationary evolution trajectory.

Example of the evolution reconstruction of the system in the process of evolution

Every controlled stationary trajectory corresponds to the personal evolution trajectory and to the personal dynamic system reorganization analyzed in the variations related to the stationary trajectory. We will not specify all the details and we will consider the example of the evolution reconstruction of the dynamic system of cutting in the variations related to the trajectory (drawing figures 1, 2). In her own turn, the stationary trajectory is synthesized recording to the control according to the criteria of the stability of diameter of the details being cut. The velocity of supply according to the proposed algorithm is varied.



Drawing figure.1. Bifurcation diagram of the points of stability in cutting process

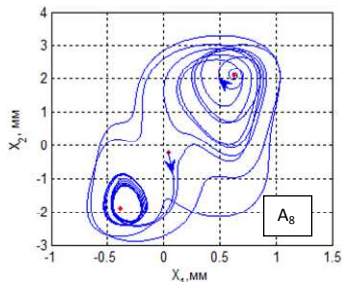
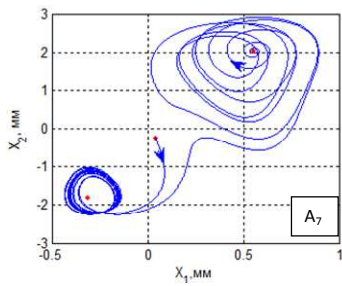
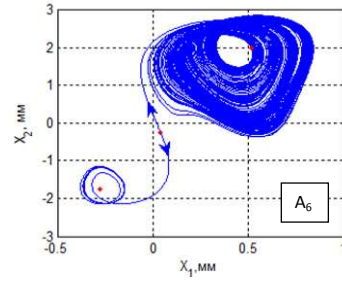
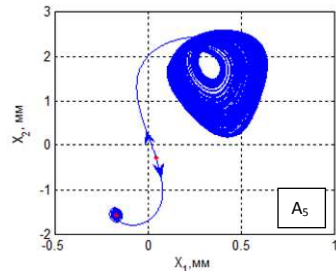
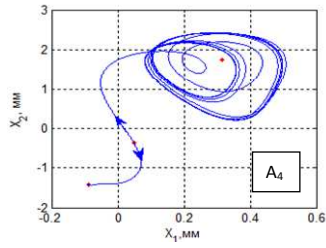
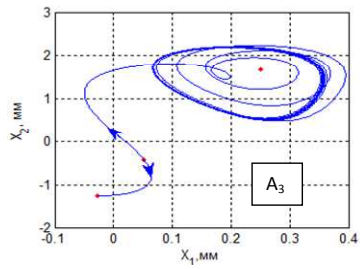
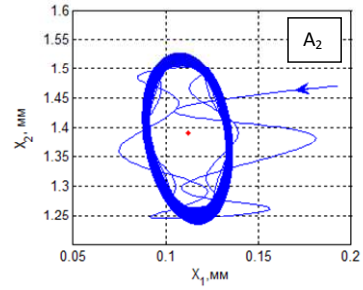
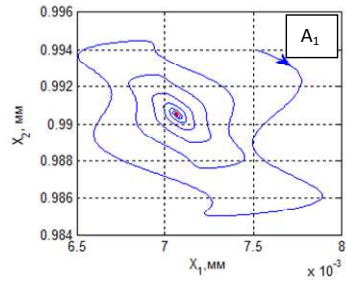
Bifurcation of stability becomes apparent when starting from the point, drawn on the figure 1 as the circle, we have the different values of the forces that correspond to the analyzed point of stability. That is why starting from this point the calculation of the evolution changes in parameters is going independently from all the branches

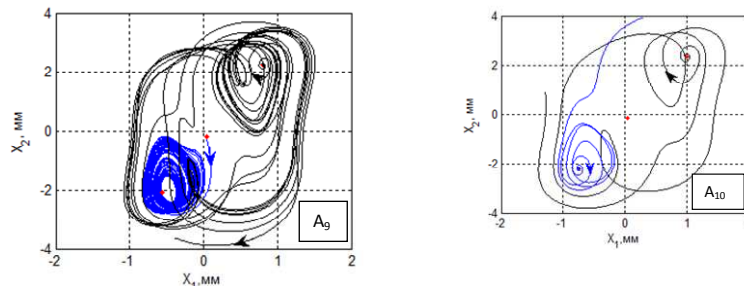
Let us characterize the bifurcation changes in the system of the irreversible transformations (drawing figure 2).

1. $\mathbf{A}_1 = [0 - 4.152 \cdot 10^4], \text{кГ} \cdot \text{м}$ - system has unique asymptotic point of stability.



2. $\mathbf{A}_2 = [4.152 - 4.4185] \cdot 10^4, \kappa\Gamma \cdot \mathcal{M}$ - sphere of orbital asymptotic stable limit circles. During the work equal to $4.4185 \cdot 10^4, \kappa\Gamma \cdot \mathcal{M}$ the branching of the points of stability is observed.
3. $\mathbf{A}_3 = [4.4185 - 4.824] \cdot 10^4, \kappa\Gamma \cdot \mathcal{M}$ - in this sphere of the neighborhood in the upper branch the orbital asymptotic stable cycle is formed, in the neighborhood in the lower branch the asymptotic stability is formed. The spheres of attraction of the two stationary states are divided by the saddle shaped separatrix curves. So, in the transition through the point of work $4.4185 \cdot 10^4, \kappa\Gamma \cdot \mathcal{M}$ in the neighborhood of the lower branch we could observe the reverse bifurcation of transformation of the limit cycle into the asymptotic stable point of stability
4. $\mathbf{A}_4 = [4.824 - 5.023] \cdot 10^4, \kappa\Gamma \cdot \mathcal{M}$ in the neighborhood of the upper branch we could observe the cascade of bifurcations of doubling of the period, in the in the neighborhood of the lower branch the asymptotic stable point is kept. The cascade of the bifurcations of the second period characterizes one of the scenarios of formation of chaotic attractor. [7].
5. $\mathbf{A}_5 = [5.023 - 5.105] \cdot 10^4, \kappa\Gamma \cdot \mathcal{M}$ in the neighborhood of upper branch the chaotic attractor is formed, in the in the neighborhood of lower branch the asymptotic stability is formed.
6. $\mathbf{A}_6 = [5.325 - 5.409] \cdot 10^4, \kappa\Gamma \cdot \mathcal{M}$ in the neighborhood of the upper branch the chaotic attractor is formed, in the in the neighborhood of lower branch the orbital asymptotic stabile limit cycle is formed.
7. $\mathbf{A}_7 = [5.325 - 5.409] \cdot 10^4, \kappa\Gamma \cdot \mathcal{M}$ in the neighborhood of the upper branch the system is unstable, in the in the neighborhood of lower branch the limit cycle is formed and his sphere of attraction is limited.
8. $\mathbf{A}_8 = [5.409 - 5.5606] \cdot 10^4, \kappa\Gamma \cdot \mathcal{M}$ in the neighborhood of the upper branch the system is unstable, in the in the neighborhood of lower branch the cascade of doubling of the period is observed.
9. $\mathbf{A}_9 = [5.5606 - 5.739] \cdot 10^4, \kappa\Gamma \cdot \mathcal{M}$ in the neighborhood of the upper branch the system is unstable, in the in the neighborhood of lower branch the chaotic attractor is formed and it has the limits in the spheres of attraction.
10. $\mathbf{A}_{10} > 5.739 \cdot 10^4, \kappa\Gamma \cdot \mathcal{M}$ in the neighborhood of the upper branch the system is unstable, in the in the neighborhood of lower branch the system is unstable, that is the system as a whole is unstable.





Drawing figure 2. Example of projections of formed multiplicities on the surface in the neighborhood of the stationary evolution trajectories on the way of work of irreversible transformations

During the synthesis of control it is taken into consideration that each trajectory of the details of the machine tool corresponds to the personal evolution trajectory, trajectory of the form creating movements of the machine tool relatively the work piece. Also it corresponds to the features of the system analyzed in the variations relatively the controlled stationary trajectory. In this case the multiplicity of trajectories exists; these trajectories show the indicators of the quality of detail production. That is why the tasks of the choice of the optimal trajectory in the multiplicity are given. The optimal choice is understood in this case as the minimization of the expenses on the production of the lot of details [8].

Conclusion

During the realization of the systemic synergetic principle of control of the machine tool production based on the correlation between the outer control and the inner dynamics of the system, it is necessary to take into consideration the inner evolution and self organization of the dynamic system. The proposed method of analysis could be useful for the control of the movement of mechanic system, separate units of which correlate with the different surroundings (frictional, aerodynamic, hydrodynamic and others).

References

1. Kolesnikov A.A. (1994). *The Synergetic Theory of Control*. Moscow, Energoatomizdat. – 238 p.
2. *Synergetics and the Problems of Control*. (2004). Ed. By A.A. Kolesnikov. // Moscow: Phisimatlit. 504 p.
3. Zakovorotny V.L., Flek M.B. (2006). *The Dynamics of the Cutting Process. Synergetic Approach*. – Rostov-on-Don: «Terra». -876 p.
4. Zakovorotny V.L., Lukyanov A.D., Nguen Dong An, Fam Dign Tung. (2008). *The Synergetic Systemic Synthesis of the Controlled Dynamics of the Metal Cutting Machine*



Tools with the Consideration of the Evolution of Relations. Rostov-on-Don, Publishing center of DGTU. – 324 p.

5. Zakovorotny V.L., Lukjanov A.D., Voloshin D.V.(2004). *The Modeling of evolution transformation in cutting in metal cutting machine tools.* Engineering & automation problems. International journal - M, № 1, 2004, P. 68-77.

6. Zakovorotny V.L., Samosudov A.A. (2006). The Problems of Managing the Evolution of the Dynamic System, Interacting with the Environment. *Engineering & Automation, International Journal* - Moscow, № 5, P. 78-91.

7. Magnitsky N.A., Sidorov S.V. (2004). *The New Methods of the Chaotic Dynamics.* Moscow, Editorial URSS. -320 p.

8. Zakovorotny V.L., Bordatchev E.V., Sankar T.S. Variational Formulation for Optimal Multi-Cycle Deep Drilling of Small Holes. *Journal of Dynamics Systems, Measurement, and Control* / ASME (Canada). -1996. -Vol.11.



Revealing chaotic features of mixing at river groyne fields using Lagrangian tools

Márton Zsugyel

MTA-BME Water Management Research Group, Budapest, Hungary
E-mail: zsugyel@vit.bme.hu

Abstract: Groynes are spur dyke type of river training works built in the river to narrow the cross section, in such a way make the river create and maintain deep enough navigation-routes in wide shallow river sections. It has been found that in the vicinity and downstream of a groyne the developing inherently unstable velocity field results in mixing process governed by chaotic advection. The investigation of this phenomenon, using Lagrangian methods originated from the chaos theory, offers a novel approach to describe such mixing processes. Recent field measurements in the river Danube have shown (Zsugyel et al., 2012) that this is an appropriate way to reveal some basic chaotic features – e.g. the sensitivity of the fate of pollutants onto the initial conditions – and to identify areas where efficient mixing occurs. Nevertheless, field measurements provide only qualitative results because of the small number of available GPS-tracked floating particles. In laboratory conditions *Particle Tracking Velocimetry* (PTV) measurements were used in order to be able to reconstruct the surface velocity field then numerical particle tracking was applied to obtain Lagrangian flow and mixing features. By the calculation of the *Finite Size Lyapunov Exponent* (FSLE) and *flushing time* fields the spatial distribution of these chaos parameters outlined the main coherent structures – e.g. stable manifolds, hyperbolic points, transport barriers – of the flow, all governing the mixing processes.

Keywords: river hydraulics, chaotic advection, mixing, Lagrangian transport, PTV

1. Introduction

At river reaches where the bed slope decreases, therefore the flow velocity is expected to be slower and the river sediment deposition is likely to increase, river training works are constructed to address the problem. One of such typical structures is groynes, built span-wise to narrow the river cross section. This accelerates the river, decreases the deposition and maintains suitable conditions for shipping.

The hydraulic situation around a groyne field is quite complicated since the developed flow field is unsteady and non-periodic.

The investigation of mixing processes in such a complex situation is essential since e.g. polluted water can be trapped between the groynes which effects longer residence time and more significant damage in the environment.

Researches until now have concentrated on the determination of the appropriate exchange rate between the groyne field and the main stream (see e.g. [1], [2]). Other investigations were done to describe the mean flow field at different groyne field geometry [3]. These investigations are based on the traditional diffusion-type description of mixing. However, it was shown that mixing is best described as Lagrangian transport [4].



Haller and his workgroup introduced Lagrangian Coherent Structures [5] and laid down its theoretical backgrounds, and recently presented some practical applications in ocean estuaries [6].

Engelhardt et al. [7] showed based on field measurements that phytoplankton distribution in a groyne field is strongly depends on the flow field properties.

Recently we collected on-site particle trajectory data using GPS-equipped floating buoys. Applying some simple mathematical tools originated from chaos theory on this measurements, areas characterized with different mixing strength rate were determined [8]. As the number of the floating buoys was a strong limitation to give a quantitative description about the mixing around the groynes, laboratory measurements were designed.

This paper is organized as follows: in Section 2 the laboratory measurements are described, which is followed in Section 3 by the report on our main results like flushing time distribution, Finite Size Lyapunov Exponents and fractal dimensions. Finally, in Section 4 we give a conclusion and outlook.

2. Laboratory measurements

For the investigations a 1 m wide and 8 m long straight, rectangular cross-section model channel was built in the laboratory of the University. Fig. 1 shows a section of the channel representing how a single groyne was built in its 2.5 m long mid-section. This groyne narrowed the channel cross-section by about 30%. Thousands of white polyethylene floaters with 9 mm diameter were released upstream of the groyne and tracked in the central area using the Particle Tracking Velocimetry technique. The main benefit of this method is to allow positioning each particle image frame by image frame, thus offering particle trajectories during the measurement in the observed area with 30 Hz temporary resolution. However, handling lost and re-found particles was an unpleasant property of the recordings. In order to overcome this difficulty we interpolated the scattered velocity field to a regular rectangular grid at every time step and released one million numerical particles which followed this interpolated flow field from each rectangular area showed in Fig 1.

Numerical particle positions were calculated using the following equation with a 4th order Runge-Kutta method:

$$\mathbf{x}_{i+1} = \mathbf{x}_i + \mathbf{v}_i \cdot dt \quad , \quad (1)$$

where \mathbf{x}_i is the 2D particle position vector at time instant i , \mathbf{v} is the instantaneous velocity vector at \mathbf{x} and dt is the time step.

In Fig 1 also the main flow structures is well observable: the main flow passing the groyne, the clock-wise recirculation zone developed downstream behind the obstacle and a shear zone between them where the small vortices shedding from the groyne head interact. Moreover, the uneven spatial distribution of the particles indicates that the surface flow is not divergence-free: up- and downwelling zones develop where the particles are sparsely or densely distributed, respectively.

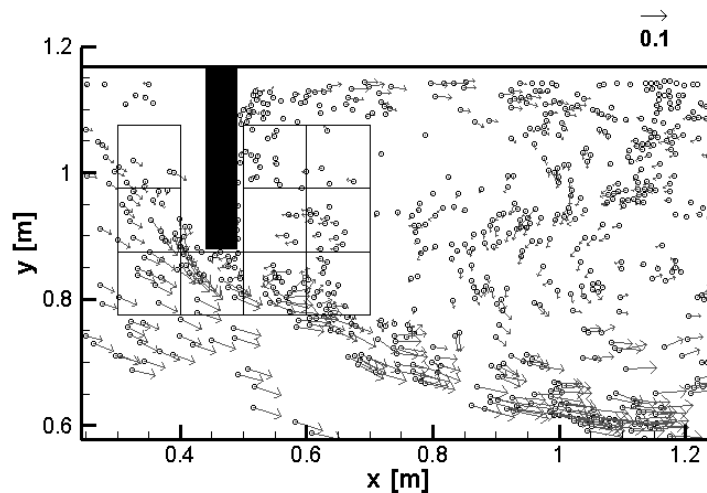


Fig 1. An extract of the model channel illustrating the groyne, the floating particles and an instantaneous scattered velocity field. The ten rectangles around the groyne show the frames for the initial positions of the numerical particles. (The reference vector in the top right corner is in ms^{-1} .)

3. Results

Different essential Lagrangian parameters were calculated in order to describe the mixing around a single groyne. The first of them was the flushing time which measures the life time of each particle spent in a prescribed flow domain. Namely, each particle was followed until it reached the cross-section at $x=1.7$ m. When this happened the elapsed time from the release was assigned to the initial position. This idea is based on the consideration that the spatial distribution of the flushing time refers qualitatively to the mixing efficiency. If the distribution is smooth, the mixing is not effective because every particle in the neighborhood reaches the border cross-section during similar time. On the other hand, efficient mixing is expected when the flushing time field is complicated.

In Fig 2 the spatial distribution of the flushing time is shown. The warmer colors mean longer flushing time. It is obvious that this implies good mixing since neighbor particles may have completely different magnitude of flushing times implying efficient spreading. Such a flushing time distribution is similar to a lifetime distribution in a chaotic system [9] and it suggests high sensitivity to the initial conditions.

The three main flow zones can be also distinguished: the main stream characterized by small flushing times, the recirculation zone behind the groyne marked with white and purplish colors. Between these areas one can identify the shear zone where the chaotic mixing essentially occurs. The reddish filaments that can be found in this area correspond to the stable manifold which is one of

the main elements of the flow in the Lagrangian description. Every stable manifold is intersected in the hyperbolic point with an unstable manifold. The particle pairs initially staying close to each other but on the different side of the stable manifold suffer from the greatest stretching after they pass the hyperbolic point because they follow different unstable manifolds [9].

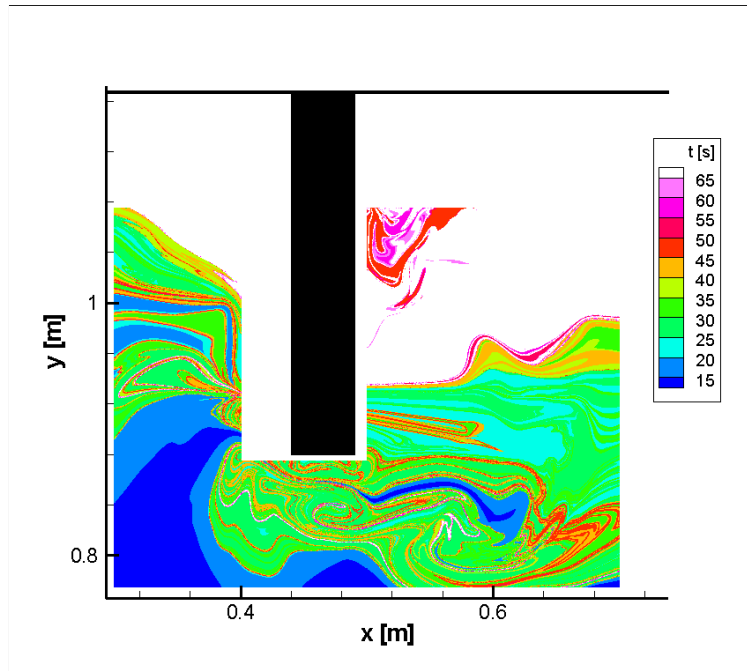


Fig. 2. Flushing time distribution around the groyne

Finite size Lyapunov exponents (FSLE) were also calculated in order to quantify the strength of mixing. On the whole domain the largest distance of the particles relative to their four initial neighbors was tracked and when it reached a given limit the following formula was evaluated:

$$\lambda(x, t_0, \delta_0, \delta_l) = \frac{1}{t'} \ln \frac{\delta_l}{\delta_0} \quad (2)$$

where λ is the FSLE which depends on the position, the initial time, the initial δ_0 and the limit distance δ_l . According to the properties of the manifolds on the mixing described in the last paragraph, the largest FSLE values are expected around the stable manifolds.

Focusing only on the release cell at the groyne head we present in Fig 3 the FSLE values at starting time $t_0=0$ s. It is obvious that the green flushing time filaments and the red FSLE filaments are indicating the same structure, that is the stable manifold. In this case the limit distance in the FSLE calculation was

1000 times larger than the initial distance, the fact responsible for some fragmented reddish filaments. On the other hand, this large limit allows to identify the really important structures.

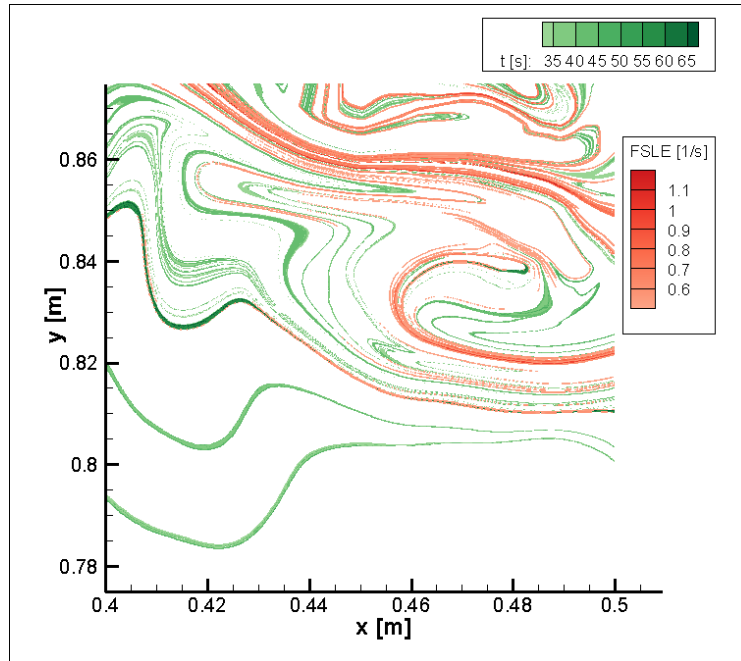


Fig. 3. Large flushing time (green) and large Finite Size Lyapunov Exponent (red) values calculated for the release cell at the groyne head ($t_0=0$ s).

It is also well visible that the stable manifolds in Fig 3. indicate fractal-like structure. Such structures often develop on the water surface during the mixing of floating organic or inorganic material. To determine the fractal dimension we applied the box-counter method [10]. It was found that flushing times larger than half of the observation period ($FT > 33$ s) provide an appropriate fractal structure with a dimension of 1.62. In a divergence free two-dimensional open flow the information dimension (D_1) of the stable manifold would be calculated using the formula

$$D_1 = 2 - \frac{\kappa}{\lambda} \quad , \quad (3)$$

where κ is the escape rate and λ is the averaged Lyapunov exponent [11]. Using this expression in our case D_1 is 1.63, implying good agreement. Further cases with different starting times were also investigated and the agreement between fractal and informational dimensions remained satisfactory.

4. Conclusion



In this paper some novel application of methods originated from chaos theory were presented. In order to better understand the mixing processes in river reaches with groynes some Lagrangian properties of mixing were calculated. Large values of flushing time and FSLE values reveal the position of Lagrangian coherent structures like stable manifolds and hyperbolic saddle points which are responsible for the most intensive mixing.

The methods outlined and applied above are simple enough also for practical applications wherever the surface velocity field is known. In fact, an improved understanding of the mixing processes at complicated flow fields can result in physically more exact numerical mass exchange models between the main stream and the recirculation zones, thus contributing to the more realistic description of the fate of not only the conventional pollutants but also their ecological impact, moreover, the identification of zones characterized with good and poor mixing may provide novel type of input data for e.g. neutralization measures.

References

1. van Mazijk A. Modelling effects of groyne fields on the transport of dissolved matter within the Rhine Alarm-Model. *Journal of Hydrology* 264, 213–229, 2002.
2. Kurzke M, Weitbrecht V, Jirka GH, Laboratory concentration measurements for determination of mass exchange between groin fields and main stream, *Proceedings of River Flow 2002 Symposium*, Elsevier Press, Louvain-la-Neuve, Belgium, 369–376, 2002.
3. Uijteteaal WSJ, Lehmann D, van Mazijk A, Exchange processes between a river and its groyne fields: Model experiments, *Journal of Hydraulic Engineering* 127 (2001), no. 11, 928–936.
4. Aref, H. Stirring by chaotic advection. *Journal of Fluid Mechanics* 143:1-21, 1984.
5. Haller, G. and Yuan G., Lagrangian coherent structures and mixing in two-dimensional turbulence, *Physica D* 147, 352-370, 2000.
6. Peacock T. and Haller G., Lagrangian Coherent Structures: The hidden skeleton of fluid flows, *Physics today* 66, 41-47, 2013.
7. Engelhardt C, Krüger A, Sukhodolov A, Nicklisch A, A study of phytoplankton spatial distributions, flow structure and characteristics of mixing in a river reach with groynes, *Journal of Plankton Research* 26, no. 11, 1351–1366, 2004.
8. Zsugyel, M., Szabó, K. G., Ciraolo, G., Nasello, C., Napoli, E., Kiss, M., Tél, T. & Józsa, J. Detecting the chaotic nature of advection in complex river flows. *Periodica Polytechnica – Civil Engineering*, 56, No. 1: 97-106, 2012.
9. Tél T and Gruiz M. *Chaotic dynamics*, Cambridge University Press, 2006.
10. Theiler J. Estimating fractal dimension, *JOSA A*, Vol. 7, Issue 6, pp. 1055-1073, 1990.
11. Lai, Y., Tél, T. *Transient chaos : complex dynamics on finite-time scales*. Springer, New York, 2011.



State and Parameter Estimation of The Lorenz System In Existence of Colored Noise

Mozhgan Mombeini^a
Hamid Khaloozadeh^b

^a Institute for Research in Fundamental Sciences (IPM), Tehran, Iran

^b Faculty of Electrical & Computer Eng., K.N. Toosi Univ. of Technol., Tehran, Iran

E-mail: mzh.mombeini@ipm.ir^a, H.Khaloozadeh@kntu.ac.ir^b

Abstract: Many researchers are interested to use Extended Kalman Filter (EKF) for state estimation of complex nonlinear dynamics with uncertainties which modeled with white noises. On the other hand behavior of the chaotic systems in time domain itself is similar to noise too. In this paper, states of the chaotic Lorenz system that its uncertainties modeled with colored noise on states and also on output are considered. For both cases, the case that parameters of Lorenz system are known and the case that parameters of the Lorenz system are unknown, EKF is used to estimate the states. In the case that parameters are unknown using a stochastic viewpoint parameters of the system and parameters of the first order filter of the colored noise are estimated. Efficiency of the method is shown with simulation.

Keywords: Colored noise, EKF, Estimation, Lorenz, Uncertainty.

1. Introduction

Extended Kalman Filter (EKF) is a powerful tool for estimation of nonlinear systems states in presence of noise and used in many nonlinear cases. In some nonlinear systems by changing parameters of the systems they get to period doubling and continuing the parameter changing then system becomes chaotic. This procedure determines the domain in which system is chaotic, where behavior of the system in time domain is similar to noise and also system is sensitive to initial condition. Then according the noise like behavior of the chaotic systems, efficiency of the EKF for state and parameter estimation of these systems is investigated in some works [1-3].

In this paper, efficiency of the EKF for separation of chaotic states from noise is investigated for Lorenz system with known parameters and for Lorenz system with unknown parameter. Where, in both cases the existent noise is a colored noise and EKF is used to estimate the filter parameters too.



2. Discrete modeling and different uncertainties

For continuous model of system in state space with

$$\dot{x} = f(x, \theta)$$

$$z = Hx(t)$$

Where $x \in \mathbb{R}^n$ denoted to state variables θ denote to system parameters, $z \in \mathbb{R}^m$ is output and H , measurement matrix is a $m \times n$ matrix, a forward difference approximation for derivations of the states is $\dot{x} = \frac{x(t + \Delta t, \theta) - x(t, \theta)}{\Delta t}$.

Choosing Δt small enough as sample time, $x_{k+1} = x(t + \Delta t, \theta)$ and

$x_k = x(t, \theta)$ result in $\frac{x_{k+1} - x_k}{\Delta t} = f(x_k, \theta)$ or equivalently a discrete model

as

$$x_{k+1} = F(x_k, \theta)$$

which can be simulated with computer codes. Note that for $x \in \mathbb{R}^n$ the forward approximation of derivatives of each state should be calculated separately. Then realization of discrete model with measured output $z \in \mathbb{R}^m$ in state space is

$$\begin{aligned} x_{k+1} &= F(x_k, \theta) \\ z &= Hx_k \end{aligned} \quad (1)$$

2.1 White noise type uncertainty

White noises are some uncertainties that are independent time series and distributed identically, which means no auto correlation between them. In particular case, the "Gaussian white noise" has normal distribution with zero mean and standard variation σ . For system(1) with Gaussian white noise $\{w\}$ on states and Gaussian white noise $\{v\}$ on output it change as following

$$\begin{aligned} x_{k+1} &= F(x_k, \theta) + Gw \\ z &= Hx_k + v. \end{aligned} \quad (2)$$

Where, mean vector and autocorrelation matrix of w and v are $\mu_w = E\{w\} = 0$, $R_{ww} = E\{ww^T\} = \sigma_w^2 I$, $\mu_v = E\{v\} = 0$, $R_{vv} = E\{vv^T\} = \sigma_v^2 I$, E is expected value operator, I is identity matrix and G is a matrix or vector that its dimension matches to size of other elements of the equation.



2.2 Colored noise type uncertainty

Colored noises are some uncertainties that are dependent to their past states then have auto correlation. In particular case passing a “Gaussian white noise” from a first order filter results in a colored noise.

Model of a first order filter which result in $\{w\}$ colored noise on states is

$$w_{k+1} = cw_k + e^1 \quad (3)$$

Where, $\{e^1\}$ is Gaussian white noise and c is a real constant. Similarly by defining

$$v_{k+1} = dv_k + e^2 \quad (4)$$

Where $\{e^2\}$ is Gaussian white noise and d is a real constant, $\{v\}$ is realization for colored noise on measured output.

2.3 Uncertain parameters

For most mathematical modeling of systems there are uncertainties in parameters of the model. Some are inherent result of the accuracy in modeling some are because of variation in realistic condition of the system among the time and etc. Then, although the θ parameters of the system (1), are considered constant in observation scale time but they may have changes among the time. In other word in bigger scale times these uncertain parameters are variable. Here, using stochastic perspective, for a unknown parameter $\bar{\theta}$ by variation in the range $[\theta - \Delta\theta, \theta + \Delta\theta]$, the parameter is consider the as a more general case a white noise with θ mean value and $\Delta\theta$ variance value or equivalently

$$\begin{aligned} \bar{\theta} &= \theta + \mathcal{G} \\ \mathcal{G} &\sim N(0, \Delta\theta) \end{aligned} \quad (5)$$

3. Extended Kalman Filter (EKF)

Extended Kalman Filter is a mathematical tool for state estimation of nonlinear systems and the method is used in many cases [1]. It called First-Order Filter too, because it uses an approximation of the system with expanding it in Taylor series getting the first order terms, and higher order terms (H.O.T.) are considered negligible. In short description, for the nonlinear model with Gaussian noise

$$\begin{aligned} x_{k+1} &= F(x_k, \theta) + G(x_k, w) \\ y &= H(x_k) + v. \end{aligned} \quad (6)$$

$$w \sim N(0, Q), v \sim N(0, R), x_0 \sim N(\bar{x}_0, Q_0)$$



Where $x \in \mathcal{R}^n$ denoted to state variables $z \in \mathcal{R}^m$ is output and v , w are white noises with zero mean and standard deviation Q , R , linearization of (6) at

$$\text{every step } k \text{ results in } \bar{A}_k = \left. \frac{\partial F(x_k, \theta)}{\partial x_k} \right|_{x_k}, \bar{C}_k = \left. \frac{\partial H(x_k)}{\partial x_k} \right|_{x_k}, \bar{G}_k = G(x_k),$$

Extended kalman filter recursively estimates the states in two phases, forecast and correction.

3.1 EKF for state estimation

For system (6) with x_k states and θ known constant parameters forecast phase is

$$\begin{aligned} \hat{x}_{k+1}^- &= F(\hat{x}_k, \theta) \\ P_{k+1}^- &= \bar{A}_k P_k \bar{A}_k' + \bar{G}_k Q \bar{G}_k' \\ \hat{x}_0^- &= \bar{x}_0, P_0^- = Q_0 \end{aligned} \quad (7)$$

And correction phase is

$$\begin{aligned} \hat{x}_k &= \hat{x}_k^- + L_k (y_k - H(\hat{x}_k^-)) \\ L_k &= P_k^- \bar{C}_k' (\bar{C}_k P_k^- \bar{C}_k' + R)^{-1} \\ P_k &= P_k^- - L_k \bar{C}_k P_k^- \end{aligned} \quad (8)$$

Where \hat{x}_k is the estimated value for the states.

3.2 EKF for state and parameters estimation

A method is introduced in literature to extend application of the EKF method for estimation of uncertain parameters too. Essence of the method is to consider the unknown parameter θ as an additional state [1-3].

In this paper, the method is used for parameter estimation of the discrete model. Consider the discrete model (2) with θ uncertain parameters. By considering this uncertainty on parameters as a noise model (5) and defining augmented vector for new states as $\zeta = [x, \theta]$, state space model (2) changes to following equation



$$\xi_{k+1} = \begin{bmatrix} x_{k+1} \\ \theta_{k+1} \end{bmatrix} = F'(\xi) + G'W' = \begin{bmatrix} F(x_k, \theta_k) \\ \theta_k \end{bmatrix} + \begin{bmatrix} G & 0 \\ 0 & I \end{bmatrix} \begin{bmatrix} w \\ \mathcal{G} \end{bmatrix} \quad (9)$$

$$y = Hx + v$$

$$w \sim N(0, Q), v \sim N(0, R), \mathcal{G} \sim N(\bar{\theta}, \Delta\theta)$$

This new description of the system with unknown parameters is in the class of system (6) and EKF method can be used for new states $\zeta = [x, \theta]$ with linearization of (9) at every sampling time instant k .

4. Effect of uncertainty on Lorenz system

The Lorenz system is a chaotic system that introduced in 1963 with equations

$$\begin{aligned} \dot{x}_1 &= \sigma(x_2 - x_1) \\ \dot{x}_2 &= -x_1x_3 + rx_1 - x_2 \\ \dot{x}_3 &= x_1x_2 - bx_3 \end{aligned} \quad (10)$$

The system is chaotic in range of parameters, here considered with $\sigma = 10, b = 1.25, r = 28$.

Discrete model (1) for system (10) is

$$\begin{aligned} x_{1k+1} &= x_{1k} + \Delta t \sigma (x_{2k} - x_{1k}) \\ x_{2k+1} &= x_{2k} + \Delta t (-x_{1k}x_{3k} + rx_{1k} - x_{2k}) \\ x_{3k+1} &= x_{3k} + \Delta t (x_{1k}x_{2k} - bx_{3k}) \end{aligned} \quad (11)$$

In this part, using simulation, effect of the different uncertainties on Lorenz system trajectory is shown. To quantify difference between states and estimation or perturbed states, error function which is used here is

$$error(x_n, y_n) = \frac{1}{N} \sum_{n=1}^N \|x_n - y_n\| \quad (12)$$

Where x_n and y_n are compared states, $N = \frac{T}{\Delta t}$ is total number of samples of

the system evolution and $\|\cdot\|$ is norm-two operator.

To model effect of noise on states and parameters the values of G and H matrix of the model (2) are chosen as $G = [1 \ 1 \ 1]^T$, $H = [1 \ 0 \ 1]$ and $\Delta t = .01$,



error function is calculated with $T = 7, dt = 0.01$ or equivalently $N = 700$. All models are run with same initial condition $(0.5622, 0.7893, 0.3509)$ for states.

4.1 Lorenz system with white noise uncertainty

Lorenz system (11) with white noise uncertainty changes to

$$\begin{aligned}x'_{1k+1} &= x'_{1k} + \Delta t \sigma(x'_{2k} - x'_{1k}) + w \\x'_{2k+1} &= x'_{2k} + \Delta t(-x'_{1k}x'_{3k} + rx'_{1k} - x'_{2k}) + w \\x'_{3k+1} &= x'_{3k} + \Delta t(x'_{1k}x'_{2k} - bx'_{3k}) + w \\z &= x'_{1k} + x'_{3k} + v \\w &\sim N(0, Q), v \sim N(0, R),\end{aligned}\tag{13}$$

Figures (1), (2) show trajectories of the ideal model (11) and noisy model (13) with $Q = 0.001$ and $R = 0.001$ in time domain and phase domain respectively. Deviation in system trajectory with adding the white noise on states is obvious in these figures. According to figures adding white noise on the states, system's behavior changes from the ideal model which is without any noise. Value of the error (12) is $error(x, x') = 61.0554$ in simulation.

4-2 Lorenz system with colored noise

According to (3), (4) Lorenz system (11) with colored noise uncertainty changes to

$$\begin{aligned}x''_{1k+1} &= x''_{1k} + \Delta t \sigma(x''_{2k} - x''_{1k}) + w_k \\x''_{2k+1} &= x''_{2k} + \Delta t(-x''_{1k}x''_{3k} + rx''_{1k} - x''_{2k}) + w_k \\x''_{3k+1} &= x''_{3k} + \Delta t(x''_{1k}x''_{2k} - bx''_{3k}) + w_k \\w_{k+1} &= cw_k + e^1 \\v_{k+1} &= dv_k + e^2 \\z &= x''_{1k} + x''_{3k} + v_k \\e^1 &\sim N(0, Q^1), e^2 \sim N(0, Q^2),\end{aligned}\tag{14}$$

Where the parameters of first order filter are chosen as $c = 0.1, d = 0.2$, $Q^1 = 0.001$ and $Q^2 = 0.001$.

Figures (3), (4) show trajectories of the real model (11) and noisy model (14) in time domain and phase domain respectively. According to figures adding colored noise on the states, system's behavior changes from the ideal model (11) which is without any noise. Value of the error (12) is $error(x, x'') = 73.1981$ in simulation.

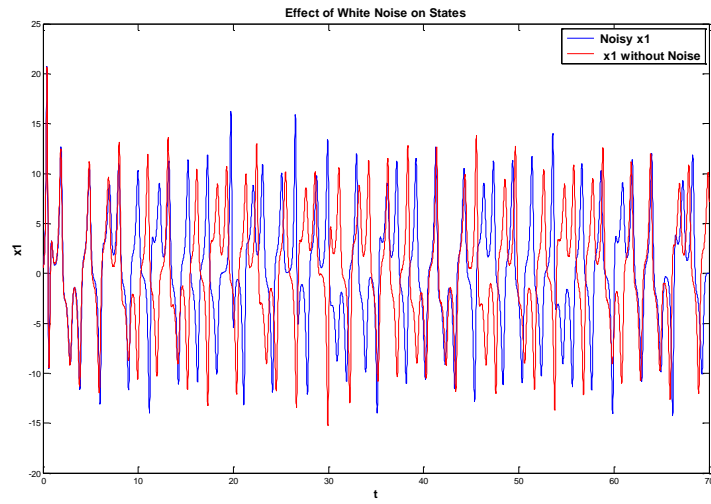


Fig.1 x_1 for ideal system (11) and x'_1 for noisy system (13)

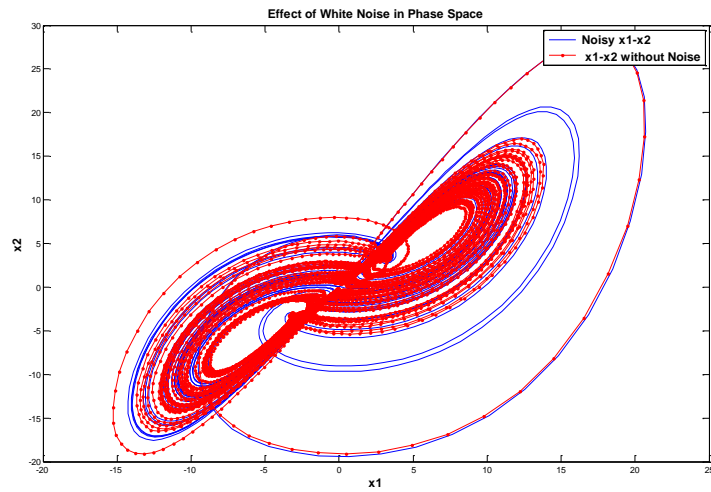


Fig.2 $x_1 - x_2$ for system (11) and $x'_1 - x'_2$ for noisy system (13)

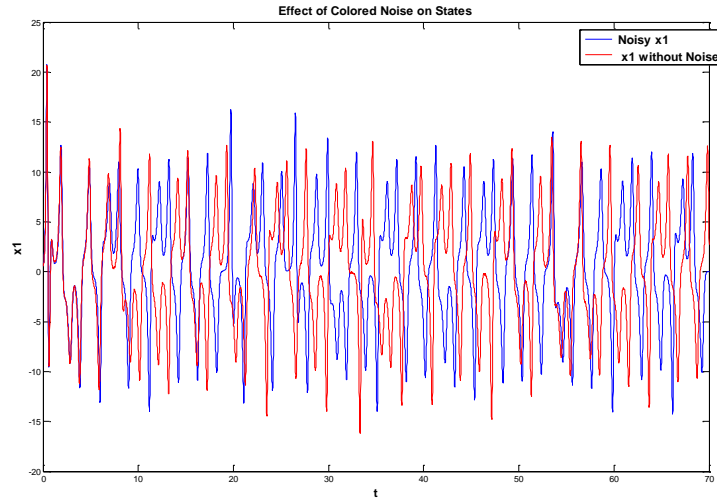


Fig.3 x_1 for ideal system (11) and x_1'' for noisy system (14)

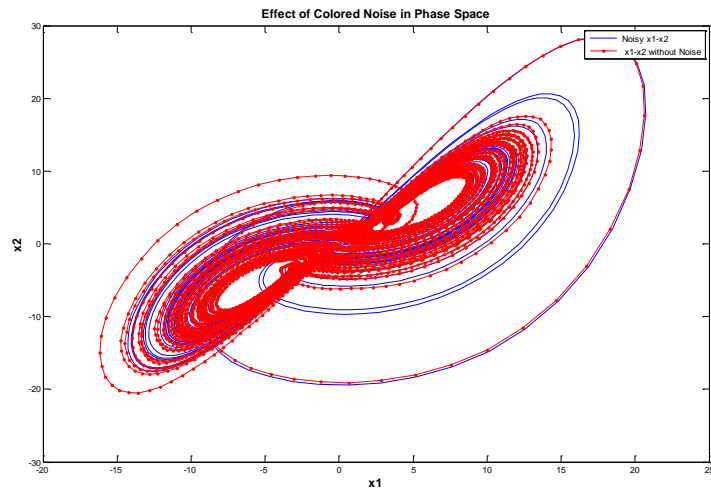


Fig.4 $x_1 - x_2$ for system (11) and $x_1'' - x_2''$ for noisy system (14)

4.3 Lorenz system with uncertain parameters



Although the chaotic systems are known with property of sensitivity to initial condition, this class of nonlinear systems is sensitive to parameters changes too. In this part this property is investigated on following uncertain Lorenz system

$$\begin{aligned}x_{1k+1}''' &= x_{1k}''' + \Delta t \bar{\sigma} (x_{2k}''' - x_{1k}''') \\x_{2k+1}''' &= x_{2k}''' + \Delta t (-x_{1k}''' x_{3k}''' + \bar{r} x_{1k}''' - x_{2k}''') \\x_{3k+1}''' &= x_{3k}''' + \Delta t (x_{1k}''' x_{2k}''' - \bar{b} x_{3k}''') \\z &= x_{1k}''' + x_{3k}'''\end{aligned} \quad (15)$$

$$\bar{\sigma} = \sigma \pm \Delta\sigma, \bar{b} = b \pm \Delta b, \bar{r} = r \pm \Delta r, \bar{c} = c \pm \Delta c, \bar{d} = d \pm \Delta d$$

Where $\bar{\sigma}, \bar{b}, \bar{r}$ are nominal or mean value of the unknown parameters and $\Delta\sigma, \Delta b, \Delta r$ are range of the parameters variations.

Figures (5), (6) show trajectories of the model (15) with nominal parameters and with small variation of σ parameter from 10 to 10.001 in time domain and phase domain respectively. According to figures with a small perturbation $\Delta\sigma = 0.005$, system's behavior changes from the nominal model. Value of the error (12) is $error(x, x''') = 65.6814$ in simulation.

5. EKF estimation of Lorenz system

In this part problem of estimation of different uncertain models are solved by changing them to model (6) which EKF is applicable for estimation of its states and parameters. For realization $x = [.]^T, \theta = [.]^T, Q' = [.]$ vectors are defined in this part. Where, x is the state vector that EKF estimates, θ is vector of known parameters, Q' is an auxiliary vector which its arrays are variance of the uncertainties that are considered as white noises in the system.

5.1 EKF for state estimation of Lorenz system with white noise on states

Realization of the Lorenz system (13) with white noise in the form (6) results in the following parameters

$$x = [x_1, x_2, x_3]^T, \theta = [\sigma, b, r]^T, Q' = [Q, R]$$

Figures (7), (8) show trajectories of the noisy model (13) and estimated value $\hat{x} = [\hat{x}_1, \hat{x}_2, \hat{x}_3]^T$ with EKF in time domain and phase domain respectively. According to figures EKF estimated the real value of x correctly. Value of the error is $error(x, \hat{x}) = 0.0013$ in simulation.

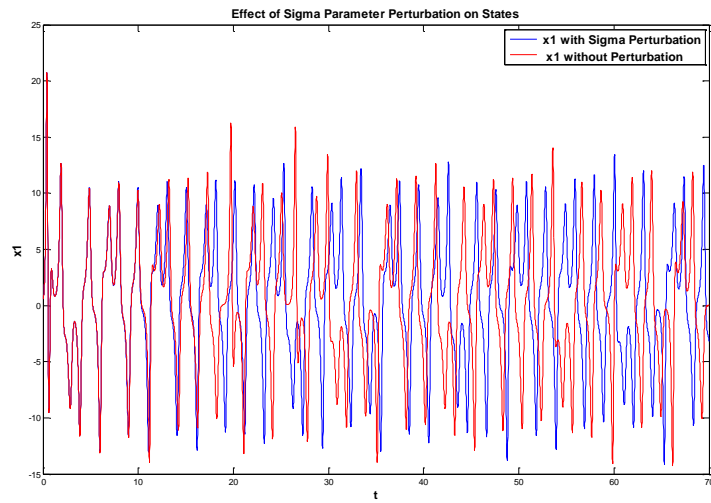


Fig.5 x_1 for ideal system (11) and x_1''' perturbed system (15) with $\Delta\sigma = 0.001$

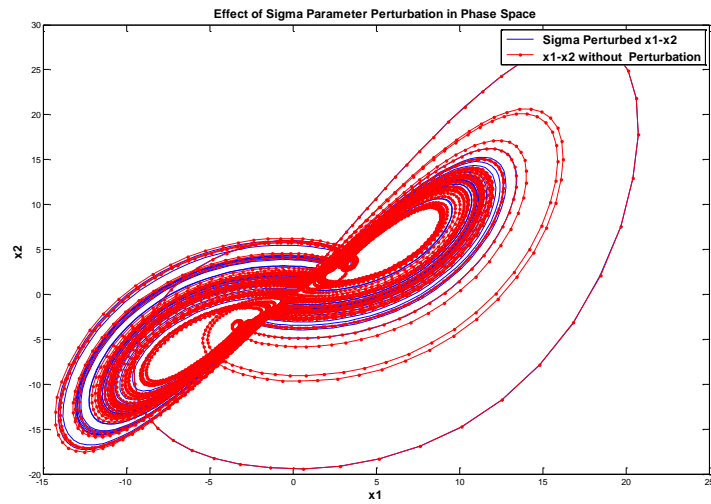


Fig.6 $x_1 - x_2$ for system (11) and $x_1''' - x_2'''$ for perturbed system (15) with $\Delta\sigma = 0.001$

5.2 EKF for state estimation of system with colored noise



Realization of the Lorenz system (14) with white noise in the form (6) results in the following parameters

$$x = [x'_1, x'_2, x'_3, v, w]^T, \theta = [\sigma, b, r, c, d]^T, Q' = [Q, R]$$

Figures (1),(2) show trajectories of the noisy model(14) and estimated value $\hat{x} = [\hat{x}'_1, \hat{x}'_2, \hat{x}'_3]^T$ with EKF in time domain and phase domain respectively.

Value of the error is $error(x', \hat{x}') = 0.0017$ in simulation.

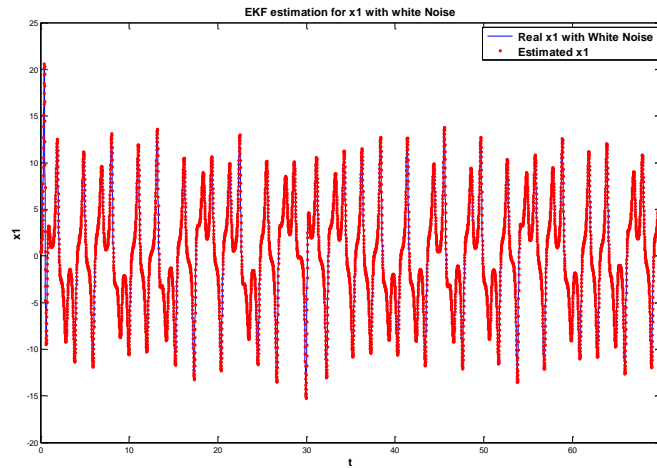


Fig.7 x'_1 for system (13) and \hat{x}'_1 estimated value with EKF

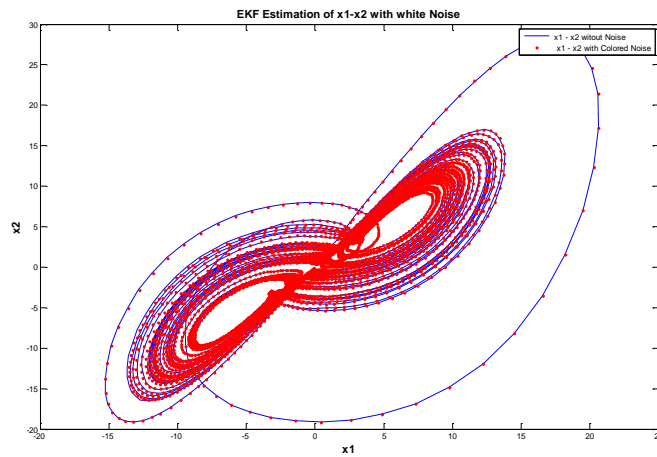


Fig.8 $x'_1 - x'_2$ for system (13) and $\hat{x}'_1 - \hat{x}'_2$ estimated values with EKF

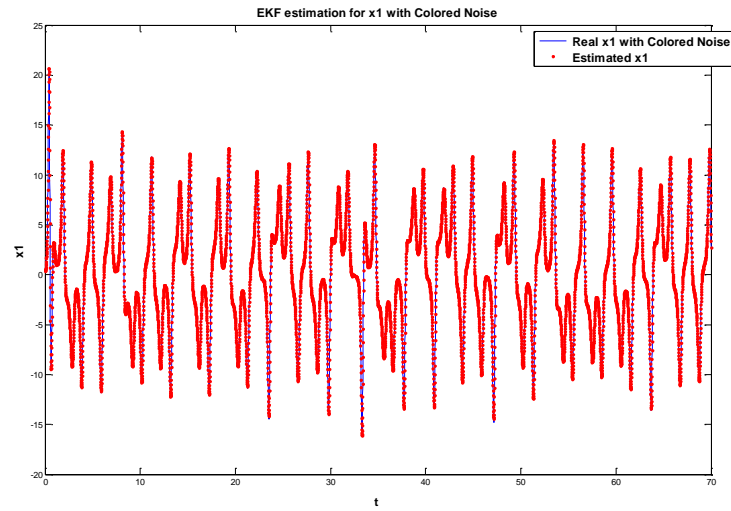


Fig.9 x_1'' for system (14) and \hat{x}_1'' estimated value with EKF

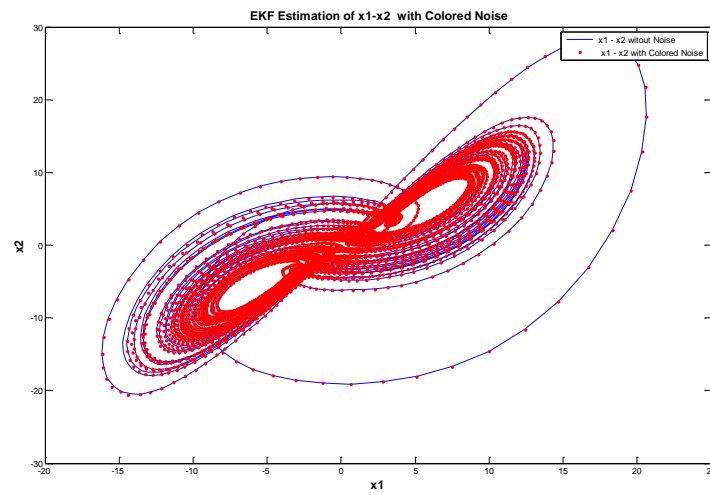


Fig.10 $x_1'' - x_2''$ for system (14) and $\hat{x}_1'' - \hat{x}_2''$ estimated values with EKF



5.3 EKF for state estimation of system with colored noise and unknown parameters

Realization of the Lorenz system with white noise and uncertain parameters results in

$$\begin{aligned}
 x_{1k+1}''' &= x_{1k}''' + \Delta t \bar{\sigma} (x_{2k}''' - x_{1k}''') + w_k \\
 x_{2k+1}''' &= x_{2k}''' + \Delta t (-x_{1k}''' x_{3k}''' + \bar{r} x_{1k}''' - x_{2k}''') + w_k \\
 x_{3k+1}''' &= x_{3k}''' + \Delta t (x_{1k}''' x_{2k}''' - \bar{b} x_{3k}''') + w_k \\
 w_{k+1} &= cw_k + e^1 \\
 v_{k+1} &= dv_k + e^2 \\
 z &= x_{1k}''' + x_{3k}''' + v_k \\
 e^1 &\sim N(0, Q^1), e^2 \sim N(0, Q^2), \\
 \bar{\sigma} &= \sigma \pm \Delta\sigma, \bar{b} = b \pm \Delta b, \bar{r} = r \pm \Delta r, \bar{c} = c \pm \Delta c, \bar{d} = d \pm \Delta d
 \end{aligned} \tag{16}$$

For realization in the form (7) parameters are

$$\begin{aligned}
 x &= [x_1''', x_2''', x_3''', v, w, c, d, \sigma, b, r]^T, \theta = [\]^T, \\
 Q' &= [Q^1, Q^2, \Delta c, \Delta d, \Delta\sigma, \Delta b, \Delta r]
 \end{aligned}$$

Figures (11) , (12) show trajectories of the noisy model(16) and estimated value with EKF in time domain and phase domain respectively. According to figures EKF estimated the real value of x''' correctly. Value of the error is $error(x_1''', \hat{x}_1''') = 0.0941$ in simulation. Figure (13) shows estimated value $[\hat{\sigma}, \hat{b}, \hat{r}]$ with EKF. According to figures EKF estimated the real value of the system parameters correctly. Value of the error is $error(\theta, \hat{\theta}) = 0.1359$ in simulation.

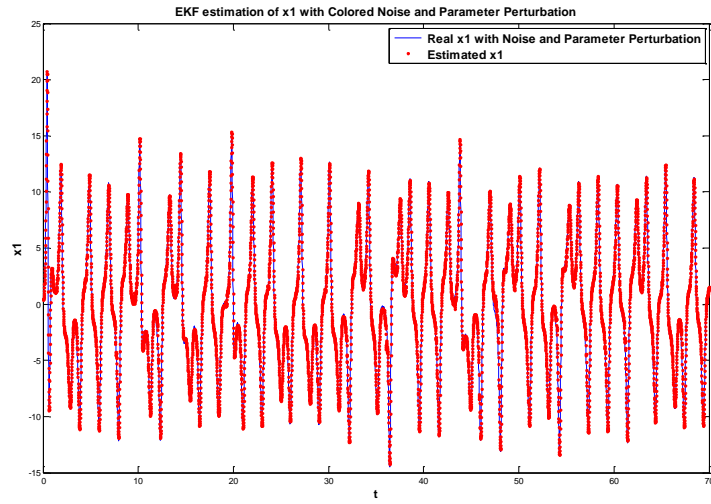


Fig.11 $x_1^{(3)}$ for system (16) and $\hat{x}_1^{(3)}$ estimated value with EKF

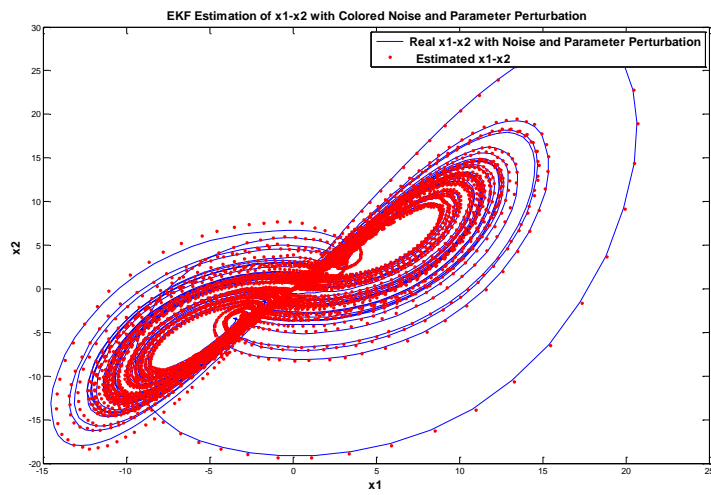


Fig.12 $x_1^{(3)} - x_2^{(3)}$ for system (16) and $\hat{x}_1^{(3)} - \hat{x}_2^{(3)}$ estimated values with EKF

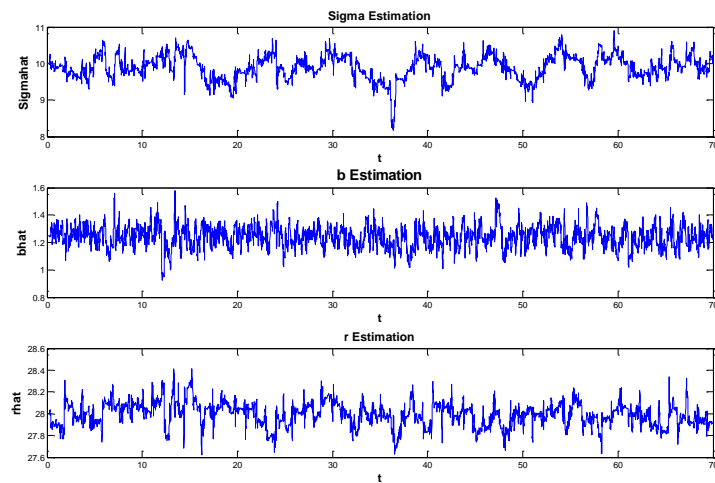


Fig.13 $\hat{\sigma}, \hat{b}, \hat{r}$ estimation for system (16) with EKF

6. Conclusion

The simulation results satisfying the efficiency of the EKF, a the first order filter which is result of Taylor expansion and neglecting higher order terms of the derivatives of the system equations, for estimation of the states and the parameters of the Lorenz system which is highly nonlinear chaotic system with noise like behavior.

References

1. J. T. Ambadan, Y. Tang. Sigma-Point Kalman Filter data assimilation methods for strongly nonlinear systems”, Journal of the Atmospheric Sciences, vol. 66, 261-285, 2009.
2. P. Li, R. Goodall, V. Kadirkamanathan, Parameter Estimation of railway Vehicle Dynamic Model Using Rao-Blackwellised Particle Filter, In (CDROM) Proceedings of the UKACC international conference on control’2004, University of Bath, UK, 2004.
3. X. Sun, L. Jin, M. Xiong, Extended Kalman filter for estimation of parameters in nonlinear state-space models of biochemical networks, Plosone, vol. 3, Is. 11, e3758, 2008.





Reconstruction of Evaporation Dynamics from Time Series

Özlem BAYDAROĞLU and Kasım KOÇAK

Istanbul Technical University, Department of Meteorology, 34469, Istanbul,
Turkey

E-mails: baydaroglu@itu.edu.tr, kkocak@itu.edu.tr

Abstract: The maximum amount of water loses from the reservoirs take place through evaporation. Thus it is important to know the dynamical system that governs the evaporation process. In this study, the Trajectory Method has been applied in order to obtain the differential equation from reconstructed phase space using evaporation time series. The trajectory method has been successfully applied in order to obtain the dynamical system that represents the periodic behavior of evaporation process.

Keywords: Dynamical system, Trajectory Method, Ordinary Differential Equations, Water Losses, Evaporation

1. Introduction

Water is the most vital substance for sustainability of life on planet earth. Unfortunately its distribution on earth both in time and in space is not uniform. This means that the water problem existed in the past, exists today and will exist in the future. On the other hand, especially in recent years water problem has gained much importance due to climate change. The state of the art climate models have shown that water related problems will be experienced more frequently in the future. This worsens the water related problems to a great extent. Thus it is mandatory to make intensive researches on the water resources and managements. In this context, water loses from all kind of water reservoirs are very important to be brought to a minimum level. As known well, the maximum amount of water loses from the reservoirs take place through evaporation. Thus it is important to know the dynamical system that governs the evaporation process. In this study, the Trajectory Method has been applied to reconstruction of differential equation that governs the behavior of evaporation process. The brief history of the trajectory method used in this study is as follows. Crutchfield and McNamara (1986) have made some important attempt to reconstruct the differential equation from time series. These two researchers have suggested two approximations about the issue. The first of them is the determination of local dynamic that considers the short-term behavior of the system while the second approach deals with the dynamic of the



whole attractor that consider the long-term behavior of the system. Almost at the same time with the aforementioned studies, Cremers and Hübler (1986) have developed the flow method that considers the sort-term behavior of the system. The flow method is applied to all points on the attractor. Thus it does not consider the long-term behavior of the system dynamic. Then Breeden and Hübler have developed this approach to include all of the system variables that could not be observed. In the end, Eisenhammer et al. (1991) have combine both short and long-term behavior of the system and they called their approach “trajectory method”. In this study, the trajectory method has been successfully applied in order to obtain the dynamical system of evaporation process.

2. Trajectory Method

Trajectory method is based on the reconstruction of differential equations which produce the trajectory resembling the original trajectory. In other word, the reconstructed model is the best possible model reflecting the original model (Perona et al., 2000).

A set first order ordinary differential equations can be given as

$$\dot{x} = f(x, t) \quad (1)$$

where x and t represent the variable vector and time, respectively. To reconstruct the equation of motion it is necessary to obtain the differential equations of model trajectory as close as possible to the original trajectory. On the other hand, mathematical form of the model should be determined ab initio.

According to theory of dynamical system, time evolution of a system can be given by its trajectories in a phase space. Coordinates of this space are formed by state variables which are necessary to reflect the time evolution of the system under study. Every trajectory in this space represents the different time evolution of the system that corresponds to different initial conditions. Phase portraits have distinct patterns that attract all trajectories. This type of a pattern is called attractor. All initial conditions of which trajectories captured from the attractor defines a domain of attraction. Systems that show deterministic evolution have low dimensional attractors like point, limit cycle and torus. These kinds of attractors can be characterized by an integer dimension. An important property of these kinds of attractors is that trajectories that converge onto them remain in a fixed distance from each other. This property ensures the system to be predictable for a long period of time (Koçak, 1996).

It is possible to reconstruct the phase space from a time series of one state variable sampled at regular time intervals Δt . For this to be done, some information and topological properties (e.g. dimension) of the attractor should be first estimated from the time series. Dimension of an attractor is the number of variable necessary to define the dynamics of the underlying system.



Packard et al., (1980) have suggested the reconstruction of phase space in order to obtain some invariant measures from an observed turbulent or chaotic flow. This can be achieved via transformation of the dynamical process to a higher dimensional space (embedding) by adding an extra independent dimension until no further information gain is impossible. One of these coordinates is formed by the time series itself and the remaining independent coordinates are formed by derivatives of the time series up to $(m-1)^{\text{th}}$ order. As a result, phase portrait of time evolution of a dynamical system can be represented in a new m -dimensional space spanned by a single state variable and its successive derivatives.

In this study, phase space is reconstructed from univariate or single time series (evaporation). Thus it is necessary to mention briefly from phase space reconstruction. Let's take a time series given as

$$x_i \in R, \quad i = 1, 2, \dots, N. \quad (2)$$

Then the reconstruction procedure is given as

$$X_i = (x_i, x_{i-\tau}, \dots, x_{i-(m-1)\tau}) \in R^m \quad (3)$$

$$i = 1 + (m-1)\tau, 2 + (m-1)\tau, \dots, N - I, N$$

where X_i is an m -dimensional vector.

This pseudo-phase space preserves the structure of the attractor embedded in the original phase space, (Takens, 1981). In Eq (3) τ is called time delay and should be calculated from time series by using autocorrelation function or mutual information function. Differential equation used in the trajectory method is assumed in the following form:

$$\dot{x}_i = \sum_{k=1}^K c_{i,k} F_{i,k}(x_1, x_2, \dots, x_D) \quad i = 1, 2, \dots, D \quad (4)$$

where $c_{i,k}$ s are coefficients of differential equation and $F_{i,k}(x_1, x_2, \dots, x_D)$ s are approximating functions. On the other hand K and D represent the number of approximating function and state variable, respectively. If $F_{i,k}$ is chosen as the 3rd degree polynomial then Eq (4) can given as

$$\dot{x}_i = \left\{ \begin{array}{l} c_{i,1} + c_{i,2}x_1 + c_{i,3}x_2 + c_{i,4}x_3 + c_{i,5}x_1x_2 + c_{i,6}x_1x_3 \\ + c_{i,7}x_2x_3 + c_{i,8}x_1^2 + c_{i,9}x_2^2 + c_{i,10}x_3^2 + c_{i,11}x_1x_2x_3 \\ + c_{i,12}x_1^2x_2 + c_{i,13}x_1^2x_3 + c_{i,14}x_1x_2^2 + c_{i,15}x_2^2x_3 \\ + c_{i,16}x_1x_3^2 + c_{i,17}x_2x_3^2 + c_{i,18}x_1^3 + c_{i,19}x_2^3 + c_{i,20}x_3^3 \end{array} \right\} \quad (5)$$

The trajectory method is very effective way of representing both short and long term behavior of dynamical system in the space of K functions.

Figure 1 outlines the trajectory method. As shown in this figure, model (Eq (4)) is run with the initial conditions ($j=1,2,\dots,j_{max}$) chosen along the original trajectory ($x_r(t_n), n=1,2,\dots,N$).

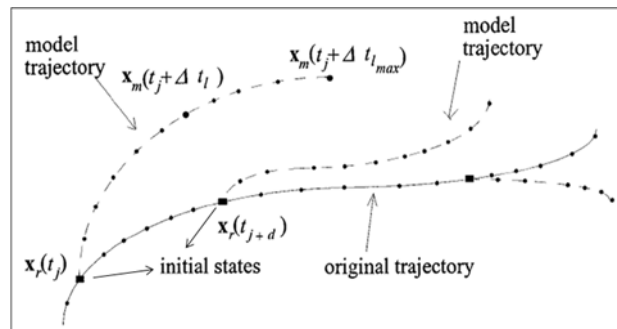


Figure 1. Schematic presentation of trajectory method in a phase space (after Perona et al., 2000).

The model equation is used to predict the state variable at the instants ($t_j + \Delta t_l$). A quality function Q is obtained by repeating this approach for different initial conditions.

$$Q = \sum_{j=1}^{j_{max}} \sum_{l=1}^{l_{max}} \|x_m(t_j + \Delta t_l) - x_r(t_j + \Delta t_l)\| \quad (6)$$

where the notation $\|\cdot\|$ shows the Euclidean norm. $x_r(t_j)$ and $x_m(t_j)$ in Eq (6) are the initial conditions on the original trajectory and trajectory produced by the model, respectively. At the beginning $x_r(t_j)$ and $x_m(t_j)$ are the same data point. On the other, hand l_{max} determines how many steps the model will be run in order to catch both sort and long-term behavior of the system. In other words, l_{max} is the number of points used for comparison between the single reconstructed trajectory and the original trajectory, starting from the initial state set on the latter. Δt_l in Eq (6) is the time interval between the integration steps of the model equation. This quantity can be calculated as

$$\Delta t_l = h(2^{l-1}) \quad (7)$$

where h is the interval between the observations or integration step in



case of numerical integration. The optimum value of $c_{i,k}$ are obtained by minimization the quality function Q .

$$Q_{\min} = \min_{c_{i,k}} Q \quad (i = 1, 2, \dots, D; k = 1, 2, \dots, K) \quad (8)$$

Eq (6) can be stated as given below

$$Q = \sum_{j=1}^{j_{\max}} \sum_{l=1}^{l_{\max}} \sqrt{\sum_{i=1}^D \left[\left(\int_{t_j}^{t_j+\Delta t_l} \dot{x}_{m_i}(\tau) d\tau \right) + x_{m_i}(t_j) - x_{m_i}(t_j+\Delta t_l) \right]^2} \quad (9)$$

The integral given in Eq (9) represents the change of $x_{m_i}(t)$ between the time interval $[t_j, t_j+\Delta t_l]$ and can be stated as

$$\int_{t_j}^{t_j+\Delta t_l} \dot{x}_{m_i}(\tau) d\tau = x_{m_i}(t_j + \Delta t_l) - x_{m_i}(t_j) = c_{i,1} \int_{t_j}^{t_j+\Delta t_l} F_{i,1}(\tau) d\tau + \dots + c_{i,k} \int_{t_j}^{t_j+\Delta t_l} F_{i,k}(\tau) d\tau \quad (10)$$

The integrals in Eq (10) should be calculated numerically because the functions $F_{i,k}$ are all unknown functions. If the partial derivative of Q with respect to unknown coefficients $c_{i,k}$ is set to zero, then the following set of linear equation is obtained:

$$\frac{\partial Q}{\partial c_{i,k}} = \left(\sum_{z=1}^K c_{i,z} A_{k,z}^{(i)} \right) - B_k^{(i)} = 0 \quad z, k = 1, \dots, K \quad (11)$$

The matrix $A_{k,z}^{(i)}$ and the vector $B_k^{(i)}$ are as given in Eqs (12) and (13), respectively.

$$A_{k,z}^{(i)} = \sum_{j=1}^{j_{\max}} \sum_{l=1}^{l_{\max}} \left[\left(\int_{t_j}^{t_j+\Delta t_l} F_{i,k}(\tau) d\tau \right) \left(\int_{t_j}^{t_j+\Delta t_l} F_{i,z}(\tau) d\tau \right) \right] \quad (12)$$

$$B_k^{(i)} = \sum_{j=1}^{j_{\max}} \sum_{l=1}^{l_{\max}} \left[\left(x_{m_i}(t_j + \Delta t_l) - x_{m_i}(t_j) \right) \left(\int_{t_j}^{t_j+\Delta t_l} F_{i,k}(\tau) d\tau \right) \right] \quad (13)$$

The matrix A is reversible. By solving Eq (11) a new set of coefficients $c_{i,k}$ are obtained then these coefficients are used in the next optimization cycle.

This process continues until the optimum values of coefficients are obtained (Perona et al., 2000).

3. Application to Evaporation Data

Daily evaporation totals used in this study are observed in the Ercan Meteorology Station located in North Cyprus. Observation period covers 2001-2010; total number of data points is 3652. In this study, before the application of the trajectory method, the original time series smoothed out by using loess method (Cleveland, 1979). Figure 2 shows the original and the smoothed out time series together.

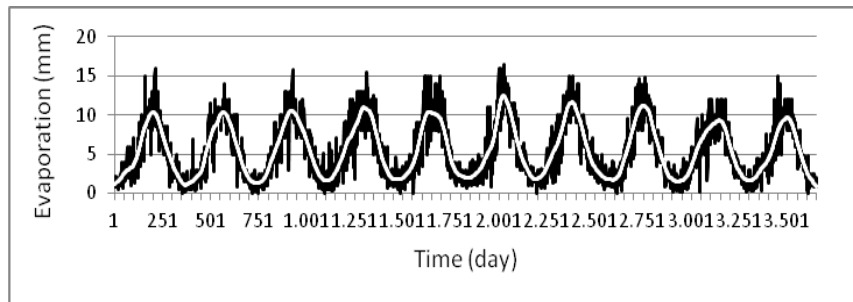


Figure 2. Evaporation time series (black) and smoothed out series (white).

By using smoothed time series phase space is reconstructed. As mentioned before, for phase space reconstruction two parameters namely time delay and embedding dimension are necessary. The time delay is determined by using Mutual Information Function (MIF) approach (Fraser, 1986). The first minimum value is taken as the optimum time delay (see Figure 3). As seen from Figure 3, the first minimum of the MIF is $\tau=112$. On the other hand embedding dimension is assumed $m=3$.

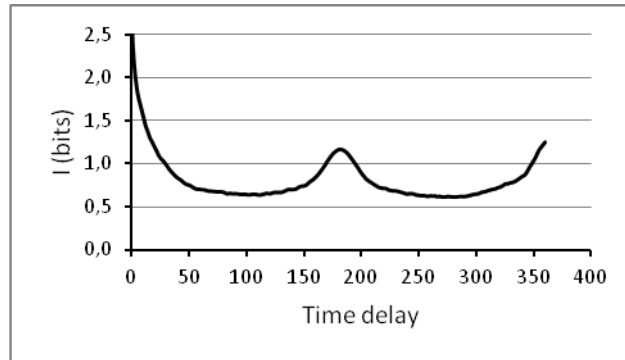


Figure 3. Mutual information of smoothed evaporation time series.

The phase space of evaporation process is reconstructed by taking time delay 112 and embedding dimension 3. Projection of the resulting attractor onto 2-dimension is given in Figure 4. As depicted in this figure smoothed attractor shows almost quasi-periodic behavior. Put another way, the behavior of this attractor in phase space is neither periodic nor aperiodic. This result shows that it will be reasonable to model the periodic structure or limit cycle of this attractor. The trajectory model has been applied to smoothed evaporation time series. The resulting limit cycle is given in Figure 5. As shown from this figure starting from an initial condition, the trajectory eventually converge the stable periodic orbit.

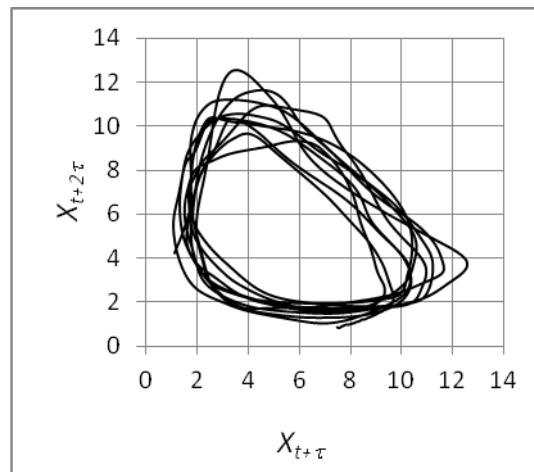


Figure 4. Projection of the attractor onto plane.

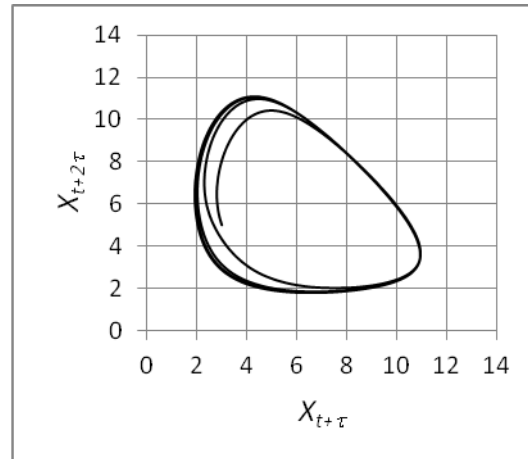


Figure 5. Periodic attractor of evaporation process.

4. Results and Discussion

Water reservoirs are very important in producing hydraulic energy, irrigation, flood control, drinking water, recreational purposes, etc. On the other hand there are some water losses from water reservoirs. The most important water losses take place by evaporation process. Thus, it is important to know the main dynamic of the evaporation.

In this study the trajectory method, the state art of the inverse problem solving method, is applied to evaporation process. Other variables that affect the evaporation such as temperature, wind speed, relative humidity, solar radiation, etc. are not considered in this application. In other words phase space reconstruction from univariate time series is used instead of multivariate approach. After the reconstruction process, the trajectory method is applied to smoothed evaporation data. The limit cycle or periodic behavior of the evaporation has been successfully reconstructed in the form of a set of differential equation which has three state variables.

References

- Breden, J.L., and Hübler, A., 1990. Reconstructing equation of motion from experimental data with unobserved variables, *Physical Review A*, 42(10), 5817-5826.



- Cleveland, W.S., 1979. Robust locally weighted regression and smoothing scatterplots. *Journal of the American Statistical Association*, 74(368), 829-836.
- Cremers, J., and Hübler, A., 1986. Construction of differential equations from experimental data, *Zeitschrift für Naturforschung A*, 42, 797-802.
- Crutchfield, J.P., and McNamara, B.S., 1986. Equations of motion from a data series, *Complex Systems*, 1, 417-452.
- Eisenhammer, T., Hübler, A., Packard, N., and Kelso, J.A.S., 1991. Modeling experimental time series with ordinary differential equations, *Biological Cybernetics*, 65, 107-112.
- Fraser A.M., Swinney H.L., 1986. Independent coordinates for strange attractors from mutual information. *Physical review A*, 33(2), 1134-1140.
- Koçak, K., 1996: Fractal Dimension Variation as a Chaotic Behaviour Criterion and its Application to Dynamical Systems. PhD Thesis, ITU Institute of Science (in Turkish).
- Packard, N.H., Crutfield, J.P., Farmer, J.D., Shaw, R.S., 1980. Geometry from a time series, *Physical Review Lett.*, 45(9), 712-716.
- Perona, P., Porporato, A., and Ridolfi, L., 2000. On The trajectory Method for the Reconstruction of Diffrential Equations from Time Series, *Nonlinear Dynamics*, 23, 13-33.
- Perona, P., D'Odorico, P., Porporato, A., and Ridolfi, L., 2001. Reconstructing the Temporal Dynamics of Snow Cover from Observations, *Geophysical Research Letters*, 28, 2975-2978.
- Takens, F. (1981) "Detecting strange attractors in turbulence", in Lectures Notes in Mathematics, edited by D. A. Rand and L. S. Young, 898, 366-381, Springer-Verlag, New York.

